INFORMATION TO USERS

This dissertation was produced from a microfilm copy of the original document. While the most advanced technological means to photograph and reproduce this document have been used, the quality is heavily dependent upon the quality of the original submitted.

The following explanation of techniques is provided to help you understand markings or patterns which may appear on this reproduction.

1. The sign or "target" for pages apparently lacking from the document photographed is "Missing Page(s)". If it was possible to obtain the missing page(s) or section, they are spliced into the film along with adjacent pages. This may have necessitated cutting thru an image and duplicating adjacent pages to insure you complete continuity.

2. When an image on the film is obliterated with a large round black mark, it is an indication that the photographer suspected that the copy may have moved during exposure and thus cause a blurred image. You will find a good image of the page in the adjacent frame.

3. When a map, drawing or chart, etc., was part of the material being photographed the photographer followed a definite method in "sectioning" the material. It is customary to begin photoing at the upper left hand corner of a large sheet and to continue photoing from left to right in equal sections with a small overlap. If necessary, sectioning is continued again — beginning below the first row and continuing on until complete.

4. The majority of users indicate that the textual content is of greatest value, however, a somewhat higher quality reproduction could be made from "photographs" if essential to the understanding of the dissertation. Silver prints of "photographs" may be ordered at additional charge by writing the Order Department, giving the catalog number, title, author and specific pages you wish reproduced.

University Microfilms

300 North Zeeb Road
Ann Arbor, Michigan 48106

A Xerox Education Company

73-7809

FOGARTY, William George, 1942-
PHYSICAL PROCESSES ASSOCIATED WITH THE INFRARED-MILLIMETER COMPONENT OF THE SPECTRA FROM THE NUCLEI OF SEYFERT GALAXIES.

The University of Arizona, Ph.D., 1972
Astrophysics

University Microfilms, A XEROX Company, Ann Arbor, Michigan

THIS DISSERTATION HAS BEEN MICROFILMED EXACTLY AS RECEIVED.

PHYSICAL PROCESSES ASSOCIATED WITH THE INFRARED-MILLIMETER COMPONENT OF THE SPECTRA FROM THE NUCLEI OF SEYFERT GALAXIES

by

William George Fogarty

A Dissertation Submitted to the Faculty of the

DEPARTMENT OF ASTRONOMY

In Partial Fulfillment of the Requirements
For the Degree of

DOCTOR OF PHILOSOPHY

In the Graduate College

THE UNIVERSITY OF ARIZONA

1 9 7 2

THE UNIVERSITY OF ARIZONA

GRADUATE COLLEGE

I hereby recommend that this dissertation prepared under my direction by William George Fogarty

entitled Physical Processes Associated with the Infrared-Millimeter Component of the Spectra from the Nuclei of Seyfert Galaxies

be accepted as fulfilling the dissertation requirement of the degree of Doctor of Philosophy

Dissertation Director — October 2, 1972 Date

After inspection of the final copy of the dissertation, the following members of the Final Examination Committee concur in its approval and recommend its acceptance:*

William J. Cocke	October 2, 1972
Ray J. Weymann	Sept. 29, 1972
James E. Felten	Oct. 5, 1972
Eugene E. Epstein	Oct. 27, 1972
Stanley Sadwick	October 2, 1972

*This approval and acceptance is contingent on the candidate's adequate performance and defense of this dissertation at the final oral examination. The inclusion of this sheet bound into the library copy of the dissertation is evidence of satisfactory performance at the final examination.

PLEASE NOTE:

Some pages may have

indistinct print.

Filmed as received.

University Microfilms, A Xerox Education Company

STATEMENT BY AUTHOR

This dissertation has been submitted in partial fulfillment of requirements for an advanced degree at The University of Arizona and is deposited in the University Library to be made available to borrowers under rules of the Library.

Brief quotations from this dissertation are allowable without special permission, provided that accurate acknowledgement of source is made. Requests for permission for extended quotation from or reproduction of this manuscript in whole or in part may be granted by the head of the major department or the Dean of the Graduate College when in his judgment the proposed use of the material is in the interests of scholarship. In all other instances, however, permission must be obtained from the author.

SIGNED: William G Fogarty

ACKNOWLEDGEMENTS

I wish to thank my dissertation director, Dr. A. G. Pacholczyk, for his guidance and specific suggestions at several critical stages during the development of the research presented herein.

I am especially indebted to Dr. Eugene E. Epstein for several reasons; for his help during five years with the observational material presented in this dissertation; for his very careful reading of and constructive criticism of the several drafts of this dissertation; for his frequent assistance in numerous practical matters; and for his constant inspiration not only to be scholarly but, even more, to be humane.

I wish to acknowledge Mary Jane Fogarty for her assistance in preparing the drawings and for many sacrifices she has made in helping me to complete this degree program.

My deepest thanks I give to Louis and Ann Epstein, who have provided me with the good atmosphere of a warm home and who have assisted me in most important ways as this dissertation was being completed.

I also wish to thank Dr. Edward Conklin for his careful reading of the observational material and the statistical analysis and Dr. Duane Dietrich, who pointed out to me the proper statistical procedures.

I wish to acknowledge Procol Harum and Franz Kafka, to whom I dedicate this dissertation, for showing me there is no way.

TABLE OF CONTENTS

		Page
	LIST OF ILLUSTRATIONS	vi
	LIST OF TABLES	viii
	ABSTRACT	ix
1.	INTRODUCTION	1
	Characteristics of Seyfert Galaxies	2
	Significance of Seyfert Galaxies	4
	Major Features of This Dissertation	6
2.	BACKGROUND MATERIAL ON SEYFERT GALAXIES	10
	Material Related to the Definition of Seyfert Galaxies	10
	Continuum Radiation	14
3.	OBSERVATIONS AT 90 GHZ OF SEYFERT GALAXIES AND RELATED OBJECTS	19
	Purposes of the Observations	19
	The Observations	21
	Equipment	21
	Observational Procedure and Data Reduction	22
	Calibration	29
	System Checks	30
	Results	34
	Discussion	39
	Estimate of the Variance of Monitored Sources	39
	An Analysis of Variance of the Monitored Sources	54
	Fluctuations in the Monitored Sources	62
	NGC 1068	63
	Other Sources	77
	Conclusions	78
4.	PRELIMINARY MODEL CONSIDERATIONS	81
	Characteristics of the Spectrum of NGC 1068	82
	Component I	84
	Component II	91
	Component III	94

TABLE OF CONTENTS--Continued

	Page
Thermal Radiation Mechanisms	95
Blackbody Radiation	95
Bremsstrahlung	100
Radiation from Dust	103
Synchrotron Radiation Mechanisms	105
The Homogeneous Model	105
Inhomogeneous Models	121
5. A SYNCHROTRON RADIATION MODEL OF THE NUCLEUS OF NGC 1068	125
Introductory Remarks	125
Component I	127
Component II	135
Discussion	138
6. PERSPECTIVES	146
Summary and Conclusions	147
Future Work	150
REFERENCES	152

LIST OF ILLUSTRATIONS

Figure		Page
1.	A Schematic Illustration of the Emission Lines Found in the Nuclei of the Two Types of Seyfert Galaxies	13
2.	A Schematic Representation of a Typical Continuous Spectrum of a Seyfert Galaxy near the Visual Region	15
3.	The ΔT vs. τ Relationship	25
4.	The Radio Spectra of Virgo A and Cygnus A	33
5.	The 90-GHz Flux vs. Time Curves of the Monitored Sources Discussed in the Test	37
6.	The 90-GHz Flux vs. Time Curves with Improved Sensitivity . .	38
7.	Long Term and Short Term Estimates of the Standard Deviation Before 1971	52
8.	Long Term and Short Term Estimates of the Standard Deviation During 1971	53
9.	Histogram of 156 Cycles of Antenna Temperature Measurements of Blank Sky	65
10.	Comparison of 713 Cycles of NGC 1068 with a Normal Distribution of 713 Cycles Around a Zero Mean	69
11.	The Observed Continuous Spectrum of NGC 1068	83
12.	The Flux Spectrum and the Variability Amplitude of the Flux for the Radio Source VRO 42.22.01	89
13.	The T_b (or ν_b) vs. R Relationship for Two Values of L_{IR} . . .	97
14.	Thermal Models of the Observed Spectrum of NGC 1068	99
15.	The Homogeneous Synchrotron Radiation Model of the Observed Spectrum of NGC 1068	119
16.	The Possible Values of N_e and T_e of the Thermal Cloud Around Component I	132

LIST OF ILLUSTRATIONS--Continued

Page

17. A Synchrotron Radiation Model Spectrum Compared to the Observed Spectrum of NGC 1068 134

18. Schematic Presentation of the Infrared Synchrotron Model of the Nucleus of NGC 1068 141

19. Schematic Presentation of a Concentric Radiation Model of the Nucleus of NGC 1068 144

LIST OF TABLES

Table		Page
1.	Observed Properties of Seyfert Galaxies	11
2.	Estimated Infrared Luminosity of Bright Seyfert Galaxies	17
3.	The 90-GHz Flux Measurements	35
4.	Confidence Intervals on σ of Monitored Sources Before 1971	48
5.	Confidence Intervals on σ of Monitored Sources During 1971	49
6.	An Analysis of Variance of the Monitored Sources Before 1971	60
7.	An Analysis of Variance of the Monitored Sources During 1971	61
8.	Runs Analysis of NGC 1068, NGC 1275, and VRO 42.22.01	72
9.	χ^2 Tests of Two Observations of NGC 1068	74
10.	Flux vs. Time Data at Four Radio Frequencies for NGC 1068	85
11.	The Constants c_5, c_6, and c_{14} for a Range of Values of γ	107
12.	Variation of the Derived Parameters of the Homogeneous Synchrotron Radiation Model	117
13.	Variation of the Derived Parameters of Component I - Double Structure	129
14.	Variation of the Derived Parameters of Component II	137
15.	Variation of the Derived Parameters of Component I - Single Source	143

ABSTRACT

Observations of Seyfert galaxies and related objects were made at a wavelength of 3.3 mm at The Aerospace Corporation. Objects which were observed extensively are NGC 1068, NGC 1275, 3C 120, 3C 273, 3C 454.3, OJ 287, and VRO 42.22.01. All were detected at a high significance level, except NGC 1068. Furthermore, all showed significant time variations, except NGC 1068. Less extensive observations were made of nine other objects, of which Cygnus A, Virgo A, and 4C 39.25 were detected with high significance.

One conclusion of the millimeter wavelength observations is the suggestion that NGC 1068 may also have a flux which is variable with time. This suggestion follows from two highly significant (as indicated by χ^2 tests and the Student's t test) detections of NGC 1068 in December 1966 and January 1967, together with the fact that the remaining observations of NGC 1068 are consistent with not having detected the source (as indicated by χ^2 tests). An analysis of variance of the observations of NGC 1068 indicates that the source is non-constant at the 0.5% significance level for all the observations between December 1966 and November 1970 and at the 5% level for the observations between April 1968 and November 1970. This suggests that variability of the flux may have occurred between December 1966 and April 1968 and probably to November 1970 (and this would be consistent with the results of the χ^2 tests). However, the results of the analysis of variance must be interpreted with caution because it is not possible to establish beyond a reasonable

doubt that the system noise was constant during the period from December 1966 to April 1968. There is no evidence for detection of NGC 1068 during 1971.

The major conclusions from these millimeter wavelength observations are that Seyfert galaxies and QSOs may be indistinguishable in their continuum millimeter flux, that both have similar variability characteristics, that the production of the millimeter radiation is more likely to be related to the radio than to the infrared radiation, and that the spectra between 10^{11} Hz and a few times 10^{12} Hz are likely to increase very rapidly with frequency.

Observations of the spectrum of NGC 1068 from radio waves to ultraviolet are reviewed, and theoretical models are discussed. Simple models involving blackbody radiation, bremsstrahlung or dust are inadequate. Homogeneous synchrotron models have severe difficulties.

A steady-state radiation model of the nucleus of NGC 1068 is determined by fitting a model to the observed spectrum. The size restrictions are satisfied by attributing different parts of the spectrum, which have different time scales of variability, to physically separate sources of radiation. In the center of the nucleus there is a small (10^{15} cm) source of optically thick synchrotron radiation, giving rise to the higher frequency infrared component of the flux spectrum. The magnetic field strength is about 2.5×10^5 gauss, and the density of the moderately relativistic electrons is about 7 cm^{-3}. Separate from this source there is a larger (3×10^{16} cm) double source of optically thick synchrotron radiation with a magnetic field strength of 400 gauss and a density of 40 cm^{-3}. This double source produces the component of the

spectrum which is sharply peaked around a wavelength of 100 μm. The double source is surrounded by a larger (3×10^{17} cm), optically thick cloud of electrons and protons with an electron temperature and density of 10^4 °K and 1.6×10^6 cm^{-3}, respectively.

The proposed model appears to satisfy simultaneously the restriction imposed by the shortest reported time scale of variability and the condition that the energy loss rate of the electrons due to inverse Compton scattering be sufficiently less than the rate due to synchrotron radiation to satisfy the observed (or presumed) ratio of the infrared luminosity to the luminosity in any higher frequency region of the spectrum. A characteristic feature of the model is that it requires a very narrow range of specification of two observed parameters, the size of the source and the frequency at which the flux density is a maximum. The model does accommodate the presently reported ranges of the values of these two parameters. The disadvantages of the model include the somewhat artificial structure of the model and the problem of the constant replenishment of the energy of the relativistic electrons because of their very short lifetime against radiation losses.

CHAPTER 1

INTRODUCTION

Seyfert galaxies have been the subject of much research since Carl Seyfert (1943) published a list of 12 galaxies with unusual morphological characteristics and line spectra. Very little research on Seyfert galaxies was done, however, until interest in them was revived by the observational work of Burbidge, Burbidge, and Prendergast (1959) and by the theoretical speculations of Woltjer (1959). Much of the subsequent study of these galaxies has been concentrated on investigating the properties which first led Seyfert to establish this class of spiral galaxies. These properties have been taken classically to be the following: 1) a very compact, or even unresolved, optical nucleus; 2) the presence of very broad Balmer series emission lines of atomic hydrogen indicating Doppler broadening velocities of several thousand km s^{-1}; and 3) the presence of narrower, but still relatively broad, lines of other elements indicating high ionization and excitation conditions (Burbidge *et al.* 1959).

A review of the existing information on Seyfert galaxies and a description of much research in progress was the result of the Conference on Seyfert Galaxies and Related Objects held at Steward Observatory in February 1968 (Pacholczyk and Weymann 1968b). Burbidge (1970) and Sargent (1971) have also discussed many of the current data and

theories on Seyfert galaxies in very comprehensive review articles on the nuclei of galaxies.

Characteristics of Seyfert Galaxies

After more careful investigation of the original list of twelve Seyfert galaxies, it has been shown that three of the galaxies do not completely satisfy the definition given above (Burbidge, Burbidge, and Prendergast 1963). In addition, the development of the new fields of radio, infrared, ultraviolet, and X-ray astronomy has enabled us to gather information about Seyfert galaxies which shows that they are not an entirely homogeneous class of objects. The attempt to discover more galaxies in this class in order to understand the Seyfert phenomenon better has led to efforts to define the phenomenon more carefully.

The Seyfert galaxies share some of their properties with other unusual galaxies of the normal spiral, elliptical, or irregular types. Of the compact galaxies identified by Zwicky (1964), most show only absorption lines and are probably ordinary elliptical galaxies or the nuclei of spirals with an unusually high concentration of stars. Only about 20 percent of the compact galaxies show emission lines at all, and only about one fourth of these show the broad emission lines characteristic of Seyfert galaxies. The only objects besides Seyfert galaxies and quasi-stellar objects (QSOs) which show lines of both high and low excitation are supernova remnants and non-Seyfert radio galaxies. Most N-type galaxies (galaxies which have an apparently very small, or even unresolved, optical nucleus - one of the characteristics of Seyfert galaxies) are not Seyfert galaxies, because they do not usually have broad

Balmer and high excitation emission lines. However, 3C 120 and Markarian 9, N-type galaxies, are Seyfert galaxies. There are also a few objects, a notable one being BL Lacertae (VRO 42.22.01), which have very compact nuclei and have many of the properties of the continuous spectrum similar to the Seyfert galaxies, but show no emission or absorption lines (Sargent 1971).

The simplest definition of a Seyfert galaxy was suggested by Sargent (1971) and follows from a discussion by Morgan and Osterbrock (1969): a galaxy whose nucleus shows broad emission lines, indicating Doppler broadening velocities of at least 500 km s^{-1}. It happens that these broad lines of galactic nuclei are seen only in spiral or irregular galaxies with very small nuclei and include, not only the emission lines generally seen in emission line galaxies, but also the emission lines indicating very high ionization and excitation conditions.

The approximately 35 galaxies now identified as belonging to the Seyfert class represent about one to two percent of the nearby spiral galaxies which have been investigated spectroscopically (de Vaucouleurs and de Vaucouleurs 1968). This result would indicate a lifetime of the Seyfert phenomenon of about 10^8 years if all spiral galaxies were to pass through such a stage at some time during their lifetimes of about 10^{10} years.

Two other important properties of several of the Seyfert galaxies are the very high infrared luminosity (Kleinmann and Low 1970) and the occurrence of variability of the flux density in one or more parts of the continuous spectrum (see, for example, the comprehensive articles by Kellermann and Pauliny-Toth 1968, Fogarty *et al.* 1971, Kleinmann and

Low 1970, and Burbidge 1970). If the light-travel time across the source is less than the characteristic time of variability of the flux, the time scale of variability may place a strong constraint on the size of the source. However, Morrison and Sartori (1968) have discussed how retardation effects can give rise to kinematic illusions. In particular, it is possible to measure images at arbitrary distances whose apparent rate of change can far exceed the speed of light, even though no actual particle or signal velocity exceeds the speed of light. This would place a much less restrictive constraint on the size of the radiating region. If the more restrictive condition is assumed to hold (as will be assumed throughout this dissertation), it is difficult to suggest a physical mechanism which can produce so high a power output in the small volume of space implied by the time scales of variability of the flux.

Significance of Seyfert Galaxies

Besides the intrinsic reasons, the Seyfert galaxies are also interesting objects for study because of the similarity of several of the properties between Seyfert galaxies and QSOs. A definition of QSOs offered by Burbidge and Burbidge (1967) is objects which show the following properties: 1) starlike objects often identified with radio sources, 2) variable light, 3) large ultraviolet flux of radiation, 4) broad emission lines in the spectra, with absorption lines sometimes present, and 5) large redshifts of the spectrum lines. We can see that the defining properties of Seyfert galaxies given above are included in this characterization of QSOs.

The sizes of QSOs and the nuclei of Seyfert galaxies are both quite small as indicated by the lack of resolution of these sources and by the time scale of variation of the flux density. Some recent high resolution studies of several QSOs show structure on an apparent scale of milliseconds of arc (Donaldson and Smith 1971, and Knight *et al.* 1971). The general shape of the continuous spectrum is remarkably similar among many of the Seyfert galaxies and QSOs from the long wavelength radio region to the ultraviolet region (Pacholczyk and Weymann 1968a), and possibly in the X-ray region also (Gursky *et al.* 1971). The presence of variability of the continuum flux density has been detected in many of both types of these sources, and the characteristics of the variability have been shown to be similar in several respects (apparent lack of periodicity, time scales, and amplitudes of the variations).

The study of QSOs is significant because of its relation to fundamental cosmological problems concerned with the size, history, and distribution of matter in the universe. It is also significant because the size of the radiating region inferred from the time scale of the variability and the distance indicated by the redshift of the spectral lines (if the cosmological interpretation of the redshift is correct), together with the apparent brightness and the probable lifetimes of these objects, lead to physical conditions and required energy mechanisms which are not yet completely understood. The probable relationship between QSOs and Seyfert galaxies indicated by their similarities makes the study of Seyfert galaxies important because they are much closer and therefore easier to observe.

The Seyfert galaxies are also intrinsically interesting. Their absolute luminosities are well known, compared to the QSOs. The small size indicated by the variability, together with the luminosity and the shape of the spectrum, leads to unusual physical conditions and to unusual required energy production mechanisms in the nucleus in order to explain the shape and strength of the continuous spectrum, the very wide emission lines, and the high excitation conditions. For those Seyfert galaxies with a very high, sharply peaked infrared spectrum and small size inferred from the observations of variability, the mechanisms of blackbody radiation, bremsstrahlung, or reradiation by a dust cloud surrounding a small ultraviolet central source either cannot produce a reasonable fit of the spectrum to the observations or cannot produce the required amount of radiation or can do neither. A spherical, homogeneous source of optically thick synchrotron radiation leads to a magnetic field strength which is not compatible with both the self-absorption feature (the peak of the flux spectrum in the infrared) and the condition that the energy losses due to inverse Compton scattering are small compared to synchrotron losses (as implied by the high ratio of the infrared luminosity to the luminosity at any higher frequencies).

Major Features of This Dissertation

The primary purposes of the research presented in this dissertation are the program of observations of Seyfert galaxies and related objects at a wavelength of 3.3 mm and the presentation of a theoretical radiation model which might be consistent with the observed continuous spectrum from the millimeter wavelength region to the near infrared

region of several Seyfert galaxies, but more specifically, to be consistent with the observed infrared spectrum of one Seyfert galaxy, NGC 1068. This source has been chosen because it is closer and brighter in most regions of its spectrum than other Seyfert galaxies. When this study was begun in 1967, it seemed to be possible that NGC 1068 is a variable source in the millimeter wavelength region (Epstein and Fogarty 1968) and in the infrared (Pacholczyk and Weymann 1968a), in which case it would be possible to place some limits on the size of the radiating region. In addition, NGC 1068 was chosen for investigation because the question has been raised [Low (1970) and Pacholczyk (1971)] whether it is possible to retain a simple synchrotron radiation model as an explanation for the observed spectra if the very rapid variability of the flux (discussed in Chapter 4) is real.

Some detailed numerical background information on the distances, sizes, and radiation characteristics of the nuclei of Seyfert galaxies is given in Chapter 2.

Chapter 3 contains the observations and some discussion of the results of a program of observing a group of Seyfert galaxies and apparently related objects at a wavelength of 3.3 mm with the 4.6-m antenna of The Aerospace Corporation in Los Angeles, California. The observations were made in order to define better the spectra of these objects, search for variability of the flux density or unusual characteristics of the spectra, and to demonstrate the relationship, or lack thereof, between Seyfert galaxies and other types of objects. A lengthy statistical discussion of the millimeter wavelength observations enables us to conclude that all the QSOs and Seyfert galaxies with strong

millimeter wavelength radiation have a variable flux density. NGC 1068 is a weak source in the millimeter region. The observations contained here indicate a low probability (≃ 1%) of not having detected the source and a low probability (≃ 5%) that the flux of NGC 1068 at a wavelength of 3.3 mm is constant.

In Chapter 4 there is a brief introduction to and discussion of some previously suggested mechanisms (Pacholczyk and Weymann 1968a) proposed to explain the large infrared flux of Seyfert galaxies, in particular, of NGC 1068. Thermal mechanisms seem to fail because they cannot satisfy the size requirements implied by the variability of the flux density. Homogeneous synchrotron radiation models fail because they cannot simultaneously satisfy the size restrictions and the condition that the energy losses due to inverse Compton scattering be sufficiently small to satisfy the observational requirements, and because they do not provide a satisfactory fit of the predicted spectrum to the observed spectrum.

The steady state model of the nucleus of NGC 1068, developed in Chapter 5, is determined by fitting a theoretical model to the observed spectrum of NGC 1068. The size restrictions of the radiating regions are satisfied by attributing different parts of the spectrum, which have different time scales of variability of the flux density, to physically separate sources of radiation. In the center of the nucleus there is a very small (10^{15} cm) source of optically thick synchrotron radiation, giving rise to the higher frequency infrared component of the flux spectrum. The magnetic field strength in this region is about 2.5×10^5 gauss, and the density of the moderately relativistic (about 10 to 50

times the electron rest mass) electrons is about 7 electrons cm^{-3}. Separate from this source there is a much larger (3×10^{16} cm) double source of optically thick synchrotron radiation with a magnetic field strength of 400 gauss and a density of 40 electrons cm^{-3}. These electrons have energies from 50 to 500 times their rest mass. This double source produces the component of the spectrum which is sharply peaked around a wavelength of 100 um. The entire source is surrounded by a larger cloud (3×10^{17} cm in radius) of optically thick electrons and protons absorbing by the free-free radiation mechanism and characterized by an electron temperature and density of 10^4 °K and 1.6×10^6 cm^{-3}, respectively. The closeness of the fit to the observed spectrum can be varied by appropriate adjustments to the size, density, temperature, and magnetic field parameters of the various components of the model source. However, the model seems to require a very narrow range of specification of some observed parameters. The model appears to satisfy the condition that the energy loss rate of the electrons due to inverse Compton scattering be sufficiently less than the energy loss rate due to synchrotron radiation to satisfy the observationally imposed restrictions.

The equations and the variables used in this dissertation are in CGS units, except for the use of MKS units or of 10^{-26} MKS units = flux units (f.u.) for the observed values of the flux density.

CHAPTER 2

BACKGROUND MATERIAL ON SEYFERT GALAXIES

In this chapter we will consider some detailed information on some of the observed and deduced parameters of Seyfert galaxies. The properties to be discussed here are those that are concerned with the definitions of Seyfert galaxies and those that are related to the parameters to be utilized in the model to be developed in Chapters 4 and 5.

Material Related to the Definition of Seyfert Galaxies

Burbidge (1970) lists 24 galaxies presently classified as Seyfert galaxies. NGC 1409, I Zw 80, I Zw 95, and II Zw 1 have been added to this list by Sargent (1970), NGC 4670 by de Vaucouleurs (1961), NGC 6814 by Ulrich (1971), 0Q 208 by Blake, Argue, and Kenworthy (1970), Markarian 3 by Sargent (1971), Markarian 205 by Weedman (1970), and 14189+12 and 1625+20 by Fairall (1971). Table 1 contains this list and some of their properties. The name of the source is given in column 1. Column 2 gives the redshift of the spectrum and column 3 the distance D derived from an adopted Hubble constant (Sandage 1968) of 75 km s^{-1} Mpc^{-1}. The widths (defined in the usual way as the full width of the line at half maximum) of the hydrogen Balmer lines and the forbidden lines of other elements, W_H and W_F, respectively, are listed in columns 4 and 5, respectively. The symbols in columns 6 and 7 indicate the regions of the spectrum where the object has been detected and where variability of the flux has been detected, respectively. The symbols have the

Table 1. Observed Properties of Seyfert Galaxies

Object	z	D[a] [Mpc]	W_H [km s^{-1}]	W_F [km s^{-1}]	Detected	Variable
NGC 1068	.00364	15	2900	2900	R,mm,IR	mm,IR
NGC 1275	.018	72	3000	3000	R,mm,IR	R,mm
NGC 1409	.00246	10	>>1000	1200		
NGC 1566		12	3500			V
NGC 3227	.00335	13	6000	3000	R,IR	
NGC 3516	.00926	37	8500	1400	R,IR	V
NGC 3783						
NGC 4051	.00233	9	3600	1200	R,IR	
NGC 4151	.00330	13	7500	1000	R,IR,X	IR,V
NGC 4670						
NGC 5548	.0166	66	5000	1000	R,IR	V
NGC 6814			6000	1500		V
NGC 7469	.0169	68	5000	1000	R,IR	
3C 120	.033	132	3300		R,mm,IR	R,mm,V
OQ 208	.077	308			R	R
Markarian 3						
Markarian 9	.038	152	6000	<6000		
Markarian 10	.029	116	6000	<6000		
Markarian 34	.0507	203	1500	<1500		
Markarian 42	.024	96	2000			
Markarian 50	.023	92				
Markarian 69	.076	304				
Markarian 205	.070	280				
VV 144	.021	84	4000	<800		
VV 150	.027	108	1000	1000		
I Zw 1	.061	244		3000		
I Zw 80						
I Zw 95						
I Zw 1535+55	.0368	154				
II Zw 1			<1000			
II Zw 136	.061	244	3000			
III Zw 2	.089	356	7000		R	
IV Zw 29	.1026	410	5000	850	IR	V
14189+12	.0947	379				
1625+20	.0124	50				

[a] For an assumed Hubble constant = 75 km s^{-1} Mpc^{-1}

following meaning: R = radio, mm = millimeter, IR = infrared, V = visual, and X = X-ray. Since the defining properties of Seyfert galaxies concern the visual region of the spectrum, V is omitted in column 6.

The feature of compact nuclei in Seyfert galaxies is, of course, a distance-dependent characteristic. The apparent nuclear sizes are typically starlike, but range up to a few seconds of arc, or about 100 pc (Burbidge 1970), and down to 0.001 pc, as inferred from the flux variability (Pacholczyk 1970b). The upper limit refers to the region containing the gas which produces the emission lines, and the lower limit refers to the region which produces the variable continuum radiation.

The permitted emission lines found in the nuclei of Seyfert galaxies include the recombination lines of H, He I, and He II, and the weak Bowen fluorescence lines of O III. The permitted lines of Fe II, probably excited by electron collisions rather than by recombination, are found in some Seyfert galaxies. The forbidden lines include the lines of [O I], [O II], [O III], [Ne III], [Ne V], [Si II], and [N II]. There is a very large range of emission lines due to iron: [Fe II], [Fe III], [Fe IV], [Fe VII], and [Fe X], and possibly even [Fe XIV] in at least one object, NGC 4151. A detailed inspection of the profiles of the emission lines shows that there are two kinds of Seyfert galaxies, those with lines as in NGC 4151 and the more rare kind like NGC 1068. These two types are illustrated schematically in Figure 1. In objects like NGC 4151 the permitted emission lines have wide wings and a sharper core, whereas the forbidden lines have only the sharp core. The half widths of the sharp cores are the same in both cases, typically about 500 km s^{-1}, while the half widths of the broad components are about

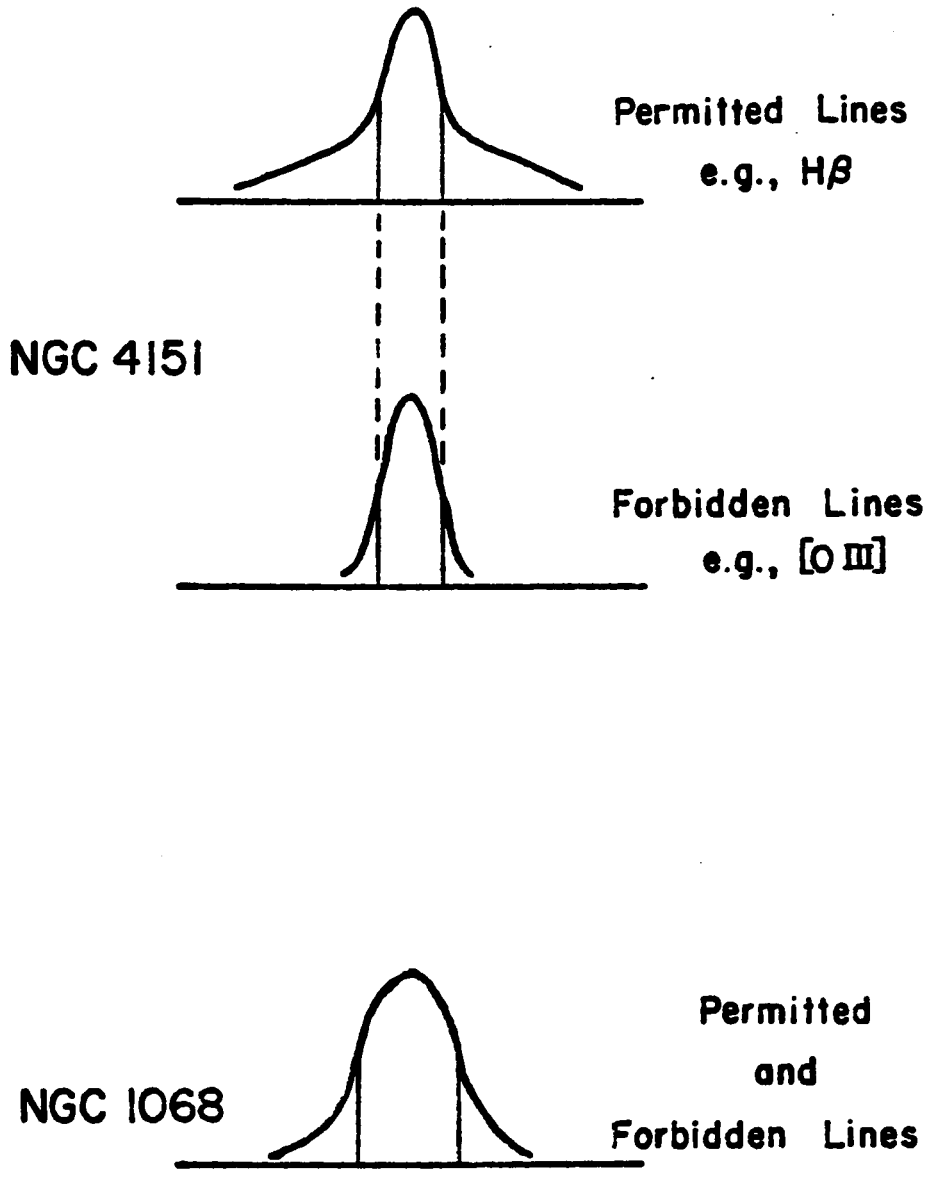

Figure 1. A Schematic Illustration of the Emission Lines Found in the Nuclei of the Two Types of Seyfert Galaxies

3000 km s^{-1}. In objects like NGC 1068 both the permitted and forbidden lines have wide profiles, which have roughly the same half width (Sargent 1971).

We see from Table I that there is a large range in the widths of the emission lines. The hydrogen lines range from 1000 km s^{-1} to 8500 km s^{-1} and are typically around 4000 km s^{-1}, while the forbidden lines range up to 3000 km s^{-1} and are typically around 1000 km s^{-1}.

Continuum Radiation

A typical continuous flux density spectrum of a Seyfert galaxy in and near the visual region has the general shape illustrated schematically in Figure 2. The ordinate is the log of the flux density, F_ν, and the abscissa is the log of the radiation frequency, ν. The bump which coincides with the Balmer discontinuity at the blue end of the optical region might be produced by the hot gas which radiates the emission lines (Oke 1968). Code (1969) has reported a very steep rise into the ultraviolet out to 1000 Å (frequency of 3×10^{15} Hz) for one of the Seyfert galaxies, NGC 1068. Two of the Seyfert galaxies, NGC 1275 and NGC 4151, have been detected in the X-ray region near a frequency of 10^{18} Hz; and there is an upper limit determined for NGC 1068 at this frequency (Gursky *et al.* 1971). More recently it has been shown (Kellogg *et al.* 1971) that the X-radiation previously attributed to NGC 1275 comes from a source which is extended beyond the visual galaxy. The amount (if any) of X-radiation emitted by the nucleus is unknown.

The discovery of the large amount of infrared radiation from the nuclei of Seyfert galaxies was first reported by Pacholczyk and

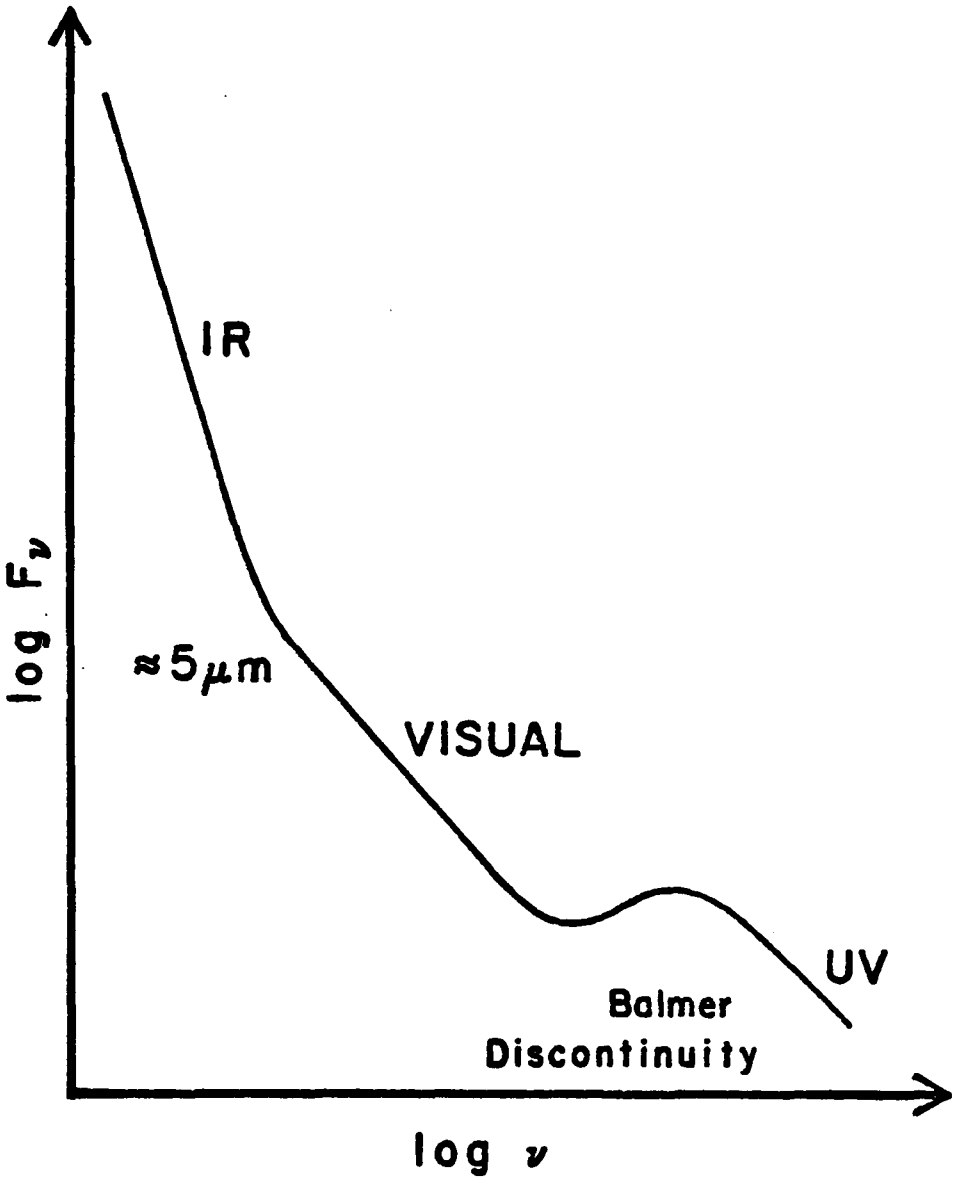

Figure 2. A Schematic Representation of a Typical Continuous Spectrum of a Seyfert Galaxy near the Visual Region

Wisniewski (1967), who observed the excess radiation from the nucleus of NGC 1068 from the visual region of the spectrum out to a wavelength of 3.4 μm. The rapid rise of the spectrum into the near infrared observed in many Seyfert galaxies implies that most of the energy of the Seyfert nucleus is radiated in the infrared. At the present time it is difficult to state how much energy is radiated because we do not know how far to extrapolate the rise into the infrared. Recent measurements of the flux density out to wavelengths as long as 22 μm (Kleinmann and Low 1970) for four of the Seyfert galaxies (NGC 1068, NGC 1275, NGC 4151, and 3C 120) indicate that at least these four are quite similar to one another and are powerful sources of radiation. The brightest of these four, NGC 1068, has been measured out to 100 μm (Low and Aumann 1970), where it is still continuing to rise very steeply. If we assume that these four sources have the same spectral distribution out to 100 um, as in NGC 1068, then the total infrared luminosity of each for an adopted distance can be calculated. The results of the calculation (after Kleinmann and Low 1970) are given in Table 2. The galactic center has been added to this table for comparison. For the brightest of these sources, the total infrared luminosity is about 10^{13} times the luminosity of the sun. In addition to these four sources, six other Seyfert galaxies have been detected in the infrared: NGC 3227, NGC 4051, NGC 5548, and NGC 7469 (Pacholczyk and Weymann 1968a), NGC 3516 (Wisniewski and Kleinmann 1968), and IV Zw 29 (Burbidge 1970).

Eleven Seyfert galaxies have been detected in the long wavelength radio region: NGC 1068 (3C 71) and NGC 1275 (3C 84) (Bennett 1962); NGC 3227, NGC 4051, NGC 4151, and NGC 7469 (Wade 1968); NGC 3516

Table 2. Estimated Infrared Luminosity of Bright Seyfert Galaxies[a]

Source	Distance [Mpc]	IR Luminosity [erg s^{-1}]
Galactic Center	0.010	3.2×10^{42}
NGC 1068	13	2.5×10^{46}
NGC 1275	70	2.7×10^{46}
NGC 4151	13	8.5×10^{44}
3C 120	120	2.9×10^{46}

[a] After Kleinmann and Low (1970)

and NGC 5548 (van der Kruit 1971); 3C 120 (Clarke, Bolton, and Shimmins 1966); 0Q 208 (Blake, Argue, and Kenworthy 1970); and III Zw 2 (Burbidge 1970). NGC 1275 and 3C 120 are well known, strong radio sources. These two are also strong sources in the millimeter wavelength region (Fogarty *et al.* 1971). NGC 1068 is a weak millimeter wavelength source.

Variability of the flux density in one or more regions of the continuous spectrum has been observed for ten of the sources listed in Table 1. Three are variable in the radio region: NGC 1275 and 3C 120 (Kellermann and Pauliny-Toth 1968) and 0Q 208 (Blake *et al.* 1970); three in the millimeter region: NGC 1068 (the uncertainty of the millimeter wavelength variability of NGC 1068 as reported in this dissertation is discussed in detail in Chapter 3), NGC 1275, and 3C 120 (Fogarty *et al.* 1971); two in the infrared: NGC 1068 (Pacholczyk 1970b; Neugebauer *et al.* 1971; and Low and Rieke 1971) and NGC 4151 (Penston *et al.* 1971); and seven in the visual: NGC 1566 (Pastoriza and Gerola 1970), NGC 3516 and IV Zw 29 (Burbidge 1970), NGC 4151 (Fitch, Pacholczyk, and Weymann 1967), NGC 5548 (Bardin, Chopinet, and Duflot-Augarde 1967), NGC 6814 (MacPherson 1972), and 3C 120 (Kinman 1968). The optical and infrared continua vary on time scales of weeks and possibly as short as one day or less (Pacholczyk 1970b). The time scales in the radio and millimeter regions appear to range from a week to perhaps several months or a year (see Chapter 3).

CHAPTER 3

OBSERVATIONS AT 30 GHZ OF SEYFERT GALAXIES AND RELATED OBJECTS

Since the major goal of the research presented in this dissertation is to suggest a model which might explain the infrared continuous radiation from the nuclei of Seyfert galaxies, it is necessary to determine the continuous spectrum as accurately as possible in order to specify the parameters of any proposed model. When this research was begun in 1967, measurements of the spectra out to wavelengths as long as 22 μm of several Seyfert galaxies were in progress (Low and Kleinmann 1968). These measurements indicated that the spectra are still rising steeply around 20 μm with increasing wavelength, that the infrared luminosity is very great (probably most of the radiation from these sources is in the infrared), and that the spectra might be variable. Measurements at wavelengths greater than 25 μm are quite difficult to make because of the very low transmission of the atmospnere in the wavelength range between 25 μm and 1 mm (1000 μm) and because of design problems and calibration uncertainties of the measuring instruments (Johnson 1966).

Purposes of the Observations

Observations at as high a frequency as possible in the radio region (as close as possible to the infrared) would help to narrow the gap between the easily observed radio and infrared regions. The highest frequency at which measurements could be made on a regular basis

(in 1967) from ground-based equipment was 90 GHz. These measurements were made at The Aerospace Corporation in Los Angeles, California. The information gained from these observations of a sample of Seyfert galaxies places constraints on the shape of the infrared spectrum in the unobservable region and indicates that the detectable millimeter radiation is probably produced in the part of the source usually associated with the radio, rather than the infrared, radiation. The time scale of any variability of the flux, determined by routine observing of these sources, can impose restrictions on the maximum size of the radiating region, a critical parameter in formulating any radiation model.

A total of five Seyfert galaxies was observed during this observing program: NGC 1068, NGC 1275, and 3C 120, which have been monitored, and NGC 4151 and OQ 208, which were not detected. Two QSOs, 3C 273 and 3C 454.3, have been monitored, while three others, 4C 39.25, 3C 380, and PKS 2134+00 and one N-type galaxy, 3C 371, were observed several times in order to compare the variability and spectral characteristics of these objects, which are believed to be related to Seyfert galaxies. The word "monitor," used in connection with the regularity with which observations were made, is to be interpreted as the attempt to measure the flux of a source at specified intervals. These specified intervals ranged from about one week to about one month, depending on the particular source.

Observations of the radio galaxies Virgo A and Cygnus A were made in order to serve as system checks, since it was believed that the value of the 3.3-mm flux could be extrapolated with reasonable confidence from the longer wavelength data (this extrapolation is less

certain for Cygnus A). The irregular galaxy M 82 was observed because some of its similarities to Seyfert galaxies and the presence of an infrared source near the nucleus had led to speculation that it is a Seyfert galaxy (Solinger 1969). It is no longer believed to belong to this class of galaxies, however (Bertola *et al.* 1969). Two other very interesting objects, OJ 287 and VRO 42.22.01 (BL Lacertae), have also been monitored. These two show the QSO-like properties of a starlike nucleus and a variable flux in both the radio and optical regions of the spectrum (possibly with time scales as short as several hours); but the optical spectra show no detectable emission or absorption lines (Dupuy *et al.* 1969; Kinman and Conklin 1971; Epstein *et al.* 1972). It is possible that no emission or absorption lines have been detected in these two objects because the lines are too broad to be measurable by the usual spectroscopic methods. If this were the reason for the non-detection of lines in these two sources, then they could possibly be considered as extreme cases of the Seyfert-type phenomenon. All seven of the sources which were monitored, except possibly NGC 1068, are known to be variable at other radio wavelengths (Kellermann and Pauliny-Toth 1971; MacLeod *et al.* 1971; Locke 1970; and Rather 1970).

The Observations

Equipment

The 90-GHz (3.3-mm) observations were made with the 15-ft (4.6-m) equatorially mounted antenna (Cogdell *et al.* 1970) of The Aerospace Corporation, located at an elevation of 40 m above sea level in El Segundo, California. For an RC time constant of 1 sec and an IF

bandwidth of 1.5 GHz, the rms output noise fluctuations of the crystal mixer were about 0.8 °K before February 1971 and about 0.25 °K after this date when several improvements of the radiometer were made. The most important of these was a widening of the bandpass of the receiver by a factor of approximately two. An antenna temperature of 0.1 °K corresponds to ≈ 40 flux units (1 f.u. = 10^{-26} W m^{-2} Hz^{-1}).

Observational Procedure and Data Reduction

A dual-beam system was used; it has two identical feed horns (with east-west polarization) mounted symmetrically east and west of the Cassegrain focus of the antenna with a corresponding separation on the sky of 18.'8. The separation was 24.'8 before May 18, 1970. The antenna half-power beamwidths are 3.'0. Each "observation" consisted of approximately 10 hours of integration, usually distributed over several days.

In the dual-beam observing procedure employed before March 1969, one of the beams was pointed at the object for an integration time of 75 sec. The output signal was a measure of the difference between the (sky + object) signal in one beam and the (sky) signal in the other beam. The other beam was then pointed at the object for 75 sec. Taking the difference of the two differences eliminated the unknown zero point in the signal scale and yielded a measure of the antenna temperature of the source. This two-step process was then repeated in the reverse sequence. This reversal tended to eliminate any linear (with time) drifts in the signal caused by variations in the receiver or the sky emission. In this observing procedure there was incomplete cancellation of the atmospheric emission and of the antenna sidelobe pickup of the ground and

atmosphere because the line losses of the two beams were unequal and because the two beams, being at slightly different zenith distances, measured slightly different amounts of atmospheric and ground emission.

An improved observing procedure (Dworetsky *et al.* 1969) was initiated in March 1969 in order to obtain nearly complete cancellation. In this later procedure each beam was alternately pointed at the position being observed. The duration in seconds of time of alternate halves of a pair of consecutive observations was equal to the beam separation in seconds of arc divided by 15 cos δ, so that the antenna traced out the same hour angle arcs during both halves of a pair. δ is the declination of the object being observed. Systematic effects due to differences in atmospheric and ground emission measured by the two beams were thereby cancelled, because in the data reduction a reading during one half of a pair was subtracted from the other.

In order to correct for the incomplete cancellation before March 1969, it is sufficiently accurate to assume that the atmosphere is a plane-parallel layer of uniform temperature. Near sea level much of the atmospheric emission at 90 GHz is produced by precipitable water vapor, which has a scale height of $\approx 1.6 \pm 0.2$ km (Stacey 1970). The emission of the atmosphere in terms of the antenna temperature, T_a^{atm}, measured by each antenna beam, has been calculated according to the equation,

$$T_a^{atm} = T_o(1 - e^{-\tau \sec z}), \qquad (1)$$

where T_o is the temperature of the atmosphere, which is taken to be 285 °K, z is the zenith distance of the object being observed, and τ is the optical depth of the atmosphere at the zenith and is the same value

used in the correction for atmospheric attenuation (described next). An empirical correction for incomplete cancellation of antenna sidelobe detection of the atmosphere and ground was determined from about 80 hours of observations of "blank" sky over ranges of declination and hour angle covered by our observations. These corrections for incomplete cancellation of atmospheric and ground emission have been applied to all the observations which were made before March 1969. The primary effect of these corrections has been to reduce the internal statistical uncertainty associated with each observation.

The corrections for daytime atmospheric attenuation have been determined from measurements of the apparent antenna temperatures of the sun. In addition, and for nighttime observations, the attenuation was calculated (before September 1968) from radiosonde measurements of atmospheric precipitable water vapor and an empirical relationship between the radiosonde measurements and the attenuation determined from solar observations (Shimabukuro and Epstein 1970). Since September 1968, the water vapor method has been replaced by a procedure involving measurements of differential atmospheric emission between the zenith and a direction with $z = 60°$ (Dworetsky *et al.* 1969):

$$\Delta T = T_o(1 - e^{-\tau \sec 60°}) - T_o(1 - e^{-\tau \sec 0°})$$

$$= T_o(e^{-\tau} - e^{-2\tau}). \qquad (2)$$

These so-called "dip" differences, ΔT, were empirically calibrated with the aid of τ values derived from simultaneous sun measurements. Figure 3 shows the empirical ΔT vs. τ relationship compared to one for a plane-parallel isothermal atmosphere at 290 °K and a perfect antenna with no

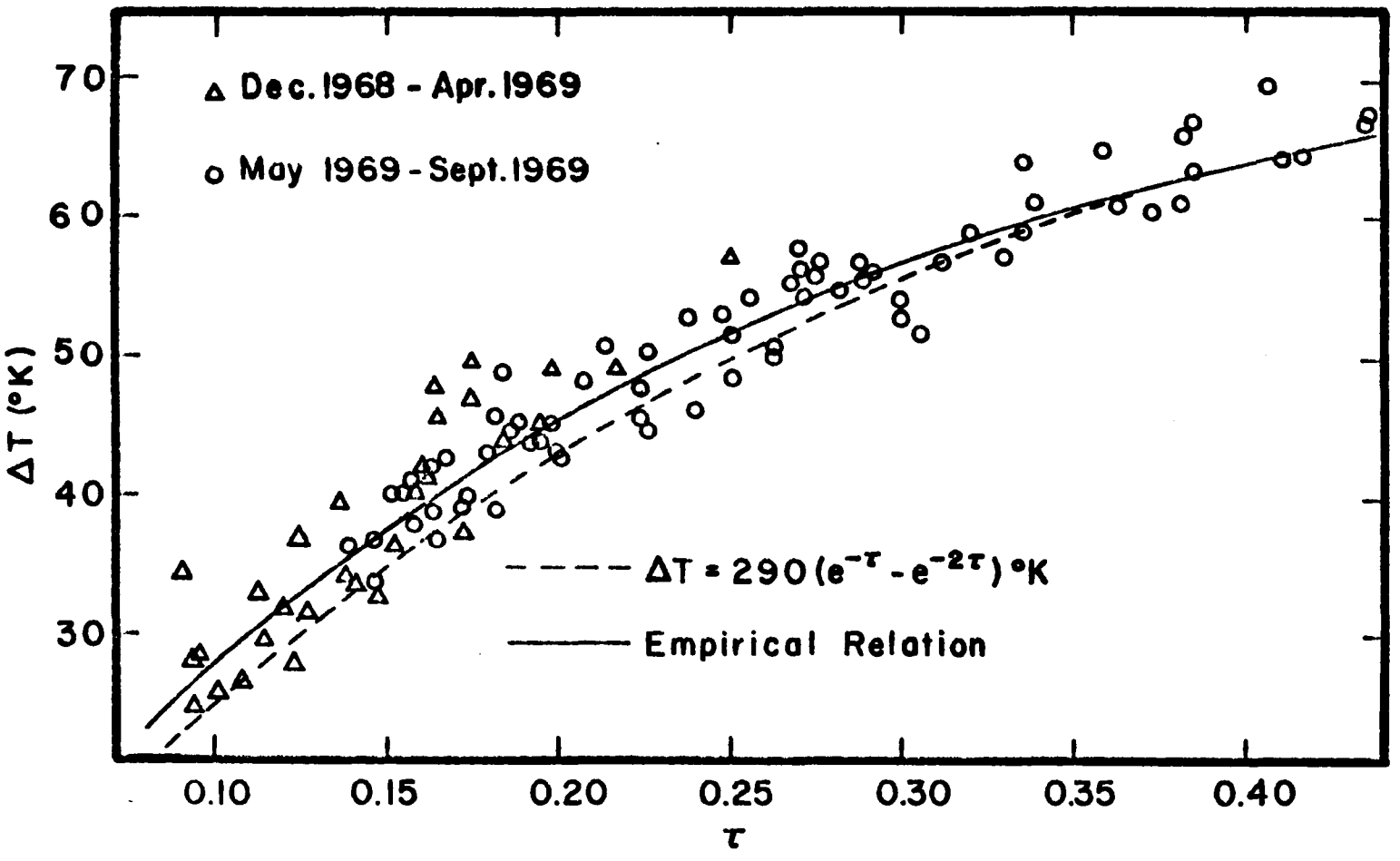

Figure 3. The ΔT vs. τ Relationship

Observed "dip" differences ΔT due to atmospheric emission vs. the 3.3-mm optical depth of the atmosphere determined by observing the sun

sidelobes. Measurements of ΔT, which were taken every two or three hours, were used both as absolute measures of τ and as an interpolation or extrapolation device when sun-derived τ's were also available in the same observing run. Dip τ's are more accurate than those derived from an empirical relationship between radiosonde measurements of precipitable water vapor and sun-derived τ's. The scatter of dip τ's is only about half as much as the scatter in radiosonde-derived τ's [compare Figure 3 with Figure 7 of Shimabukuro (1966) and Figure 3 of Shimabukuro and Epstein (1970)]. Dip measurements have two further advantages: they can be made as frequently as desired, and their results are immediately available. The estimated one-standard-deviation (1-σ) uncertainty of the corrections for attenuation for each observation, $\langle e^{\tau \sec z} \rangle$, is 3%. Typical values of τ at 3.3 mm ranged from 0.09 in winter to 0.35 in summer.

Most of the observations reported here were obtained when the sky was clear or almost clear of clouds. About 20% of the observations were made through thin ($\lesssim$ 300 m) stratus clouds or thin cirrus clouds, and about 15% of the observations were made through stratus or altocumulus layers between 300 m and 600 m thick. The observations were almost always restricted to zenith distances of less than 60°.

Shimabukuro (1966) has discussed the accuracy of the formula,

$$R_o = \frac{21.3}{T}\left(P + \frac{4810\ h\ P_w}{100\ T}\right)\tan z, \qquad (3)$$

used to correct for radio refraction. R_o is the refraction correction, T is the temperature of the atmosphere in °K, P is the pressure of the atmosphere, h is the % relative humidity, and P_w is the partial vapor

pressure of water. The pressures are in millimeters of mercury. The formula is generally accurate to 15" at zenith distances smaller than 70°. Antenna pointing corrections were determined a few times a day on an almost daily basis throughout each year by observing the opposite radio limbs of the sun in each coordinate. (These corrections were confirmed by observations at night of Jupiter and Venus.) These corrections are usually reproducible to ± 5" to 10" on a day-to-day basis. Small scaling factors (≃ 1.02 ± 0.02) were applied to the data to allow for small (≃ 5" to 10") residual antenna pointing errors (not corrected for while observing) and antenna jitter, which is typically ≲ 5".

A correction of the observed antenna temperatures was necessary for Cygnus A and Virgo A, which are not point sources to the 3' beams. A 2.7-GHz map and a 5-GHz map of the distribution of the brightness temperature of Cygnus A are shown in Figures 1 and 2, respectively, of Mitton and Ryle (1969). The distributions of the brightness temperature at 2.7 GHz and 5 GHz are quite similar to each other and also similar to the distributions of the brightness temperature at 408 MHz and 1.4 GHz measured by Macdonald, Kenderdine, and Neville (1968) and by Ryle, Elsmore, and Neville (1965), respectively. It was assumed here that the distribution of the brightness temperature at 90 GHz is similar to the distributions at the lower frequencies. The two main components of Cygnus A have been taken to have Gaussian distributions of brightness temperature with half-power diameters of 15" and a separation on the sky of 2'. It was assumed (for a further justification, see the last page of the later section of this chapter, Discussion) that the flux ratio at 90 GHz of the two components is the same as at 5 GHz. The observations

were made at the positions of the two main components and at the central position between the two components. The correction factor for Virgo A, 1.1, follows from the assumption that at 3 mm Virgo A has a Gaussian distribution of brightness temperature with a half-power diameter of $1\overset{'}{.}0$, a size inferred from the beam broadening measured by Mayer and McCullough (1971) at 1.65 cm, the shortest radio wavelength at which the size of Virgo A has been measured. [It should be noted, however, that Allen , Barrett, and Crowther (1968) derived a size of $0\overset{'}{.}5$ at 1.94 cm. If the 3-mm size of Virgo A is $0\overset{'}{.}5$, the correction factor, 1.03, is much smaller than for the size of $1\overset{'}{.}0$.]

The correction factors CF were calculated for the half-intensity diameters D of the sources and for the offset distance d under the assumption that the dual antenna beams could both be represented by Gaussian profiles with a half-power beamwidth of $3'$ according to equation (1) of Dworetsky *et al.* (1969):

$$CF = \left[\frac{1}{\pi a^2} \int_{-\infty}^{\infty} \int_{-\infty}^{\infty} e^{-\frac{x^2+y^2}{a^2}} e^{-\frac{(x-d)^2+y^2}{b^2}} \, dy \, dx \right]^{-1} . \quad (4)$$

In equation (4), a and b are parameters used to make the source and beam intensities one half of their center values at their respective half-power radii (a and D are proportional). The correction factors, equal to 1.1 for Virgo A, 1.38 at the center position of Cygnus A, 1.51 at the position of the eastern main component of Cygnus A, and 1.56 at the position of the western main component of Cygnus A, have been applied to the observations by multiplying the measured values of the flux by the correction factors. This corrected value of the measured flux is the

"integrated" total flux (for Cygnus A this "integrated" total flux is the integrated flux from both components of Cygnus A). The uncertainty in the correction factor, estimated from the uncertainty in the source positions and sizes, is 10%. The values listed in Table 3 are the corrected values, but the uncertainty in the correction factor is not included in the quoted uncertainty of the flux.

The uncertainty caused by possible confusion noise from unknown sources is very unlikely to be much greater than 0.01 f.u., which is much smaller than the internal uncertainties. This estimate is based on another estimate made by Kellermann, Pauliny-Toth, and Tyler (1968) of the confusion noise at 11.3 cm (having a value of 0.04 f.u.) and on the assumption that the spectra of any unknown sources are unlikely to be turned up sharply between 11 cm and 3 mm.

Because the east-west polarized antenna is equatorially mounted, there is a constant angle between the accepted polarization angle of the incoming radiation and the actual polarization angle of the incoming radiation if it is polarized. Therefore there can be no confusion of any possible time variability of the flux caused by detecting different polarization angles of the incoming radiation at different times.

Calibration

The calibration of the antenna gain was done with the aid of a standard gain horn and a transmitter in the antenna's far field; the estimated 1-σ uncertainty is $\approx$ 9%. The calibration of the antenna temperature scale is based on a semi-theoretical calculation of the antenna's diffractive efficiency over the solid angle subtended by the sun

and the value, 6600 ± 200 °K, for the 90-GHz brightness temperature of the quiet sun (Shimabukuro and Stacey 1968; Reber 1970). Before October 28, 1968, a secondary calibration was obtained about every 20 minutes from a gas discharge tube; it has since been obtained from a hot resistive load. Approximately twice a year the secondary calibration standard is checked against loads in liquid nitrogen and ice water. The estimated overall absolute calibration uncertainty is 10%. An approximate check on the calibration was provided by observations of Virgo A (see below).

System Checks

Because the observations reported here are absolute measurements, rather than measurements relative to standard sources, several checks on the calibration and performance of the system were performed.

1. Each observation is composed of from 20 to 40 antenna temperature measurements, each representing an integration time of about 20 minutes. It was verified that the histogram of the antenna temperatures in each observation resembles a Gaussian distribution and that the histogram width is consistent with the short-term noise characteristics of the radiometer, the major source of the overall system noise. Other possibly significant contributors to the measurement errors are the uncertainties in pointing, tracking, atmospheric emission and attenuation, confusion noise from unknown sources, and the corrections for extended sources, which are all discussed above. Other less quantitatively correctable effects include small unknown changes in

the system, both continuous and discontinuous, due to variations in the ambient temperature, system gain, and atmospheric conditions. These latter effects, if present and not rejected during the data reduction, are probably small (compared to the major causes of the overall measurement errors discussed above), probably occur on time scales of the order of an hour or less, and furthermore are taken into account by the observational procedure of accumulating the set of 20 to 40 antenna temperature measurements of about 20 minutes each from a total integration time span of about 10 hours spread over several days (usually about one week). This spreading out of the set of antenna temperature measurements will tend to make the variations which occur on a time scale of an hour or less appear to be random noise.

2. Frequent observations of "blank" sky were made in order to verify that the dual-beam procedures caused no systematic bias (see Figure 8 of Shimabukuro and Epstein 1970). The results of the observations of blank sky are discussed in more detail later in connection with the analysis of system noise and measurement errors and the results of the measurements of the flux of NGC 1068.

3. In October 1970, simultaneous observations of five sources were made at the 36-ft NRAO antenna at the Kitt Peak site (Wilson 1971) and at The Aerospace Corporation. The 36-ft data are indicated by the triangles in Figure 5. There is good agreement between the Aerospace and NRAO data.

4. Virgo A was observed in order to determine whether its measured flux agrees with the predicted value. This source was chosen because its 3-mm flux can be predicted with reasonable confidence by extrapolating the longer wavelength data, because the spectrum (Figure 4) is approximately linear, and because there is no evidence of variability. [See, however, Graham (1971) concerning the possibility that a small part of the flux might be variable.] The agreement between the extrapolation and the measurement at 90 GHz, 6.1 ± 0.5 f.u. (± 0.8 f.u. for the estimated total error), is satisfactory. The average flux, $\langle F_\nu \rangle$, shown in Figure 4 is the weighted mean of the individual observed fluxes, F_ν^i, weighted by the associated 1-σ uncertainties, σ_i, which are listed in Table 3:

$$\langle F_\nu \rangle = \frac{\sum_i \frac{F_\nu^i}{\sigma_i^2}}{\sum_i \frac{1}{\sigma_i^2}} . \qquad (5)$$

The standard deviation of the mean, σ_m, is given by

$$\frac{1}{\sigma_m^2} = \sum_i \frac{1}{\sigma_i^2} . \qquad (6)$$

[For a discussion and derivation of equations (5) and (6), see, for example, Hoel 1971, pp. 127-9.] The data for Cygnus A and Virgo A shown in Figure 4 have been taken from compilations by Baars, Mezger, and Wendker (1965) and Kellermann, Pauliny-Toth and Williams (1969). Other data were taken from Medd and Ramana

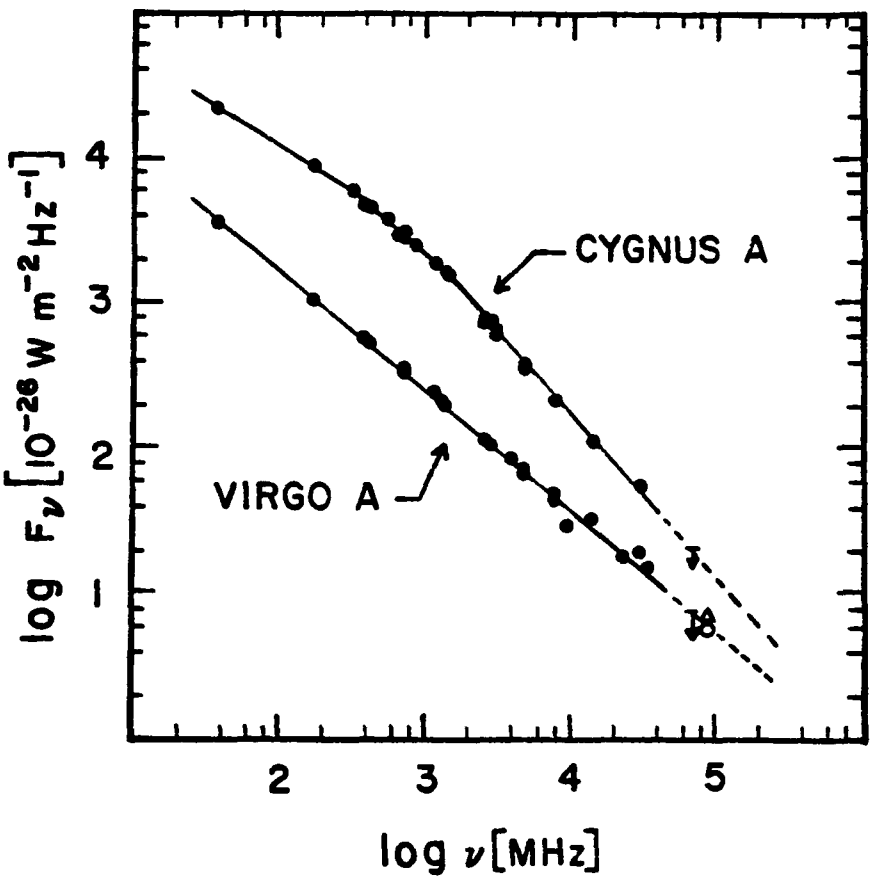

Figure 4. The Radio Spectra of Virgo A and Cygnus A

The 3.3-mm data are indicated by the open triangle for Cygnus A and by the open circle for Virgo A. References for the other data are cited in the text. The error bars of any of the points are comparable to or less than the size of the symbols. These 3.3-mm observations of Virgo A and Cygnus A replace the preliminary observations reported by Schorn *et al.* (1968). The dashed portions of these lines represent extrapolations from the longer wavelength radio data. We see that the 3.3-mm flux of Virgo A is in good agreement with the extrapolated value, but the 3.3-mm flux of Cygnus A is only one half of the extrapolated value.

(1967); Guidice (1966); Hobbs, Corbett, and Santini (1968,1969); Berge and Sielstad (1969); Mitton and Ryle (1969); and Rather (1970).

5. In order to check the repeatability of the measurements of sources which are presumed to be constant, Virgo A was observed frequently (see Table 3) and Saturn has been monitored (see Figure 2 of Epstein *et al.* 1970). The repeatability is quite good for both Virgo A and Saturn; that is, the scatter in the data is consistent with the 1-σ uncertainties. The consistency of the scatter in the data with the 1-σ uncertainties is discussed in more detail later in connection with the results shown in Tables 4 to 7. (Note that the data were taken during both winter and summer when the corrections for atmospheric attenuation were considerably different.)

On the assumption of the non-variability of Virgo A and Saturn, the consistency of the scatter in the data with the 1-σ uncertainties indicates that the observing procedures, long-term relative calibration, corrections for atmospheric attenuation, refraction, and pointing errors, and uncertainty estimates are satisfactory.

Results

Table 3 contains the results of observations of nine extragalactic sources for which only a few observations of each were made. The name of the source is given above the data. Column 1 contains the inclusive dates (month/date/year) of the observations. In column 2 the flux, F_ν^i, and the one-standard-deviation statistical uncertainty, σ_i,

Table 3. The 90-GHz Flux Measurements[a]

Dates	$F_\nu \pm \sigma$	Dates	$F_\nu \pm \sigma$
NGC 4151		Virgo A	
Sep/2-26/68	-2.1 ± 2.7	Dec/2/67-Jan/23/68	7.4 ± 2.8
Nov/26-Dec/2/68	0.9 ± 1.8	Jun/19-Jul/23/68	8.6 ± 2.2
		Aug/31-Sep/20/69	2.0 ± 2.6
OQ 208		Sep/22-27/69	5.7 ± 2.8
Jan/1-21/68	30.9 ± 14.7	Sep/28-Oct/1/69	7.0 ± 2.1
Nov/24-Dec/27/69	10.8 ± 7.8	Oct/3-10/69	6.1 ± 2.5
Jan/1-Feb/2/70	-5.0 ± 1.9	Aug/7-18/71	6.3 ± 1.0
Aug/8-16/70	-1.4 ± 2.1	Aug/30-Sep/5/71	5.8 ± 0.8
4C 39.25		$\langle F_\nu \rangle \pm \sigma_m$	6.1 ± 0.5 (± 0.8)
Nov/11-Dec/1/67	3.2 ± 8.1		
Jan/14-18/68	-5.4 ± 2.6		
Feb/2-29/68	8.9 ± 5.2	Cygnus A	
Apr/9-11/68	0.8 ± 4.2	May/18-23/68	8.9 ± 4.7
		May/23-Jul/17/68	9.7 ± 3.1
3C 380		Sep/12-Dec/29/68	10.3 ± 3.2
Oct/18-22/68	1.0 ± 2.1	May/30-Jun/18/70	3.0 ± 3.5
Aug/8-13/70	3.4 ± 2.2	Jun/19-24/70	7.3 ± 3.9
		Jun/25/29/70	8.9 ± 3.0
PKS 2134+00		Jul/3-11/70	5.3 ± 2.7
Jan/6-20/68	-0.8 ± 3.4	Sep/5-10/70	8.8 ± 2.5
Aug/9-12/70	-3.5 ± 2.3	Sep/20-26/70	3.3 ± 2.2
3C 371		$\langle F_\nu \rangle \pm \sigma_m$	7.9 ± 1.0 (± 1.3)
Oct/14-24/69	4.7 ± 2.1		
Oct/25-Nov/2/69	-1.6 ± 4.5		
Dec/2-26/69	-0.3 ± 3.7		
Aug/5-7/70	0.7 ± 1.8		
M 82			
Mar/27-31/69	0.8 ± 1.8		

[a] In units of 10^{-26} W m^{-2} Hz^{-1}

(in flux units) are listed. The uncertainty is calculated from the scatter in the set of 20-minute samples making up each observation and from the uncertainty in the corrections for pointing and attenuation. The 10% uncertainty in the correction for extended sources (where applicable) and the 10% uncertainty in the overall absolute calibration are not included here. Column 2 also contains the weighted average flux and the standard deviation of the mean for Virgo A and Cygnus A. The calculation of the weighted mean, together with its uncertainty, has been described earlier in equations (5) and (6). The 10% uncertainty in the correction made for extended sources and the 10% uncertainty in the overall absolute calibration are included in the uncertainty (shown in parentheses) of the weighted mean for Virgo A and Cygnus A.

Figures 5 and 6 display the results of extensive monitoring of seven objects which are, or may be, time varying. These sources have been described at the beginning of this chapter. Figure 5 contains the observations made before December 1970, while Figure 6 contains the results obtained since February 1971. This separation of the results was made because of the significant difference in the observational uncertainties before and after February 1971 (due to significant improvements in the sensitivity of the receiver, as described above). The errors indicated in Figures 5 and 6 are computed in the same way as those given in column 2 of Table 3 and represent 1-σ statistical uncertainties. In Figure 5 the size of the error is indicated by the vertical lines through the point (the lack of an error bar indicates that the 1-σ error is comparable to or less than the size of the dot), while in Figure 6 the error is indicated by the size of the open circle.

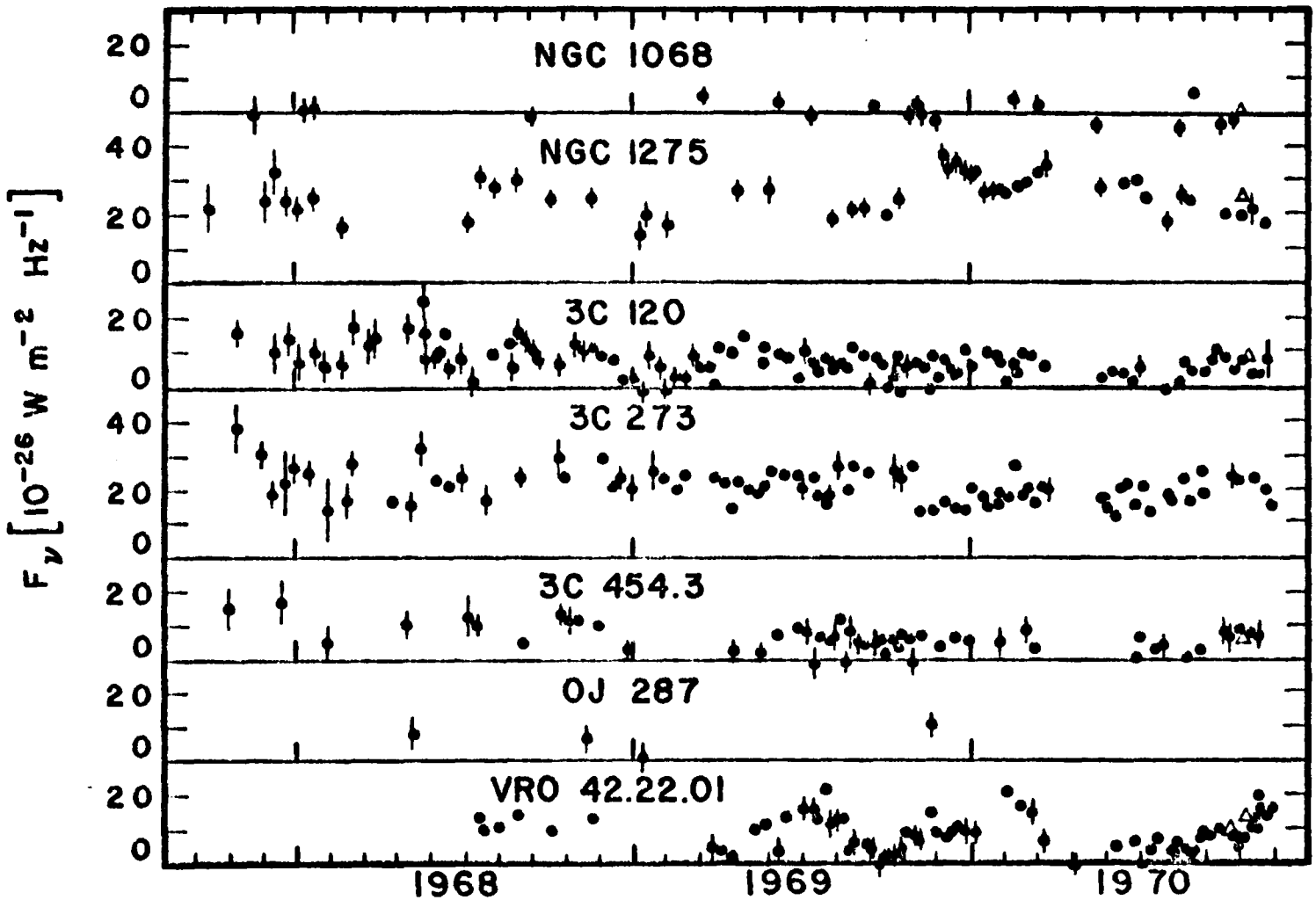

Figure 5. The 90-GHz Flux vs. Time Curves of the Monitored Sources Discussed in the Text

The error bars indicate 1-σ relative uncertainties. The open triangles (October 1970) represent observations made by Wilson (1970) with the NRAO 36-ft antenna.

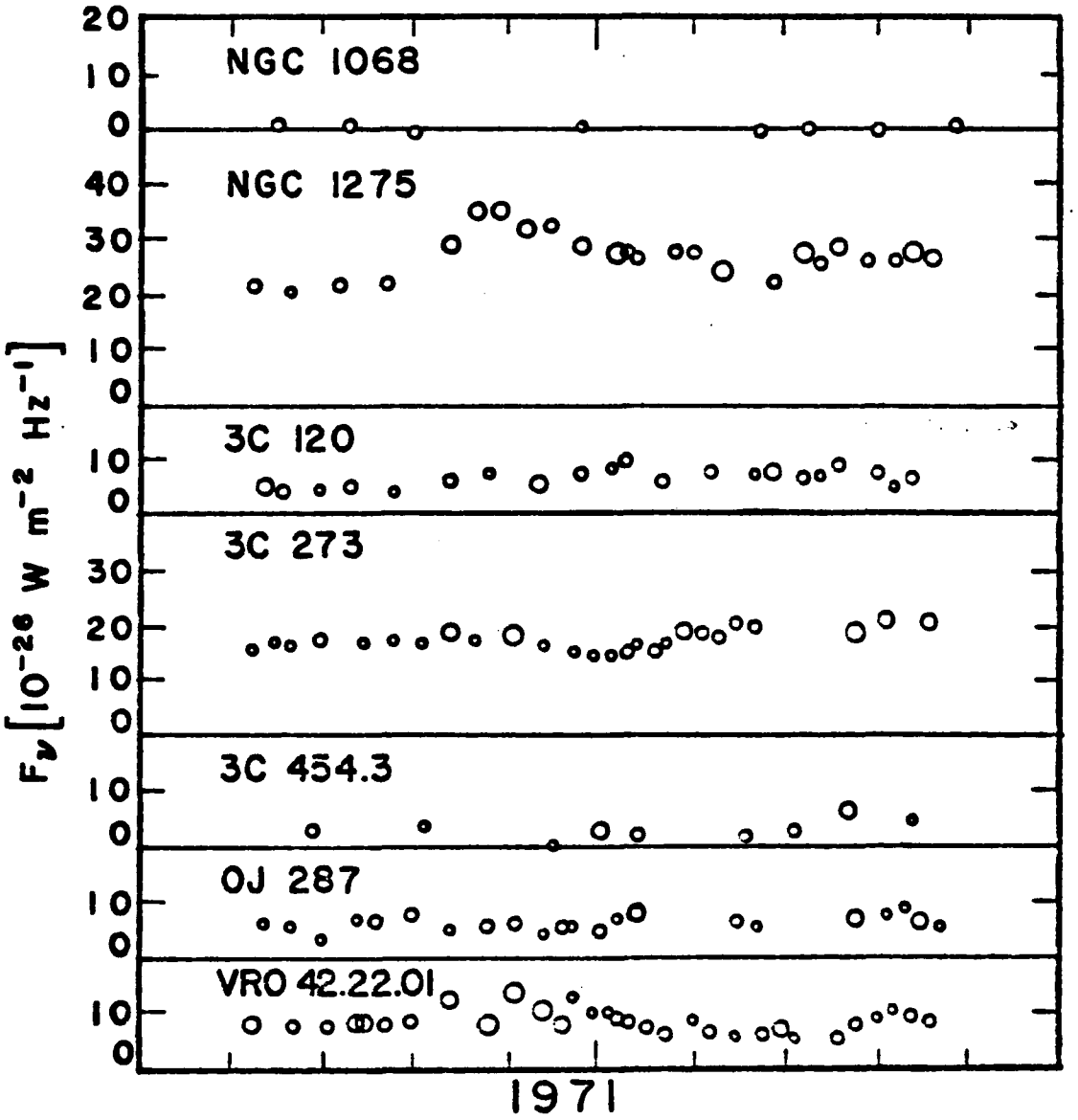

Figure 6. The 90-GHz Flux vs. Time Curves with Improved Sensitivity

The radius of the open circle indicating each data point is equal to the 1-σ relative uncertainty of the measurement.

Discussion

An inspection of Figures 5 and 6, illustrating the flux measurements of the seven monitored sources, together with their 1-σ error bars, might enable one to see whether those sources have been detected and whether or not the flux is variable with time. It is not clear from this inspection that NGC 1068 has been detected; but for the other six sources, it is quite clear that they have been detected and that variability of the flux with time occurs.

It is also possible to make some statistical calculations concerning the certainty of the detection of the flux and the probability of the flux being variable with time. In this section no fundamental relationships or quantities of statistics are derived, proved or explained in any great detail. Such quantities as distribution functions, variances, and confidence intervals are discussed in sufficient detail in any elementary textbook on statistics and probability, for example, Hoel (1971).

In the first two parts of this section we shall consider the two usual major areas of statistical inference. The first area is concerned with the estimation of parameters by means of a sample of measurements and the second area is concerned with the significance of the measured parameters. In this section we will be estimating and then testing the significance of the variance.

Estimate of the Variance of Monitored Sources

Consider the measurements, x_{ij}, of a variable X to be normally distributed with mean μ and variance σ^2. The sample variance is

$$s_1^2 = \frac{1}{N} \sum_{i=1}^{k} \sum_{j=1}^{n_i} (x_{ij} - \bar{x})^2 \ , \tag{7}$$

where the sample mean is given by

$$\bar{x} = \frac{1}{N} \sum_{i=1}^{k} \sum_{j=1}^{n_i} x_{ij} = \frac{1}{N} \sum_{i=1}^{k} n_i \bar{x}_i \ , \tag{8}$$

and where

$$N = \sum_{i=1}^{k} n_i \ . \tag{9}$$

The subscripts i and j refer to the manner in which the measurements are acquired. The total of N measurements are grouped into k samples of sizes n_i. The subscript i refers to the ordering of the samples, and the subscript j refers to the ordering of the measurements within each sample. The random variable s_1^2 does not take into account the order of the measurements, but treats each measurement as independent and of equal weight. This estimate, s_1^2, of the population variance, σ^2, will be referred to as a long term estimate. If the x_{ij} are normally distributed with mean μ and variance σ^2, it can be shown (Hoel, p. 254) that the random variable, $N\, s_1^2/\sigma^2$, has a χ^2 distribution with N - 1 degrees of freedom. This statement can be written in the notation:

$$\text{if } x_{ij} \text{ are } N[\mu,\sigma^2] \text{ and independent,}$$

$$\text{then } \frac{N\, s_1^2}{\sigma^2} \text{ is } \chi^2[N-1] \ . \tag{10}$$

We can calculate a confidence interval of percentage 100P on the variance σ^2 in the usual manner:

$$a_1 \equiv \frac{N s_1^2}{\chi^2_{(1-P)/2}} \leq \sigma^2 \leq \frac{N s_1^2}{\chi^2_{(1+P)/2}} \equiv b_1 \ . \tag{11}$$

The meaning of the confidence interval is given by the following: we can state with 100P percent confidence that the unknown parameter σ^2 lies in the interval (a_1,b_1).

Since the measurements, x_{ij}, of the variable X are grouped into k samples of sizes n_i, we can obtain another estimate of the population variance. For the i-th sample we can write the sample mean and sample variance as

$$\bar{x}_i = \frac{1}{n_i} \sum_{j=1}^{n_i} x_{ij} \ , \tag{12}$$

$$s_i^2 = \frac{1}{n_i} \sum_{j=1}^{n_i} (x_{ij} - \bar{x}_i)^2 \ . \tag{13}$$

An unbiased estimate of the i-th sample variance is given by

$$\sigma_{ei}^2 = \frac{1}{n_i - 1} \sum_{j=1}^{n_i} (x_{ij} - \bar{x}_i)^2 \ , \tag{14}$$

while the random variable

$$\frac{n_i s_i^2}{\sigma^2} = \frac{(n_i - 1)\sigma_{ei}^2}{\sigma^2} \quad \text{is} \quad \chi^2[n_i - 1] \tag{15}$$

It can be shown (Hoel, p. 253) that the sum of several independent χ^2 variables, V_i, each with ν_i degrees of freedom, is itself a χ^2 variable with the number of degrees of freedom given by the sum over ν_i; that is,

$$\text{if} \quad V_i \quad \text{are} \quad \chi^2[\nu_i] \quad \text{and independent,}$$

$$\text{then} \quad \sum_i V_i \quad \text{is} \quad \chi^2[\sum_i \nu_i] \ . \tag{16}$$

Since successive values of $(n_i - 1)\sigma_{ei}^2/\sigma^2$ are independent χ^2 variables with $n_i - 1$ degrees of freedom,

$$\sum_{i=1}^{k} \frac{(n_i - 1)\sigma_{ei}^2}{\sigma^2} \text{ is } \chi^2[\sum_{i=1}^{k} (n_i - 1)] \ . \tag{17}$$

If we define a weighted mean of the unbiased sample variances by

$$<\sigma_{ei}^2> \equiv \frac{1}{N} \sum_{i=1}^{k} (n_i - 1)\sigma_{ei}^2 \ , \tag{18}$$

then we can write equation (17) in the form,

$$\frac{N<\sigma_{ei}^2>}{\sigma^2} \text{ is } \chi^2[N-k] \ . \tag{19}$$

The random variable $<\sigma_{ei}^2>$ takes into account the ordering of the measurements according to time by grouping into samples of size n_i. Since each σ_{ei}^2 is calculated from measurements made over a time short compared to the time required to make all of the measurements, $<\sigma_{ei}^2>$ will be called a short term estimate of the population variance σ^2. We can now calculate another confidence interval of percentage 100P on the population variance in a manner similar to equation (11):

$$a_s \equiv \frac{N<\sigma_{ei}^2>}{\chi^2_{(1-P)/2}} \leq \sigma^2 \leq \frac{N<\sigma_{ei}^2>}{\chi^2_{(1+P)/2}} \equiv b_s \ ; \tag{20}$$

that is, we can state with 100P confidence that the unknown parameter σ^2 lies in the interval (a_s, b_s).

We now have two methods of estimating the population variance σ^2, a long term estimate and a short term estimate, s_1^2 and $<\sigma_{ei}^2>$, respectively. If both methods estimate the same parameter, the two

estimates should agree to within their statistical uncertainties; that is, the two confidence intervals, (a_l, b_l) and (a_s, b_s), should overlap. If, however, the mean of the measurements is not constant in time from sample to sample, the long term estimate of σ^2 will be increased compared to the short term estimate. If the mean varies on a time scale shorter than the time required to complete the measurements of one sample, both estimates of σ^2 will be increased. Therefore the lack of agreement of the two estimates of σ^2 is an indication that the basic variable, X, varies on a time scale greater than the time required to complete one sample and less than the time required to complete all the measurements. We can interpret the comparison of the two confidence intervals in the following way: if P is chosen such that the two 100P percent confidence intervals do not overlap, then either an event of probability less than $(1 - P)/2$ has occurred or the hypothesis that the x_{ij} have a time-independent distribution, $N(\mu,\sigma^2)$, is false. We can pick a value of P for which, if the two 100P percent confidence intervals do not overlap, we will reject at the $(1 - P)/2$ significance level the hypothesis that μ and σ are constant. In the application of this test we shall choose P = .95 since this gives a sufficiently high significance level (2.5%) to decide whether to accept or reject the hypothesis.

Although the above estimates of σ^2 are rigorously correct, there is a drawback in trying to draw conclusions about the variability of the mean from these two estimates. The test does not have sufficient sensitivity (unless the number of measurements is much larger than in the

cases discussed here) to assign a highly significant rejection of the implied hypothesis that the mean is constant unless the overall change in the mean is comparable to the standard deviation σ. This drawback is related to the fact that the parameter being estimated investigates the behavior of the individual measurements since all ordering of the measurements is ignored in the calculation of s_1^2, whereas the desired test should investigate the behavior of the means of the samples of measurements.

There is another method of estimating the population variance. This third estimate is called a long term estimate because the determination involves using the scatter of the sample means about the long term, or overall, average. We can define a sample variance, s_2^2, by

$$s_2^2 = \frac{1}{k} \sum_{i=1}^{k} n_i \, (\bar{x}_i - \bar{\bar{x}})^2 \, . \tag{21}$$

It can be shown (see Cramér 1945, pp. 537-8) that $k\, s_2^2/\sigma^2$ has a χ^2 distribution with $k - 1$ degrees of freedom:

$$\frac{1}{\sigma^2} \sum_{i=1}^{k} n_i \, (\bar{x}_i - \bar{\bar{x}})^2 \quad \text{is} \quad \chi^2[k-1] \, . \tag{22}$$

We can show that s_2^2 is an estimate of the variance σ^2 by considering the expectation value of s_2^2:

$$\begin{aligned} E[s_2^2] &= E\left[\frac{1}{k} \sum_{i=1}^{k} n_i (\bar{x}_i - \bar{\bar{x}})^2\right] \\ &= \\ &= \frac{1}{k} \sum_{i=1}^{k} n_i \, E[(\bar{x}_i - \bar{\bar{x}})^2] \\ &= \frac{1}{k} \sum_{i=1}^{k} n_i \left\{ E[(\bar{x}_i - \mu)^2] - E[(\bar{\bar{x}} - \mu)^2] \right\} \end{aligned}$$

$$E[s_2^2] = \frac{1}{k}\sum_{i=1}^{k} n_i\left(\frac{\sigma^2}{n_i} - \frac{\sigma^2}{N}\right)$$

$$= \frac{k-1}{k}\sigma^2 \ . \tag{23}$$

The corresponding unbiased estimate of σ^2 is then given by

$$\sigma_{e_2}^2 = \frac{1}{k-1}\sum_{i=1}^{k} n_i(\bar{x}_i - \bar{\bar{x}})^2 \ . \tag{24}$$

We can now calculate another confidence interval of percentage 100P on the population variance σ^2 in a manner similar to equation (11):

$$a_2 \equiv \frac{k\, s_2^2}{\chi^2_{(1-P)/2}} \leq \sigma^2 \leq \frac{k\, s_2^2}{\chi^2_{(1+P)/2}} \equiv b_2 \ ; \tag{25}$$

that is, we can state with 100P percent confidence that the unknown parameter σ^2 lies in the interval (a_2, b_2).

Following equation (20), we have discussed the significance of the agreement, or lack thereof, between the short term, $\langle\sigma_{ei}^2\rangle$, and long term, s_1^2, estimates of σ^2 with respect to the constancy of the mean of all the measurements. All of the comments made there are relevant to the agreement, or lack thereof, between the short term, $\langle\sigma_{ei}^2\rangle$, and long term, s_2^2, estimates of σ^2 , except that the comparison of these latter two estimates is a more sensitive indicator of a non-constant mean.

We should indicate here that the value of χ^2 for a given percentage level P and number of degrees of freedom ν is obtained from statistical tables such as Abramowitz and Stegun (1964) for the values of P and ν for which χ^2 is tabulated. If ν is very large ($\gtrsim 100$), the value of χ^2 can be obtained from a standard normal distribution in the

following way. A given percentage $P(y_1)$ of the normal distribution, $f(y)$, is included between the normal deviates, $\pm y_1$. For the χ^2 distribution it is a good approximation for large ν that the given percentage P is included between the deviates, $\pm y_1$, of the normal distribution,

$$P[\chi^2] = P[y_1] \ , \tag{26}$$

where in this case y_1 is given in terms of χ^2 and ν by

$$y_1 = \sqrt{2\ \chi^2} - \sqrt{2\nu - 1} \ . \tag{27}$$

In particular, for a given P we determine y_1 from the standard normal distribution; and for this value of y_1, together with the value of ν, we can determine the values of $\chi^2_{(1-P)/2}$ and $\chi^2_{(1+P)/2}$.

We now wish to apply the above statistics results to the data concerning the monitored sources shown in Figures 5 and 6 in order to estimate the population variance, σ^2. In this application the $\bar{x}_i$ and $\sigma_{ei}/\sqrt{n_i}$ of the above discussion correspond to the $F_\nu{}^i$ and σ_i, respectively, shown in Figures 5 and 6. The x_{ij} correspond to the raw data (not presented in this dissertation). They are the antenna temperature measurements (described in the section discussing antenna system check), each representing an integration time on the source of about 20 minutes bracketed by about 3 minutes of calibration time. These measurements are also referred to as cycles or cycles of observations. The sets of from 20 to 40 cycles or measurements are referred to as sets, samples, groups, or observations, depending on the context of the discussion.

The three estimates of σ^2, together with their 95% confidence intervals, have been calculated according to equations (7), (11), (18),

(20), (21), and (25). The results of these calculations, presented in Tables 4 and 5, refer to the observations presented in Figures 5 and 6, respectively. As explained in the previous section, this separation of the results was made because of the significant difference in the precision of the measurements before and after February 1971. Table 4 does not use all of the observations shown in Figure 5 because of the apparently greater system noise in the early part of the period of October 1967 to November 1970. Only the observations made between April 1968 and November 1970 are included in the results of Table 4. This beginning date was chosen because the observations appear to have more uniform uncertainties and because a change in the observing procedure, which may have contributed to the improved system noise, was made near that date. This change was described earlier in connection with the discussion of the observing procedure. For comparison, Table 4 contains the results of these same calculations from the measurements of Virgo A and Cygnus A from Table 3, and Table 5 contains the results of two sets of Virgo A; but the comparison should be made with caution since the values of k for these two sources are much smaller than for the seven monitored sources. The comparison is suggested because (as discussed earlier) Virgo A and Cygnus A are believed to be non-variable radio sources. Table 5 contains all the results shown in Figure 6.

In the case of NGC 1068, Table 4 gives the results determined from all of the samples between December 1966 and November 1970. These samples include all of those shown in Figure 5 plus two measurements reported previously by Fogarty *et al.* (1971), 10.5 ± 3.2 f.u. in December 1966 and 9.1 ± 3.5 f.u. in January 1967. The statistical results

Table 4. Confidence Intervals on σ of Monitored Sources Before 1971[a]

Source	N	k	$\bar{x} \pm \frac{s_1}{\sqrt{N-1}}$	$\sqrt{\langle\sigma_{ei}^2\rangle}$	s_1	s_2
NGC 1068*	713	21	1.9 ± 0.6	15.7 $^{16.8}_{15.1}$	16.2 $^{17.1}_{15.4}$	23.0 $^{34.1}_{18.1}$
NGC 1068	505	16	0.8 ± 0.6	12.4 $^{13.5}_{11.9}$	12.7 $^{13.6}_{12.0}$	16.1 $^{25.7}_{18.1}$
NGC 1275	947	42	25.7 ± 0.4	12.1 $^{13.0}_{11.8}$	13.3 $^{14.0}_{12.7}$	27.1 $^{35.0}_{22.6}$
3C 120	2528	106	7.3 ± 0.3	12.9 $^{13.5}_{12.7}$	13.6 $^{14.0}_{13.2}$	21.8 $^{25.5}_{19.3}$
3C 273	1850	78	21.8 ± 0.3	12.5 $^{13.2}_{12.3}$	13.4 $^{13.8}_{13.0}$	23.6 $^{28.2}_{20.5}$
3C 454.3	1204	50	6.6 ± 0.4	13.2 $^{14.1}_{12.9}$	13.7 $^{14.4}_{13.3}$	18.9 $^{23.8}_{15.9}$
OJ 287	101	4	6.4 ± 1.9	19.1 $^{22.9}_{17.1}$	19.5 $^{22.9}_{17.2}$	20.8 $^{89.5}_{13.6}$
VRO 42.22.01	1709	69	9.1 ± 0.3	12.4 $^{13.1}_{12.2}$	13.5 $^{14.0}_{13.1}$	27.1 $^{32.8}_{23.4}$
Virgo A	191	6	6.5 ± 1.1	14.3 $^{16.3}_{13.2}$	14.5 $^{16.4}_{13.3}$	12.1 $^{32.5}_{8.3}$
Cygnus A	252	9	7.9 ± 1.1	17.2 $^{19.3}_{16.1}$	17.4 $^{19.5}_{16.2}$	12.0 $^{24.3}_{8.6}$

[a] Columns 4 to 7 are given in units of 10^{-26} W m^{-2} Hz^{-1}

Table 5. Confidence Intervals on σ of Monitored Sources During 1971[a]

Source	N	k	$\bar{x} \pm \frac{s_1}{\sqrt{N-1}}$	$\sqrt{\langle\sigma_{ei}^2\rangle}$	s_1	s_2
NGC 1068	221	9	-0.1 ± 0.3	$4.8^{5.4}_{4.5}$	$4.8^{5.4}_{4.4}$	$3.3^{6.6}_{2.3}$
NGC 1275	639	26	27.1 ± 0.3	$5.9^{6.4}_{5.7}$	$7.0^{7.5}_{6.7}$	$19.4^{27.4}_{15.5}$
3C 120	576	23	6.3 ± 0.2	$4.5^{4.8}_{4.3}$	$4.7^{5.0}_{4.5}$	$8.3^{12.0}_{6.6}$
3C 273	724	29	17.6 ± 0.2	$5.0^{5.3}_{4.8}$	$5.3^{5.6}_{5.0}$	$9.5^{13.0}_{7.6}$
3C 454.3	236	10	3.3 ± 0.3	$4.5^{5.1}_{4.2}$	$4.7^{5.2}_{4.4}$	$7.5^{14.5}_{5.5}$
OJ 287	636	26	6.8 ± 0.2	$4.5^{4.9}_{4.4}$	$4.9^{5.2}_{4.6}$	$9.3^{13.0}_{7.4}$
VRO 42.22.01	842	35	8.1 ± 0.2	$4.7^{5.1}_{4.6}$	$5.2^{5.5}_{5.0}$	$10.8^{14.3}_{8.9}$
Virgo A	55	2	6.1 ± 0.6	$4.7^{6.0}_{4.0}$	$4.7^{6.0}_{4.0}$	$1.9^{11.7}_{1.2}$

[a] Columns 4 to 7 are given in units of 10^{-26} W m^{-2} Hz^{-1}

referring to all of the measurements made before November 1970 are indicated by the use of an asterisk after the source name, that is, by NGC 1068*. Where there is no asterisk after the name of the source, the results do not include data obtained before April 1968. This convention will also be used later in Tables 6 and 8 and Figure 7. We should emphasize that the results of NGC 1068* must be interpreted with caution or scepticism since they mix together results from times when the system noise was different. Nevertheless, they probably give some indication of what was really occurring with regard to the flux of NGC 1068 as a function of time.

In both Tables 4 and 5 column 1 gives the name of the source. Columns 2 and 3 contain the total number of individual measurements or cycles, N, and the number of sets or samples, k, respectively. The mean of all of the individual cycles, $\bar{x}$, and the one-standard-deviation uncertainty of the mean, $s_1/\sqrt{N-1}$, are given in column 4. Columns 5, 6, and 7 contain the short term, $\sqrt{\langle\sigma_{ei}^2\rangle}$, the long term, s_1, and the long term, s_2, estimates of the population standard deviation, σ, the square root of the variance, together with their 95% confidence intervals, respectively. The limits of the 95% confidence intervals on the estimates of σ are indicated by the small numbers to the right and above and below the estimates of σ. The values of the means and of the estimates of the standard deviation are all given in flux units.

The certainty of the detection of the flux of the monitored sources is indicated by the ratio, $\bar{x}\sqrt{N-1}/s_1$, commonly referred to as the signal-to-noise ratio. The detection is 97.5% certain when this ratio is 2 and 99.8% certain when the ratio is 3. The significance

level of the detection determined by the observed signal-to-noise ratio is found from the Student's t distribution. [For a discussion of the properties and applications of the Student's t distribution, see Hoel (1971), pp. 257-69.] Therefore we have certainly detected all the objects in Tables 4 and 5, except possibly NGC 1068. That we have detected NGC 1068 is not clear from Tables 4 and 5 alone. NGC 1068 was not detected with certainty by the measurements made in 1971. The certainty of the detection of NGC 1068 is somewhat greater than 99% if all the observations made before 1971 (NGC 1068*) are included (this estimate of the certainty is only approximate and must be interpreted with caution because the results contain observations made at times when the system noise was not constant), whereas the certainty of detection falls to 83% if only the measurements made between April 1968 and November 1970 are included. The results of the measurements of NGC 1068 will be discussed in more detail later in this chapter in a separate section.

We have explained above [following equations (20) and (25)] that the detection of variability is indicated by the lack of agreement between the long term, s_2^2, and the short term, $\langle\sigma_{ei}^2\rangle$, estimates of the population variance (or of the population standard deviation). The three estimates of the standard deviation σ, together with their 95% confidence intervals from the values in Tables 4 and 5 are presented in Figures 7 and 8, respectively. Note that the confidence interval on s_2 is much larger than the confidence intervals on s_1 and on $\sqrt{\langle\sigma_{ei}^2\rangle}$ because the number of degrees of freedom of the χ^2 variable associated with s_2^2 is much smaller (and therefore the estimate is much less certain) than the number of degrees of freedom for the other two associated χ^2

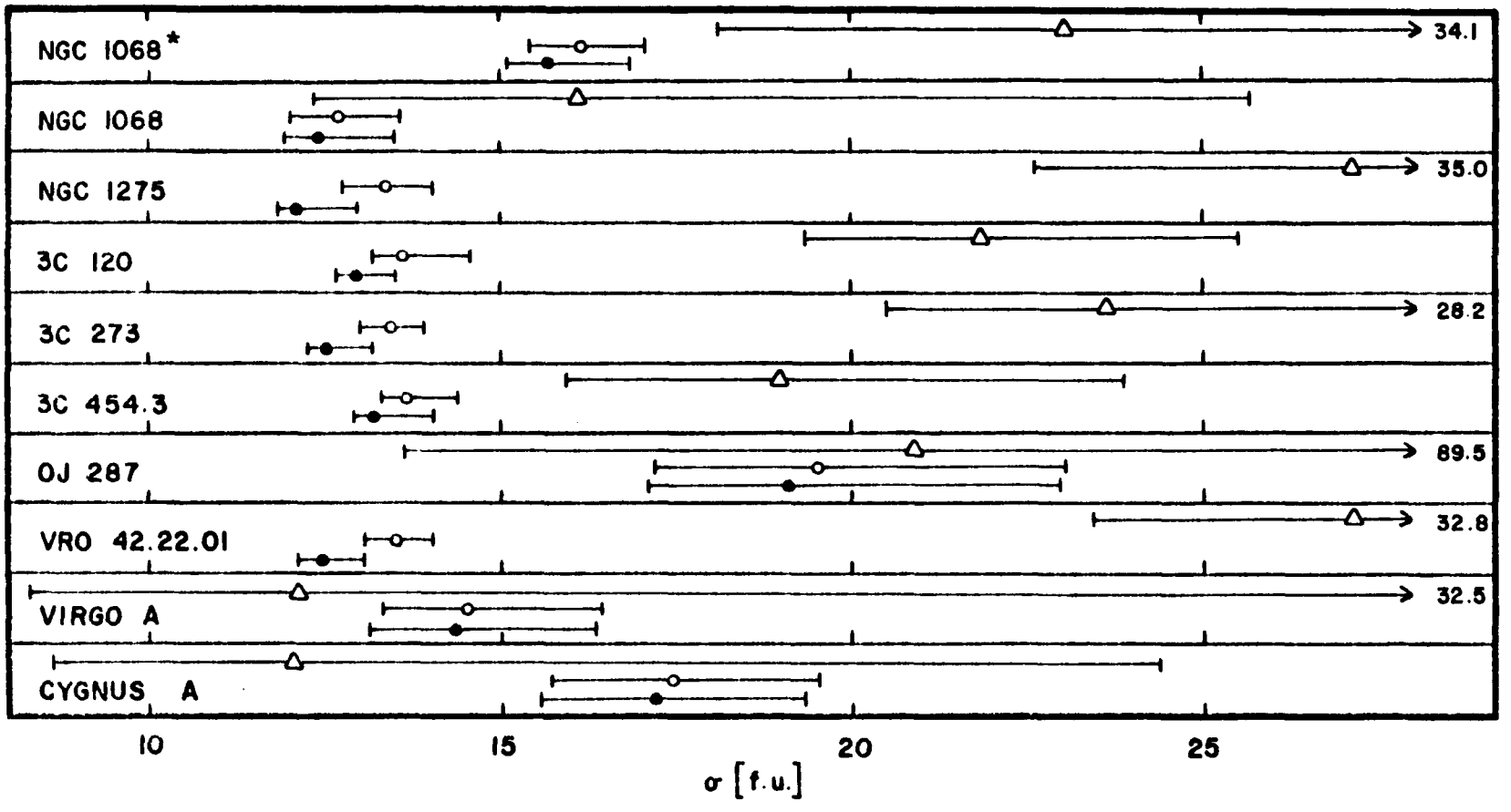

Figure 7. Long Term and Short Term Estimates of the Standard Deviation Before 1971

The uncertainty of the estimates of σ are indicated by the 95% confidence intervals for both long term estimates, s_1 (⊢—○—⊣) and s_2 (⊢—△—⊣), and the short term estimate, $\sqrt{\langle \sigma_{ei}^2 \rangle}$ (⊢—●—⊣).

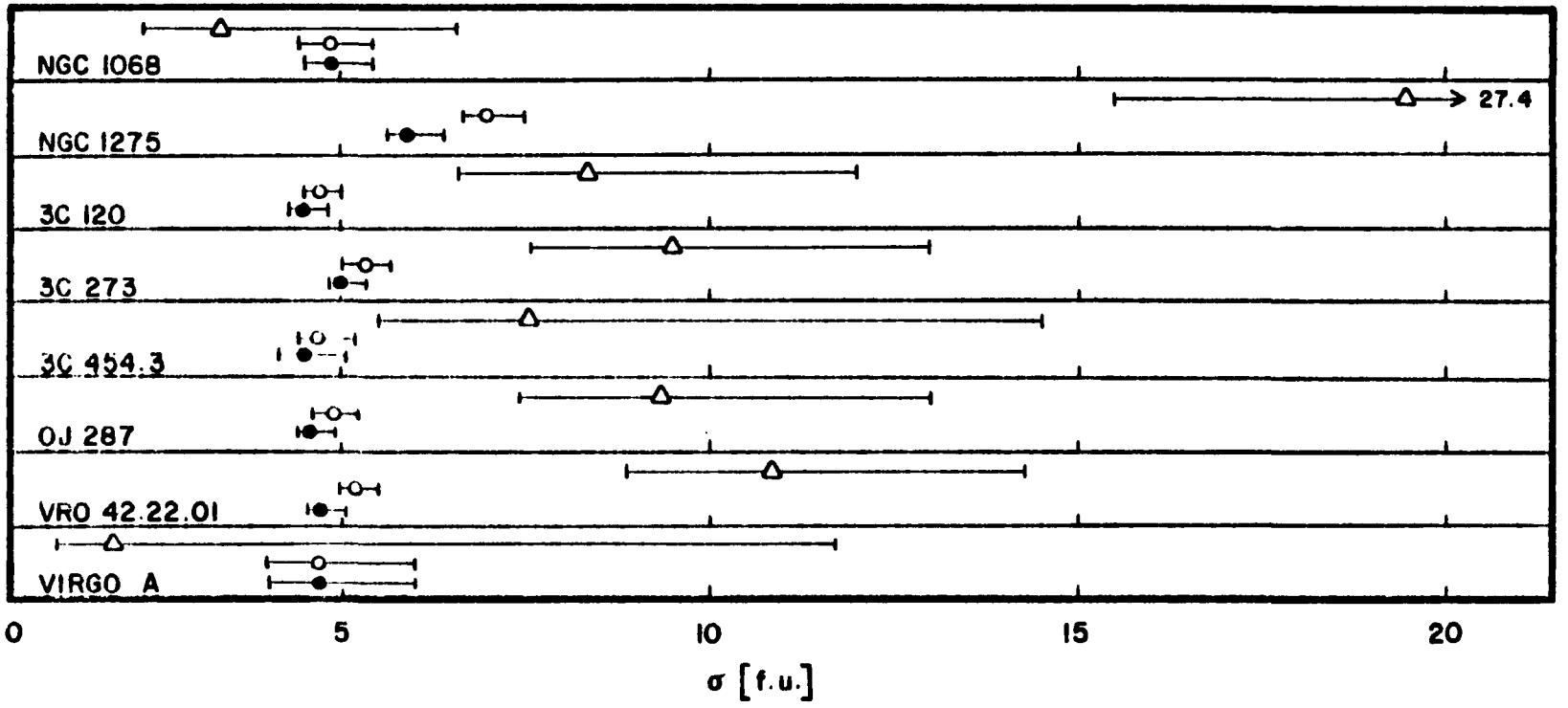

Figure 8. Long Term and Short Term Estimates of the Standard Deviation During 1971

The uncertainty of the estimates of σ are indicated by the 95% confidence intervals for both long term estimates, s_1 (⊢—○—⊣) and s_2 (⊢—△—⊣), and the short term estimate, $\sqrt{\langle \sigma_{ei}^2 \rangle}$ (⊢—●—⊣).

variables. There seems to be a significant lack of agreement between the two estimates, s_2^2 and $\langle\sigma_{ei}^2\rangle$, for all of the monitored sources except NGC 1068 (and 0J 287 before 1971 and possibly 3C 454.3 during 1971), implying that all except NGC 1068 (and, of course, Virgo A and Cygnus A) are likely to be variable. We should point out that the above specification of confidence intervals on the various estimates of the variance is a procedure of estimation of a parameter; but we still need to present a procedure for making a stronger significance test of a measured parameter, an analysis of variance, before we can draw more firm conclusions about the variability of the sample means.

An Analysis of Variance of the Monitored Sources

We will now proceed to the discussion of a parametric model, an analysis of variance technique with one-way classification. For a discussion of the classical analysis of variance models, see, for example, Johnson and Leone (1964), Vol. II, pp. 1-242 or Cramér (1945), pp. 536-42.

The parametric model of analysis of variance with one-way classification can be represented by the statement:

$$\text{(Observed value)} = \text{(Term representing the appropriate parameter)} + \text{(Random residual)} \quad (28)$$

The observed value is the individual measurement, x_{ij}, of the variable X. The subscripts i and j refer to the manner in which the measurements are acquired. The N measurements are grouped into k groups or samples of sizes n_i. The subscript $i(= 1,2,\ldots,k)$ denotes the group and the subscript $j(= 1,2,\ldots,n_i)$ identifies the observation within the group.

Since there is a separate random residual for each observation, it is convenient to use the similar notation, z_{ij}, to represent the residuals. The phrase, "term representing the appropriate parameter," refers in our case to the time variation of the mean across the blocks of time.

We will need to make several assumptions about the random residuals, z_{ij}, in the development of this analysis of variance. These assumptions can be summarized by the following:

1. The expectation value of z_{ij} is zero for all i and j:

$$E[z_{ij}] = 0 .$$

2. The z_{ij} are all mutually independent.
3. The variance of z_{ij} is the population variance, σ^2, for all i and j:

$$Var[z_{ij}] = \sigma^2 .$$

4. z_{ij} is normally distributed.

We will assume that the expectation value of each x_{ij} in the i-th group is a constant, which we write as $A + B_i$. Stated simply, $E[x_{ij}] = A + B_i$. Since there are $k + 1$ parameters, $A, B_1, B_2, \ldots, B_k$, representing the k expectation values, we can impose one linear restriction on the B_i's. The restriction will be

$$\sum_{i=1}^{k} n_i B_i = 0 . \tag{29}$$

The model is now described by

$$x_{ij} = A + B_i + z_{ij} \tag{30}$$

Because of equations (29) and (30), the B_i's represent the expectation

values of the deviation of the i-th average value from the expectation value of the overall average value.

If we wish to investigate differences between groups (that is, the possibility of the variation of the mean), we need to compare the values of the B_i's. In particular, if we are testing the hypothesis that the mean is constant, all of the B_i's are zero:

$$B_i = 0 \ . \tag{31}$$

The sample means, $\bar{x}_i$, and the overall mean, $\bar{x}$, are given by

$$\bar{x}_i = \frac{1}{n_i} \sum_{j=1}^{n_i} x_{ij} = A + B_i + \bar{z}_i \ , \tag{32}$$

$$\bar{x} = \frac{1}{N} \sum_{i=1}^{k} n_i \bar{x}_i = A + \bar{z} \ , \tag{33}$$

where

$$\bar{z}_i = \frac{1}{n_i} \sum_{j=1}^{n_i} z_{ij} \ , \tag{34}$$

$$\bar{z} = \frac{1}{N} \sum_{i=1}^{k} n_i \bar{z}_i \ . \tag{35}$$

We now note that

$$x_{ij} - \bar{x} = (x_{ij} - \bar{x}_i) + (\bar{x}_i - \bar{x}) \ ; \tag{36}$$

and the sum of the squares over all the measurements is given by

$$\begin{aligned} \sum_{i=1}^{k} \sum_{j=1}^{n_i} (x_{ij} - \bar{x})^2 &= \sum_{i=1}^{k} \sum_{j=1}^{n_i} (x_{ij} - \bar{x}_i)^2 + \sum_{i=1}^{k} \sum_{j=1}^{n_i} (\bar{x}_i - \bar{x})^2 \\ &\quad + 2 \sum_{i=1}^{k} \sum_{j=1}^{n_i} (x_{ij} - \bar{x}_i)(\bar{x}_i - \bar{x}) \\ &= \sum_{i=1}^{k} \sum_{j=1}^{n_i} (x_{ij} - \bar{x}_i)^2 + \sum_{i=1}^{k} n_i (\bar{x}_i - \bar{x})^2 \ . \end{aligned} \tag{37}$$

It is customary to give names to the quantities in equation (37). This equation is then expressed as

(Total sum of squares) = (Within groups sum of squares)
+ (Between groups sum of squares)

or as

$$TSS = WGSS + BGSS. \tag{38}$$

We need to determine the expected values of the quantities in equation (37). By employing the assumptions 1 to 3 given above, we can show that

$$\begin{aligned} E[WGSS] &= E\left[\sum_{i=1}^{k}\sum_{j=1}^{n_i}(x_{ij} - \bar{x}_i)^2\right] \\ &= \sum_{i=1}^{k} E\left[\sum_{j=1}^{n_i}(z_{ij} - \bar{z}_i)^2\right] \\ &= \sum_{i=1}^{k}(n_i - 1)\,\sigma^2 \\ &= (N - k)\,\sigma^2 , \end{aligned} \tag{39}$$

and that

$$\begin{aligned} E[BGSS] &= E\left[\sum_{i=1}^{k} n_i(\bar{x}_i - \bar{x})^2\right] \\ &= E\left[\sum_{i=1}^{k} n_i(\bar{z}_i - \bar{z} + B_i)^2\right] \\ &= E\left[\sum_{i=1}^{k} n_i(\bar{z}_i - \bar{z})^2\right] + \sum_{i=1}^{k} n_i B_i^2 \\ &= \sum_{i=1}^{k} n_i\, E\left[z_i^2\right] - E\left[N\,\bar{z}^2\right] + \sum_{i=1}^{k} n_i B_i^2 \end{aligned}$$

$$E[BGSS] = \sum_{i=1}^{k} n_i\left(\frac{\sigma^2}{n_i}\right) - N\left(\frac{\sigma^2}{N}\right) + \sum_{i=1}^{k} n_i B_i^2$$

$$= (k - 1)\,\sigma^2 + \sum_{i=1}^{k} n_i B_i^2 \quad . \tag{40}$$

The multipliers of the σ^2 in the expected values are called the degrees of freedom of the corresponding sums of squares. If we define the mean squares as the sums of squares divided by their degrees of freedom, we will find from equations (14), (18), (21), (39), and (40) that

$$E[BGMS] = E\left[\frac{k}{k - 1}\, s_2^2\right] = \sigma^2 + \frac{1}{k - 1}\sum_{i=1}^{k} n_i B_i^2 \quad , \tag{41}$$

$$E[WGMS] = E\left[\frac{N}{N - k}\,\langle\sigma_{ei}^2\rangle\right] = \sigma^2 \quad . \tag{42}$$

A considerable excess of the BGMS over the WGMS can reasonably be ascribed to the existence of some nonzero B_i's, that is, to some real difference between groups, or to the variability of the mean. If we use the assumption 4 above and assume further that all the B_i's are zero, it can be shown that

$$R = \frac{BGMS}{WGMS} \tag{43}$$

has an F distribution (for a description of the properties of the F distribution see Hoel, pp. 269-73) with k - 1 and N - k degrees of freedom (see Johnson and Leone, Vol. II, p. 9). Therefore the value of $R = F_{k-1,N-k,1-\alpha}$ is a significance level test of the hypothesis that all the B_i's are zero and by implication that the mean is constant. The significance level of the test is 100α percent.

Now the quantities in brackets on the left and right of equations (41) and (42) are identically equal in each case. From the values in Tables 4 and 5 we can then evaluate R and construct a significance test of the hypothesis that the mean of a monitored source is constant. The results of this test are presented in Tables 6 and 7. Column 1 lists the name of the source. Columns 2 and 3 give the number of degrees of freedom of the BGMS and WGMS, respectively, while columns 4 and 5 list the BGMS and WGMS, respectively. Column 6 gives the value of R from equation (43), and column 7 presents the significance level of rejection of the hypothesis that the mean of the corresponding source is constant. The results of the observations of Virgo A and Cygnus A are included here for comparison. We see that the observations of Virgo A and Cygnus A (as expected), OJ 287 before 1971 (however, note that only four observations were made during that period), and NGC 1068 during 1971 are all consistent with a constant mean. The significance of rejection of a constant mean of NGC 1068 before 1971, 5%, is low, but not so low as to allow one to conclude that NGC 1068 is definitely constant. We feel that this 5% significance level is not sufficiently high to enable us to conclude that NGC 1068 is definitely variable. The results of the observations of NGC 1068 will be discussed in more detail in the next section. The remainder of the monitored sources show a very high significance for the rejection of the hypothesis of a constant mean both before and during 1971; that is, the flux of the sources is quite definitely variable with time.

Table 6. An Analysis of Variance of the Monitored Sources Before 1971

Source	k - 1	N - k	BGMS	WGMS	R	α
NGC 1068*	20	692	530.30	253.51	2.09	.005
NGC 1068	15	489	258.12	159.13	1.62	.05
NGC 1275	41	905	734.08	152.39	4.82	$<< 10^{-3}$
3C 120	105	2422	475.79	172.39	2.76	$<< 10^{-3}$
3C 273	77	1722	557.24	162.61	3.43	$<< 10^{-3}$
3C 454.3	49	1154	356.77	181.40	1.97	$< 10^{-3}$
OJ 287	3	97	432.37	381.38	1.13	$\approx .35$
VRO 42.22.01	68	1640	732.07	160.44	4.56	$<< 10^{-3}$
Virgo A	5	185	146.34	212.43	0.69	$\approx .70$
Cygnus A	8	243	143.03	307.80	0.47	$\approx .90$

Table 7. An Analysis of Variance of the Monitored Sources During 1971

Source	k - 1	N - k	BGMS	WGMS	R	α
NGC 1068	8	212	10.62	24.04	0.44	$\approx .90$
NGC 1275	25	613	377.52	36.08	10.46	$<< 10^{-3}$
3C 120	22	547	68.81	20.66	3.33	$<< 10^{-3}$
3C 273	28	695	89.35	25.51	3.50	$<< 10^{-3}$
3C 454.3	9	226	56.85	21.16	2.67	.01
OJ 287	25	610	85.77	21.21	4.04	$<< 10^{-3}$
VRO 42.22.01	34	807	116.49	23.36	4.99	$<< 10^{-3}$
Virgo A	1	53	3.45	23.17	0.15	$\approx .70$

Fluctuations in the Monitored Sources

For five of the seven monitored sources (NGC 1275, 3C 120, OJ 287, 3C 273, and VRO 42.22.01), repeated outbursts of the flux can be clearly seen from Figures 5 and 6 and Figure 2 of Fogarty *et al.* (1971). The specific outbursts for 3C 454.3 are less clearly seen. Every Seyfert galaxy and QSO, including OJ 287 and VRO 42.22.01, which was easily detected at 3 mm (that is, all of the monitored sources except NGC 1068) shows variability of the flux with a range of characteristic time scales and amplitudes of the variations which are, as well as have been determined, similar for both types of objects. The rise time from an apparent quiescent level to the maximum flux, which ranges from a week to several months, implies that the sizes of the radiating regions are no larger than a few times 10^{16} cm, if the light-travel time across the source of the radiation is less than the time scale of variability. The increase in the flux compared to the quiescent level ranges from being just discernible from the noise level to perhaps a factor of five to ten times the quiescent level in the cases of 3C 120 and VRO 42.22.01.

The time scales and the amplitudes of variation of the flux at 3.3 mm, as well as the quiescent level of the flux, seem to be correlated with the respective quantities observed in the centimeter wavelength region. For example, compare the flux density versus time graphs (the "light" curves) of VRO 42.22.01 in Figures 5 and 6 with the centimeter wavelength results reported by MacLeod *et al.* (1971). MacLeod *et al.* have also made comparisons of some of the variations with

predictions of the expanding source model of radio sources (see, for example, Pauliny-Toth and Kellermann 1966).

There is some indication that the measured values of the flux tend to scatter more during an outburst than during the quiescent phase. This would indicate that when the flux increases from its quiescent value, it also tends to become more unstable on a time scale much shorter than that of the overall increase and decrease of the flux. Although some evidence for this effect can be seen in Figure 5, it is more clearly indicated by the size of the errors in Figure 6 for VRO 42.22.01. However, the effect is by no means clearly demonstrated for any of the sources.

NGC 1068

NGC 1068 will be discussed here separately from the other monitored sources because the results of the flux measurements and the statistical tests presented in Tables 4 to 7 are less clear for this source and because the results from NGC 1068 are more important than the results from the other sources for the radiation model to be presented later. It would be worthwhile to see whether these millimeter observations of NGC 1068 can give any additional information concerning the shape of the spectrum in the millimeter wavelength region or concerning the possibility that the flux is variable with time. The variation of the flux with time would help to specify more carefully the parameters of the radiation model to follow. In particular, several statistical tests will be applied to the results of the observations in

order to investigate quantitatively the probability that NGC 1068 is a non-zero source and the probability that the flux from the source is variable with time.

The most obvious observational difficulty in measuring the flux from NGC 1068 with the Aerospace antenna is that the flux expected from an extrapolation of the long wavelength radio data (≈0.2 f.u.) is much less than the usual system noise level even with total integration times of about 10 hours (≈2.5 f.u.). Therefore the first tests to be made will test the statistical characteristics of the total system noise determined from observations of "blank" sky. As indicated in a previous section discussing antenna system checks, an observation is composed of from 20 to 40 antenna temperature measurements, each representing an integration time of about 20 minutes. The word cycle or measurement will be used to denote the integration time of about 20 minutes bracketed by about 3 minutes of calibration time, and the word set or sample or group will denote the set of from 20 to 40 cycles.

The observations of blank sky include 156 cycles obtained over the same period as the observations of the sources discussed in this chapter. The histogram of these cycles is shown in Figure 9. The mean antenna temperature $\langle T_a \rangle$, standard deviation of the mean $\sigma_{T,m}$, and the standard deviation of a single cycle σ_T are 0.0002 °K, 0.0034 °K, and 0.042 °K, respectively. The hypothesis that this set of 156 cycles is normally distributed can be checked by making a χ^2 test of the goodness of fit of the 156 cycles to a normal distribution (with 10 groups) with a mean = 0.0 °K and a standard deviation = 0.042 °K. [For a discussion

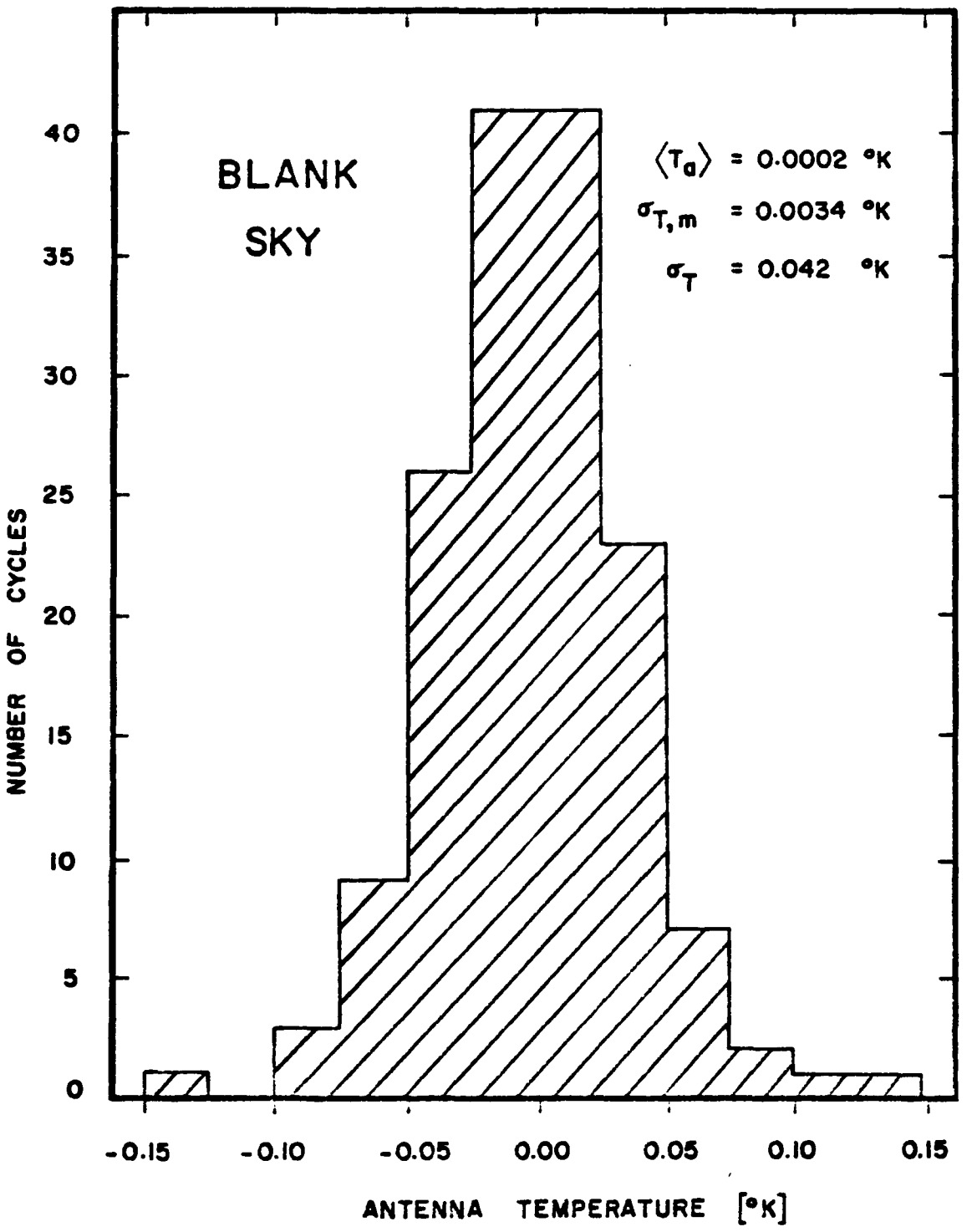

Figure 9. Histogram of 156 Cycles of Antenna Temperature Measurements of Blank Sky

of the χ^2 test see, for example, Hoel (1971), p. 226.] The results of the χ^2 test with 7 degrees of freedom show that there is a 35% chance of having a value of χ^2 greater than the value found in the test. We can therefore accept the hypothesis that the distribution of the 156 cycles is consistent with a normal distribution around a zero mean. It is consistent at the 35% significance level.

We can make another test of the system noise by examining the measurements of Virgo A, a source which is known to be constant [however, see Graham (1971) concerning the possibility that there may be a slight amount of variability in the small nuclear component of Virgo A], and for which adequate data are available to make the test. The six observations (made before 1971) of Virgo A in Table 3 represent six sets with a total of 191 cycles of observation. In this case the mean antenna temperature of the set will not be near zero, since Virgo A is a positively detected object (a six-standard-deviation detection). However, it is the dispersion of this sample which yields the required information about the system noise. The standard deviation of a single cycle determined from the sample of 191 cycles is 0.039 °K, in good agreement with the value of 0.042 °K determined from the 156 samples of blank sky. χ^2 tests of the goodness of fit of the 191 cycles (in ten groups) to normal distributions with a mean = 0.015 °K (the sample mean) and with a standard deviation = 0.039 °K or with a standard deviation = 0.042 °K show that there is a 33% or 11% probability, respectively, of having a χ^2 value greater than the values found in the two tests. The number of degrees of freedom in the two tests is seven and eight, respectively. The distribution of the 191 cycles of measurements of

Virgo A is in good agreement with a normal distribution whose dispersion is determined from the sample of 191 cycles or from the sample of 156 cycles of blank sky at the 33% or 11% significance levels, respectively. It is therefore acceptable to use the distribution of measurements either from Virgo A or from the blank sky or to use the total sample of both Virgo A and the blank sky in specifying the assumed noise characteristics of the system. In the following tests we shall use the noise characteristics determined from the total sample of 347 cycles, namely that the standard deviation of a single cycle is 0.040 °K.

We have seen in the previous section from the test results shown in Tables 4 and 6 and Figure 7 that there was a suggestion of variability with time of the flux of NGC 1068 before February 1971. The cause of this suggestion is the presence of the two observations of NGC 1068 in December, 1966 to January, 1967 reported previously by Fogarty *et al.* (1971), both being approximately 3 standard deviation detections. We can make more quantitative tests of the NGC 1068 data. There are 21 sets comprising 713 cycles of measurements of NGC 1068 made between December 1966 and November 1970 (from Figure 5 plus two values from Fogarty *et al.*). A χ^2 test of the goodness of fit of the 713 cycles to a normal distribution with a mean = 0.0 °K and a standard deviation = 0.040 °K (from the 347 cycles of blank sky and Virgo A) shows that there is less than a 10^{-5} probability of having a χ^2 value as large as is found for this test (91.8 for 11 degrees of freedom).

It is therefore unlikely that the 713 cycles are normally distributed around a mean of zero with a standard deviation = 0.040 °K,

but this is apparent from the histogram of the 713 cycles shown in Figure 10. There is a significantly large number of cycles at large positive antenna temperatures, which contribute most of the amount to the value of χ^2. Many of these positive cycles are from the two observations from December 1966 to January 1967. If these two observations are removed from the sample, we are left with a sample size of 621 cycles. A χ^2 test of the goodness of fit of the 621 cycles to a normal distribution with a mean = 0.0 °K produces a χ^2 = 23.8 with 11 degrees of freedom and a probability of .014 of having a χ^2 this large or larger. It is still not a good fit to a normal distribution, but it is much closer to a normal distribution than the sample of 713 cycles.

A possible explanation of the lack of fit follows from an inspection of the histogram of Figure 10. There is a strong indication that most of the cycles are normally distributed around a mean of zero, but there are too few cycles just below and around a mean antenna temperature = 0.0 °K and an excess of cycles at positive values of the antenna temperature beyond 0.060 °K. It is possible to attribute this shift of the distribution to occasional variation (increase of the observed antenna temperature) of the source with time.

We can make a better test of the goodness of fit of the NGC 1068 cycles to a normal distribution by choosing more carefully the standard deviation of the blank sky. If we restrict our attention to the data acquired between April 1968 and November 1970 (when there is ample evidence that the system noise level was approximately constant), then the appropriate choice of the blank sky is the five samples including 148 cycles of measurements of Virgo A. (Most of the 156 cycles of blank

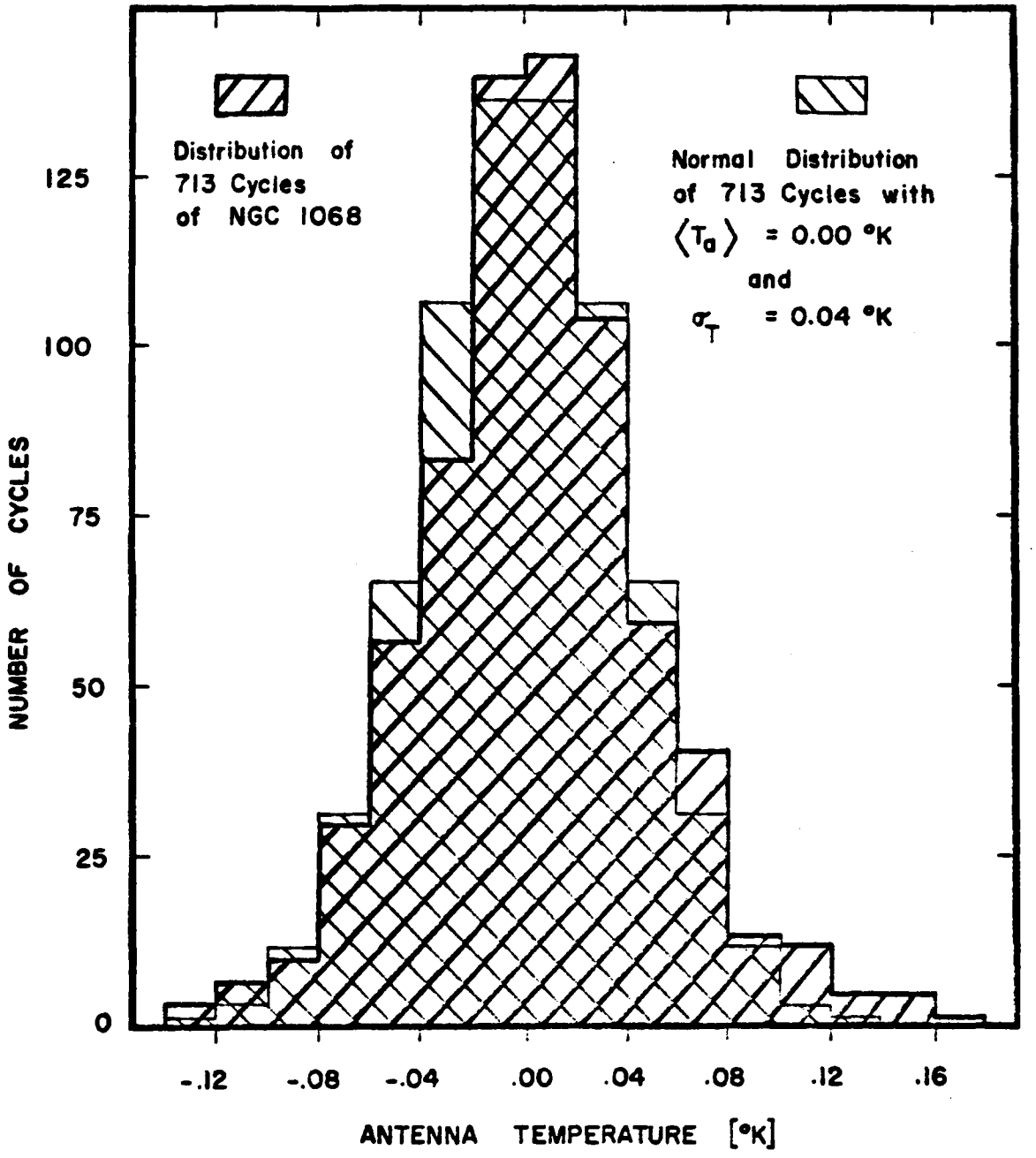

Figure 10. Comparison of 713 Cycles of NGC 1068 with a Normal Distribution of 713 Cycles Around a Zero Mean

sky were acquired earlier than April 1968.) The standard deviation of these 148 cycles is 0.037 °K. A χ^2 test of the goodness of fit of these 148 cycles to a normal distribution with the same standard deviation leads to a value of $\chi^2 = 9.26$ with 8 degrees of freedom and a probability of 32% of having a χ^2 this large or larger. The distribution of the 148 cycles is thus consistent with a normal distribution at the 32% significance level, and we can safely compare the distribution of the NGC 1068 cycles to the Virgo A cycles.

Now we can compare the distribution of the 16 sets including 505 cycles of measurements of NGC 1068 from April 1968 to November 1970 to a normal distribution with a mean = 0.0 °K and with a standard deviation = 0.037 °K. In this case a χ^2 test of the goodness of fit leads to a value of $\chi^2 = 13.75$ with 9 degrees of freedom and a probability of 0.25 of having a value of χ^2 this large or larger. The distribution of the 505 cycles of NGC 1068 is consistent with a normal distribution at the 25% significance level. We cannot conclude from the results of this test that the individual cycle measurements of NGC 1068 scatter any more than for the presumed constant source, Virgo A, nor therefore that NGC 1068 might have a variable flux; but we should notice that this test is not a very sensitive test for variability.

So far the statistical tests which we have applied to the NGC 1068 observations neglect the time ordering of the observations; that is, the results of the tests would be the same regardless of the position in time of the various samples. It might be interesting to look at a test which investigates the randomness of the sequential ordering of the samples. There is a statistical test called runs

analysis [see, for example, Johnson and Leone (1964) Vol. I, pp. 262-4] which can be used to test the randomness of the distribution of sample means about the overall mean. The procedure is to count the number of groups, G, of consecutive sample means above and consecutive means below the overall mean. G is then the total number of groups or "runs" about the overall mean. Let M_1 and M_2 be the number of sample means above and below, respectively, the overall mean. If the distribution is random, most of the groups will contain 1, 2, or 3 sample means, so that the number of groups of means will usually be around one third to two thirds of the total number of sample means. Occasionally, because of statistical fluctuations, there will occur groups with more sample means; but there is a smaller probability for the occurrence of large groups of sample means. As an example, if $M_1 = M_2 = 20$, we would expect that 95% of the time the total number of groups, G, above and below the overall mean will lie between 14 and 27, which we will call here the 95% range, or $R_{.95}$.

The runs analysis of NGC 1068 is presented in Table 8. The values of $R_{.95}$ are taken from Johnson and Leone (1964), Vol.I, pp. 486-7. For comparison, we have included the runs analyses for NGC 1275 and VRO 42.22.01, two sources which we have shown to be definitely variable. In addition, the analyses for NGC 1068 are done for the cases where we consider the scatter of the means about the overall mean and about zero. We see from the results in Table 8 that the scatter of the means is very non-random for NGC 1275 and VRO 42.22.01. The means tend to group above and below the overall mean, and therefore the number of groups is smaller than would be likely to occur as a result of a random

Table 8. Runs Analysis of NGC 1068, NGC 1275, and VRO 42.22.01

Source	Before or During 1971	Scatter About Overall Mean Or About Zero	M_1	M_2	G	$R_{.95}$	Random?
NGC 1068*	Before	Overall	8	13	12	6-15	yes
NGC 1068*	Before	Zero	12	9	14	6-15	≈ yes
NGC 1068	Before	Overall	6	8	11	4-13	≈ yes
NGC 1068	Before	Zero	8	8	11	4-13	yes
NGC 1068	During	Overall	5	4	8	2-8	≈ no
NGC 1068	During	Zero	5	4	8	2-8	≈ no
NGC 1275	Before	Overall	20	22	11	14-27	no
NGC 1275	During	Overall	13	13	8	8-19	≈ no
VRO 42.22.01	Before	Overall	32	37	17	24-45	no
VRO 42.22.01	During	Overall	16	19	11	12-24	no

distribution of sample means. The distributions of the sample means of NGC 1068 are not usually significantly different from what would be expected from a random distribution. Note that the meaning of NGC 1068* is the set of all measurements from December 1966 to November 1970, as explained on p. 47 and p. 50. However, the tendency for the means is to scatter more than the expected random scatter of means. A physical explanation of why the means might scatter more than an expected random scatter is that the sample means vary about the overall mean with a time scale of variation which is comparable to the interval of time between successive sample means. A favorable phase relationship during part of the observing run could cause a surplus of runs. The last column of Table 8 attempts on the basis of the runs analysis to answer whether or not the means tend to be distributed randomly.

We have indicated that the two observations of NGC 1068 during December 1966 to January 1967 show a highly significant positive result. Let us look with more detail at those two observations separately from the other observations. The number of cycles in the two observations of December 1966 to January 1967 is 92, a number which is sufficiently large to enable us to perform χ^2 tests of the goodness of fit to some assumed distributions. Appropriate assumed distributions are those with a mean = 0.0 °K (in order to test the probability of having detected the source) and a mean = 0.027 °K (the mean of the 92 cycles) and with a standard deviation = 0.040 °K (determined from the 347 cycles of blank sky and Virgo A) and a standard deviation = 0.067 °K (determined from the 92 cycles). The results of the χ^2 tests are shown in Table 9. P is the probability of having a value of χ^2 equal to or larger than the

Table 9. χ^2 Tests of Two Observations of NGC 1068

Assumed Mean[a]	Assumed Standard Deviation[a]	Degrees of Freedom[b]	χ^2	P
0.000	0.040	7	99.2	$< 10^{-5}$
0.027	0.040	6	47.2	$< 10^{-5}$
0.000	0.044	7	60.7	$< 10^{-5}$
0.027	0.044	6	24.0	5×10^{-4}
0.000	0.067	8	18.7	.017
0.027	0.067	7	8.4	.43

[a] The assumed mean and standard deviation are in units of °K.

[b] The number of groups is 10 in the cases where the assumed standard deviation is 0.067 °K and 8 otherwise.

test value for the given number of degrees of freedom. We can see that it is very unlikely that the distribution of the 92 cycles is drawn from a normal distribution having a mean = 0.0 °K or 0.027 °K and having a standard deviation like that determined from Virgo A and the blank sky. The distribution is consistent with a normal distribution having a mean antenna temperature = 0.027 °K and a standard deviation = 0.067 °K at the 43% significance level.

A better χ^2 test might be made with an assumed distribution whose parameters are determined from observations which had a system noise much like the system noise during the period of the two observations of NGC 1068. The only good comparison observations are the 43 cycles of the one sample of Virgo A during the winter of 1967-68 (see Table 3), for which the standard deviation was 0.044 °K. The system noise was approximately constant throughout the period of late 1966 to early 1968. The results of this χ^2 test with the standard deviation = 0.044 °K and the mean = 0.0 °K and = 0.027 °K are also given in Table 9. We see from this last test that it is not very likely that the 92 cycles are drawn from a normal distribution having a mean = 0.0 °K or 0.027 °K and a standard deviation = 0.044 °K.

We have noted above that the system noise level was approximately the same during the times of the two observations of NGC 1068 and the one observation of Virgo A. However, the standard deviation of a single measurement was found to be 0.067 °K for NGC 1068 and 0.044 °K for Virgo A. We can test the hypothesis that the two values of the sample standard deviation arise from a single constant (but unknown) population standard deviation. It can be shown that the ratio of any

two independent χ^2 variables leads to an F distribution (see Hoel 1971, pp. 269-73). In our case the unbiased estimates of the variances are independent χ^2 variables. We therefore wish to consider the ratio

$$R = \frac{\frac{91}{92}(0.067)^2}{\frac{42}{43}(0.044)^2} = 2.35 \qquad (44)$$

This ratio leads to the conclusion that the hypothesis of a single constant standard deviation can be rejected at the 0.001 significance level. We might conclude then that the standard deviation for the measurements of NGC 1068 was larger than the usual system noise level at that time.

The very low likelihood that the mean of the 92 cycles is around zero is, of course, consistent with the fact that both observations are approximately three-standard-deviation detections. The significantly larger value of the standard deviation of a single cycle for the 92 cycles than is found for the usual system noise level at that time may be an indication that variation was occurring on a time scale less than the time required to make an observation, or it may be an indication that the system noise was greater than usual during December 1966 and January 1967. However, as was pointed out above, the system noise was approximately constant from late 1966 to early 1968. Therefore it might seem that the more likely conclusion to be drawn is that the flux of NGC 1068 was variable during the two months during which the two observations were made. This would indicate a time scale of variability of less than one month, possibly as short as two weeks.

Other Sources

The two Seyfert galaxies, NGC 4151 and OQ 208, were clearly not detected (see Table 3); and the detection of the N-type galaxy, 3C 371, does not have high statistical certainty (about 80% certainty) according to the same test for significance (the Student's t test; see Hoel, pp. 257-69) described for column 4 of Tables 4 and 5. The weighted mean of the four measurements shown in Table 3 and the associated 1-σ error, 1.8 ± 1.2 f.u., are calculated according to equations (5) and (6). These results are consistent with extrapolations from the longer wavelength data.

Only one, 4C 39.25, of the three QSOs listed in Table 3 has been detected with certainty. For the four measured values of the flux density of 4C 39.25 listed in Table 3 plus two more values, 9.4 ± 3.9 f.u. and 7.2 ± 2.4 f.u., reported by Fogarty *et al.* (1971), the weighted mean flux and the associated 1-σ uncertainty of the mean is 4.3 ± 1.7 f.u. The certainty (according to the Student's t test) of this detection is 99.7%. The large scatter in the observations of 4C 39.25 may be due to observational uncertainties rather than intrinsic variation with time, but it does not conflict with the variability detected at 2.8 cm and 4.5 cm wavelengths (Locke 1970). The certainty of the detection of 3C 380 is about 95%. (The weighted mean and the associated 1-σ uncertainty is 2.1 ± 1.5 f.u.) No detectable milimeter radiation was found at the position of the infrared source near the nucleus of M 82.

The measured value of the flux of Cygnus A, 7.9 ± 1.0 f.u. (± 1.3 f.u., estimated total error), seems to be significantly less than the approximately 13 f.u. predicted by a straight line extrapolation

from the longer wavelength data (see Figure 4), indicating that the spectrum must be curved downward between 30 and 90 GHz. The weighted mean and the standard deviation of the mean were computed according to equations (5) and (6). Wilson (1970) measured a flux at 3.5 mm for Cygnus A of 8.4 ± 2.0 f.u. (estimated total error) with the 75" beam of the NRAO 36-ft antenna. His observations indicate that the flux ratio at 3.5 mm of the two main components is approximately the same as at 6 cm (5 GHz) as shown in Figure 2 of Mitton and Ryle (1969) and discussed earlier in this chapter.

Conclusions

The major conclusions from these millimeter wavelength observations are that Seyfert galaxies and QSOs may be indistinguishable (in the shape of their spectra) in their continuum millimeter flux and that both have similar variability characteristics. Because of the similarity of the variability of the millimeter wavelength flux to that of the longer wavelength radio flux and because of the lack of any indication of a strong increase of the millimeter flux from the radio toward the infrared, the production of the millimeter radiation is probably related to the radio rather than to the infrared radiation for most Seyfert galaxies and QSOs. There is some indication that during an outburst there is a tendency for the flux to vary additionally on a much shorter time scale than the overall time scale of the outbursts.

While the source of the millimeter flux may be unrelated to the source of the infrared (since the observable characteristics seem to be unrelated, with the possible exception of the case of NGC 1068 to be

discussed in Chapter 4), the values of the millimeter flux help to specify the shape of the spectrum in the as yet unobserved very far infrared (submillimeter) region of the spectrum. The spectra of those objects which show a high infrared flux must begin to rise very steeply with frequency somewhere beyond 10^{11} Hz. For instance, for NGC 1068 the spectral index, α, defined by $F_\nu \propto \nu^\alpha$, must be at least 2.0 and more likely about 3.0. The smaller value of α occurs if $F_\nu = 10^4$ f.u. at 100 μm (3×10^{12} Hz) (Kleinmann and Low 1970; Low and Aumann 1970) and if $F_\nu = 10$ f.u. at 90 GHz, while the larger value is the more likely value since the 90-GHz flux is likely to be $\simeq$ 0.2 f.u. at most times (Kellermann and Pauliny-Toth 1971).

Probably the most useful conclusion of these millimeter wavelength observations (with respect to the specification of the parameters in the radiation model discussed later) is the suggestion that NGC 1068 may have a flux which is variable with time. This suggestion follows from the apparent positive detection (a statistical certainty $\gtrsim$ 99.9%) of NGC 1068 in December 1966 and January 1967 at a flux level ($\simeq$ 10 f.u.) four standard deviations above the level found by extrapolation from the longer wavelength radio data ($\simeq$ 0.2 f.u.) together with the fact that the mean of the remainder of the set of observations of NGC 1068 is consistent with the extrapolated value and not with the higher detected value. Variability of the flux is also suggested by the results of the analysis of variance of NGC 1068 and by the apparently higher values of the standard deviation of the above mentioned detections of NGC 1068. While it is not shown with high certainty that NGC 1068 is variable with time, it is also not shown with high certainty

that NGC 1068 is not variable with time nor that the flux is always equal to the extrapolated value. The statistical tests presented in this chapter do not take into account large systematic errors. Therefore if there are no large systematic errors present in the observing procedure or the data reduction, it would appear from this data that variability of the flux of NGC 1068 is more likely than constancy.

CHAPTER 4

PRELIMINARY MODEL CONSIDERATIONS

In the previous chapters we have surveyed some of the existing data concerning Seyfert galaxies and some apparently related objects. We have considered the continuous spectrum (from the radio to the X-ray region) and the characteristics of the variability of the flux in several objects. We have also shown that the results of the millimeter wavelength observations, presented in Chapter 3, have helped to establish more clearly the similarity of Seyfert galaxies and QSOs and the shape of the spectrum from the millimeter through the infrared portions of the spectrum. An important conclusion that follows from these results is that the infrared spectra of Seyfert galaxies are very similar to one another. However, the spectra are not very accurately determined because of the observational and instrumental difficulties. The fact of the similarity of the spectra and the fact that the spectra are not yet accurately determined suggest that an extremely rigorous attempt to explain the source of the infrared radiation from the nuclei of Seyfert galaxies is not justified at this time. It is probably sufficient to specify the parameters of any proposed radiation model by fitting the model to the observed spectrum of one source, NGC 1068, the Seyfert galaxy with the most thoroughly determined spectrum and variability characteristics. We will therefore discuss the characteristics of the spectrum of NGC 1068 in the next section and then look briefly

in the remainder of this chapter at some thermal and synchrotron radiation mechanisms which have been proposed to explain the infrared spectrum of NGC 1068.

Characteristics of the Spectrum of NGC 1068

The observed continuous spectrum of NGC 1068 is shown in Figure 11. The data, which range from the radio region of the spectrum to the X-ray region, have been taken from the following sources: the radio data from Kellermann and Pauliny-Toth (1971) and Brandie and Stull (1971); the millimeter wavelength data from Rather (1970) and Fogarty *et al.* (1971); the infrared and visual photometric data from Pacholczyk and Weymann (1968b), Kleinmann and Low (1970), Low and Aumann (1970) Pacholczyk (1970b), and Low and Rieke (1971); and the upper limit in the X-ray region from Gursky *et al.* (1971). The relative uncertainties of the measurements are $\lesssim 5\%$ in most regions of the spectrum. In the region of 1 - 22 μm, the uncertainties are 10%, while at 100 μm the relative uncertainty is about one third. The one-standard-deviation errors of the measurements by Rather and by Fogarty *et al.* range from about 1 to 2 f.u. and from about 2.0 to 3.5 f.u., respectively. The upper limit at 90 GHz represents the measurements by Kellermann and Pauliny-Toth and many of the measurements by Fogarty *et al.* for which NGC 1068 was not detected.

The continuous spectrum will be discussed in terms of several numbered spectral components: Components I, II, and III, which correspond to the respective components of the model to be presented in Chapter 5.

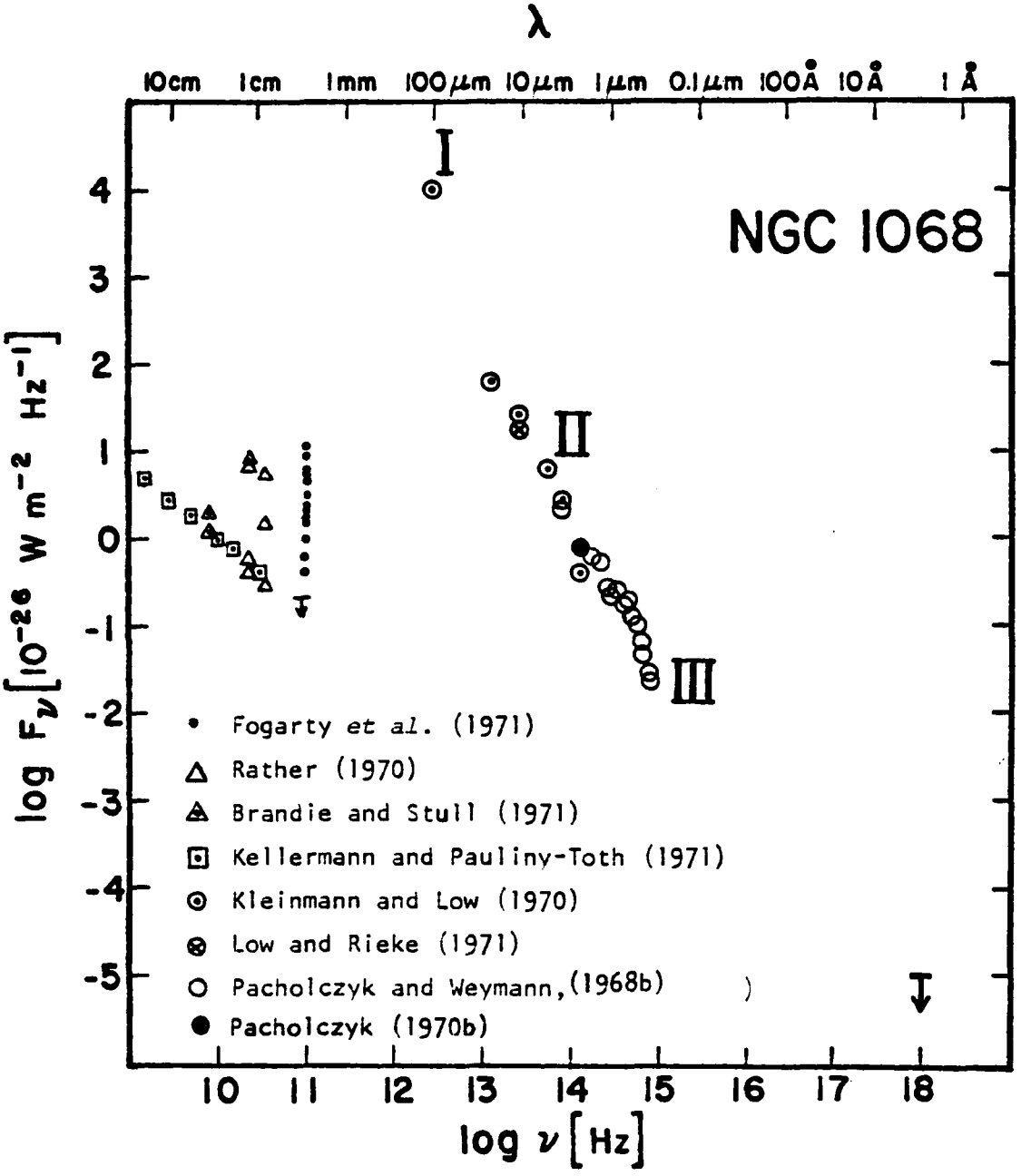

Figure 11. The Observed Continuous Spectrum of NGC 1068

The relative uncertainties of the measurements are discussed in the text. The upper limit at 90 GHz is from several of the measurements by Fogarty *et al.* and by Kellermann and Pauliny-Toth. The upper limit in the X-ray region is by Gursky *et al.* (1971).

Component I

The portion of the spectrum which lies in the frequency range from 3×10^{10} Hz to 3×10^{13} Hz and is sharply peaked near 3×10^{12} Hz (a wavelength of 100 μm) is called Component I. The frequency of the peak of Component I is not well known, but lies between 1.5×10^{12} Hz and 4.5×10^{12} Hz, as discussed later with the 100-μm measurement. The radio spectrum for frequencies < 10^{10} Hz seems to be a normal radio source spectrum with a spectral index, $\alpha = -0.8$. The spectral index is defined by the relation, $F_\nu \propto \nu^\alpha$. There is no reported indication of variability of the flux at frequencies less than 15 GHz. On the contrary, there is abundant evidence which shows that the flux is not variable at wavelengths longer than 2 cm (Kellermann and Pauliny-Toth 1971). However, variability in the millimeter wavelength region on a time scale of one month is indicated at 90 GHz (as discussed in Chapter 3) and possibly at several other frequencies, by the data presented in Table 10. Table 10 lists the flux data at 90 GHz shown graphically in Figures 5 and 6 plus two values reported by Fogarty *et al.*, at 35.5 GHz and 23.7 GHz by Rather, and at 8 GHz by Brandie and Stull. The values of the flux at the respective frequencies, F_ν^{extr}, extrapolated from the longer wavelength radio data (see Figure 11) are also given in Table 10. The extrapolated value of the flux at 90 GHz is about 0.2 f.u.; however, the observed 90-GHz flux has been greater than 2.0 f.u. on seven different occasions. The signal-to-noise ratio, S/N, was > 2 (a certainty of detection of 97% according to the Student's t test) for four of these seven measurements; and S/N was > 3 (a certainty of detection of 99.7%) for three of the seven measurements. For 20 of the

Table 10. Flux[a] vs. Time Data at Four Radio Frequencies for NGC 1068

Date	90 GHz	35.5 GHz	23.7 GHz	8 GHz
1966.99	10.5 ± 3.2			
1967.07	3.1 ± 3.5			
1967.89	-0.9 ± 5.1			
1968.03	0.4 ± 2.5			
1968.07	1.4 ± 2.8			
1968.71	-0.7 ± 2.1			1.5 ± 0.05
1968.82				1.3 ± 0.30
1968.90				1.6 ± 0.05
1968.94				1.4 ± 0.10
1969.16			7.2 ± 1.2	
1969.22	5.7 ± 2.1			1.9 ± 0.30
1969.44	2.9 ± 2.0			
1969.46		5.5 ± 2.1		
1969.54	-0.3 ± 2.5			
1969.65				1.5 ± 0.05
1969.72	2.0 ± 1.7			1.5 ± 0.05
1969.74			0.4 ± 1.9	
1969.76		0.3 ± 1.5		
1969.77		1.5 ± 1.6		
1969.83	-0.6 ± 2.5			1.3 ± 0.15
1969.84	2.4 ± 2.0			
1969.86	0.2 ± 2.3			
1969.91	-2.2 ± 2.2		0.6 ± 0.7	
1970.14	4.3 ± 2.5			
1970.21	1.8 ± 2.4			
1970.30			8.5 ± 1.0	
1970.38	-3.1 ± 2.1			
1970.63	-3.9 ± 2.2			
1970.68	5.6 ± 1.8			
1970.75	-2.1 ± 2.8			
1970.80	-1.0 ± 2.2			1.4 ± 0.10
1971.15	0.2 ± 0.9			
1971.23	0.4 ± 0.9			
1971.30	-0.9 ± 1.0			
1971.48	0.6 ± 0.7			
1971.67	-0.5 ± 1.0			
1971.73	0.0 ± 1.0			
1971.80	-0.7 ± 0.9			
1971.89	0.9 ± 1.3			
1971.93	-0.8 ± 0.9			
F_ν^{extr}	0.2	0.4	0.5	1.4

[a] In units of 10^{-26} W m^{-2} Hz^{-1}

total of 30 measurements, S/N was $\leq$ 1. These considerations and the discussion in Chapter 3 indicate that the apparent detections of the 90-GHz radiation from NGC 1068 may have statistical significance. If the apparent detections are really a measure of the flux of NGC 1068, the lack of detection at other times would imply that the radiation at 90 GHz is probably variable.

There is further (but scant) evidence for variability at 35.5 GHz (8 mm) and 23.7 GHz (12.5 mm) reported by Rather. The extrapolated values of the flux at 8 mm and 12.5 mm are 0.4 f.u. and 0.5 f.u. respectively. The weighted means and the associated 1-σ uncertainties [determined according to equations (5) and (6)] at the two wavelengths are 2.3 $\pm$ 1.0 f.u. and 4.0 $\pm$ 0.9 f.u., respectively. The statistical certainty of detection of the weighted means at the two wavelengths is $\approx$ 98% and $\approx$ 99.99%, respectively; but the statistical certainty of detection of some of the individual measurements is clearly much higher. The statistical certainty of detection is determined from the Student's t test (see Hoel 1971, pp. 257-69). Rather's observed values of the flux of NGC 1068, along with the 90-GHz values, indicate that an outburst may have occurred during the first half of 1969. The 8-GHz observations of the flux reported by Brandie and Stull showed no significant time variations, but there is an interesting coincidence in time of their highest measured value of the flux, 1.9 $\pm$ 0.3 f.u., with the possible outburst in the spring of 1969 indicated by the 35.5-GHz and 90-GHz values. The value of the flux of 1.9 f.u. is two standard deviations above the extrapolated value and the mean of the other eight observed values of the flux at 8 GHz. The mean of the other eight values,

1.45 ± 0.02 f.u., agrees well with the extrapolated value. At each of these frequencies the flux has been found occasionally to be considerably higher than the extrapolated values. These observations tend to confirm (but with not very great certainty) the preliminary suggestion of variability of the flux of NGC 1068 reported previously by Epstein and Fogarty (1968). It must be pointed out here that there is no attempt to show that it is convincing that NGC 1068 has been detected at 90 GHz or that variability of the flux in the millimeter region has occurred. There is only the attempt to show that it is not absolutely convincing that the flux of NGC 1068 in the millimeter wavelength range has remained constant since late 1966 and equal to the values extrapolated from the longer wavelength radio data.

There is ample room for scepticism regarding the millimeter wavelength variation of the flux of NGC 1068. One objection could be that there are no other sources known to be variable at millimeter wavelengths which are not variable in the centimeter and longer wavelength regions also. It is possible to imagine a situation where such characteristics of the variability might occur. Suppose that in a hypothetical source producing variable millimeter radiation there is another source which produces the bulk of constant centimeter (and longer wavelength) radiation. The spectrum from the source producing the variable millimeter radiation might be dropping, or even remain flat, toward longer wavelengths. If the source producing the centimeter radiation were a much stronger source at centimeter wavelengths than the source producing the variable millimeter radiation is at centimeter wavelengths (as seems to be the case for NGC 1068), we would not expect to detect

the component of the flux or its variability at centimeter or longer wavelengths from the source producing the variable millimeter wavelength component.

There is at least one other source, VRO 42.22.01 (BL Lacertae), which shows characteristics similar to the hypothetical, two-component source under discussion. Figure 12 shows the flux spectrum of VRO 42.22.01, together with the range of amplitude of variation of the flux, as a function of frequency. We see that in this case the quiescent level of the flux is approximately flat from the centimeter to the millimeter range whereas the amplitude of the variation of the flux increases with frequency and has its maximum reported value in the short millimeter wavelength range. The percentage variability of the flux of VRO 42.22.01 becomes very small according to Weiler and Ekers (1972) at a wavelength of 21 cm. If the quiescent component were not flat, but increasing with wavelength, with the variable component decreasing with wavelength (as it is for NGC 1068), then the wavelength at which variability would remain detectable would be much shorter, probably around 2 cm to 5 cm. In the case of NGC 1068, as noted above, there is much evidence indicating that the flux is not variable (or, at least, the percentage variability is very small) at wavelengths greater than 2 cm. Of course, this explanation is not offered as a proof that NGC 1068 is variable, but only as a suggested resolution of the apparently incompatible results between high and low frequency radio observations. An explanation would be required if it were shown conclusively that the millimeter wavelength flux of NGC 1068 is variable.

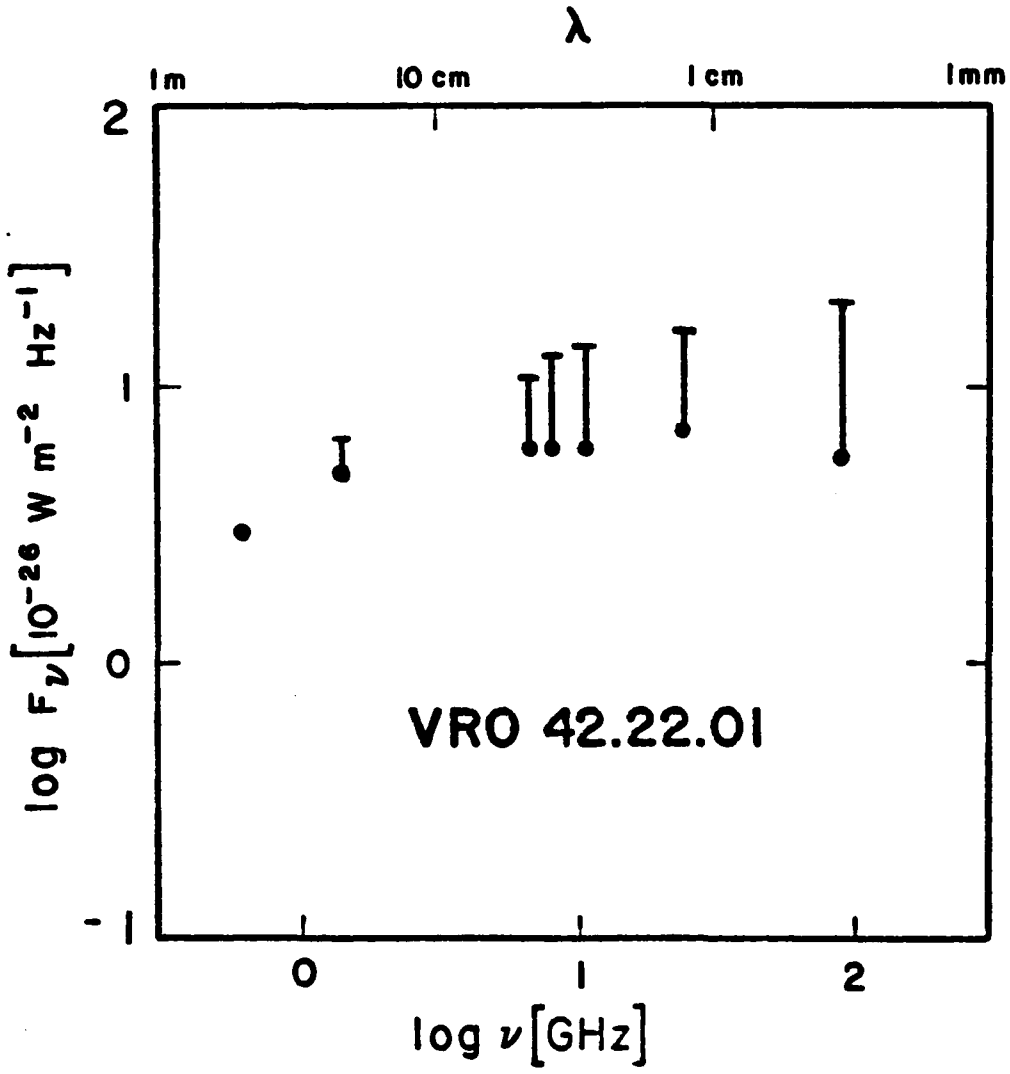

Figure 12. The Flux Spectrum and the Variability Amplitude of the Flux for the Radio Source VRO 42.22.01

The dots indicate the quiescent level of the flux and the length of the bar above the dots indicates the amplitude of the variability of the flux. The data have been taken from Chapter 3 of this dissertation, Kellermann and Pauliny-Toth (1971), MacLeod *et al.* (1971), Rather (1970), and Weiler and Ekers (1972).

In the model to be presented later, the size of Component I will be assumed to be restricted by the millimeter wavelength variability, having a time scale of the order of one month, and will be taken to be $\lesssim 10^{17}$ cm. This restriction will be made, even though it is not shown conclusively that the millimeter radiation is variable, in order to satisfy the most stringent condition which might be required, namely that the millimeter radiation is associated with Component I and that the millimeter radiation is variable.

The peak of Component I is determined by the reported value of the flux (Aumann and Low 1970, Kleinmann and Low 1970, Low 1970, and Low and Aumann 1970) at a wavelength near 100 μm. The reported value, $\approx 10^4$ f.u., shows that the spectrum must rise very rapidly with frequency between 10^{11} Hz and 3×10^{12} Hz and fall even more rapidly on the high frequency side of the peak between 3×10^{12} Hz and 1.5×10^{13} Hz. The 100-μm observations were performed several times with good agreement between the observed values. The relative statistical error of this measurement is about one third with an estimated calibration uncertainty of 10%; however, there are considerable systematic uncertainties in the observations. The uncertainties (as discussed by the investigators cited above) include the response of the detector (bolometer) over the bandpass ($\approx$ 50 μm to $\approx$ 300 μm), the weighted centroid of the bandpass, and the inability to reject from a measurement any constant and smoothly varying instrumental or sky background. The response of the detector is approximately flat over much of the bandpass. The high frequency cut-off, determined by the filter characteristics, is rather sharp and occurs between 50 μm and 70 μm, while the

low frequency end, eventually cut off by the effect of diffraction at wavelengths greater than 350 μm, has a very gradual drop in sensitivity. Because of the very broad bandpass of the detector and the lack of prior knowledge of the spectrum of NGC 1068, it is not possible to state precisely at which frequency the flux spectrum has its maximum, but the peak must lie somewhere between the approximate limits, 1.5×10^{12} Hz and 5×10^{12} Hz (between the wavelength limits, 200 μm and 60 μm). Since the 100-μm observations were made at an altitude of 10 miles from a jet aircraft, the attenuation of the atmosphere did not contribute to the uncertainty of the observations.

There are no reported observations in the wavelength region between 3 mm and 300 μm, although there are currently some attempts being made to measure the flux near a wavelength of 350 μm with a very broad bandpass detector (Rieke 1972). The current state of these measurements indicates a preliminary upper limit of 350 f.u. at 350 μm.

Component II

Component II of the spectrum of NGC 1068, which spans the frequency range from 10^{13} Hz to 3×10^{14} Hz, is determined by the observations between 1 μm and 22 μm. From the size of the error bars of the observations between 5 μm and 100 μm (up to 10% relative errors), it can be seen that the spectrum cannot be represented by a single straight line, or even by a simple curve without inflection points. There must be an inflection point around 20 μm in the spectrum, and this suggests (but does not necessarily require) the presence of two spectral components. If the infrared spectrum between 1 μm and 100 μm is separated

into two components, the second component seems to have a maximum around 2×10^{13} Hz (somewhere between 1.5×10^{13} Hz and 3×10^{13} Hz) and appears to be curved downward at frequencies greater than 6×10^{13} Hz.

Variability of the flux at 2.2 μm (1.4×10^{14} Hz) on a time scale of days, or even less than one day, and with an amplitude of a factor from two to four has been reported by Pacholczyk (1970b). This result would imply that the emitting region is no larger than 10^{15} cm. Pacholczyk notes that some of the apparent variability may be due to centering errors in the 15" diaphragm (the angular aperture of the photometric instrument) if the source is extended. Neugebauer *et al.* (1971) have raised some questions concerning the 2.2-μm variability reported by Pacholczyk. Their observations with diaphragm sizes ranging from 2" to 20" of the nucleus of NGC 1068 indicate that 56 percent of the 2.2-μm flux detected with a 15" aperture originates from outside a central circle of 2" diameter. The size of the source is probably of the order of 10". (At the distance of 13 Mpc, 10" corresponds to about one-half kpc.) This would limit the amplitude of the variation of the flux to not more than a factor of about two if the source of the variable flux lies within 1" of the nucleus. Pacholczyk (1971) has pointed out that the limit on the variability implied by the observations of Neugebauer *et al.* depends on the assumption that the centering errors at the smallest apertures are negligible. In reality, any errors in centering with apertures as small as 2" will tend to overestimate the percentage of flux from the source beyond 1" from the source center and are more likely to occur with the 2" diaphragm than with Pacholczyk's 15" diaphragm. We might conclude from the above discussion that the

very rapid variability of the flux is doubtful, but possibly not excluded (if the amplitude of the variability is less than twice the quiescent value) by the apparent resolution of the source of the 2.2-μm radiation.

There is a more direct objection to the existence of the rapid variability of the flux. Frequent observations of NGC 1068 at 2.2 μm, 5 μm, and 10 μm by Low (1971) have failed to detect variability of the flux on time scales less than the order of a month. (The possibility of variability with longer time scales is discussed below.) If the variability at 2.2 μm is real, then it is quite likely that the flux at nearby wavelengths would be variable with a similar time scale, contrary to what is observed. Of course, if the 2.2-μm flux is not rapidly variable at all times, but is only occasionally rapidly variable, the apparently conflicting results by the different observers would not then be incompatible. An explanation for the existence of very rapid variability at 2.2 μm, together with the non-existence of variability at 5 μm and 10 μm will be discussed at the end of the section Component II of Chapter 5. We might also mention here that Penston *et al.* (1971) have reported the possibility, based on rather weak evidence at the present time, that the Seyfert galaxy NGC 4151 may also exhibit rapid variability of the flux at wavelengths of 2.2 μm and 3.4 μm with a time scale of the order of one day. Rapid variability on a time scale of several hours in the radio, infrared, and optical regions of the spectrum has also been reported for VRO 42.22.01 and OJ 287 by Epstein *et al.* (1972). The evidence for rapid variability in these latter two sources is not overwhelmingly convincing, but is certainly based on more comprehensive

and more accurate observations than the observations cited above for NGC 1068 and NGC 4151. The above discussion is not intended to prove that the rapid variability of the flux of NGC 1068 is convincingly demonstrated, but only that there are some indications of the possibility of the occurrence of very rapid variability.

Kleinmann and Low (1970) have suggested previously that the flux of NGC 1068 between 5 μm and 25 μm may be variable, and the 10-μm flux data of Neugebauer *et al.* (1971) are not in conflict with this possibility. Low and Rieke (1971) have confirmed that the 10-um flux from the nucleus of NGC 1068 is variable. They found a 30% variation of the flux in a time of the order of a few months, which is comparable to the time scale of variability of the 3.3-mm flux (if that latter variability is real).

In spite of the above objections to the existence of time scales of variability of the flux as short as one day, or even less, the model presented in the next chapter will retain the most restrictive condition of the shortest reported time scale of variability for NGC 1068; and the size of Component II will therefore be required to be $\lesssim 10^{15}$ cm. This restriction will be kept because of the possibility that the 1-day variability may be real and because of the consequent necessity to have a very small source model for the infrared radiation of Component II.

Component III

The radiation source of Component III of the spectrum at frequencies greater than 10^{14} Hz can be identified with the normal background radiation from the near infrared to the near ultraviolet produced

by the stars, gas, dust, etc. in the nuclear region of a normal spiral galaxy (Johnson 1966). There is no reason to expect coherent variability of the flux from a source whose radiation is produced in this way, and therefore there is no reason to assume any size restrictions for this component.

Thermal Radiation Mechanisms

Blackbody Radiation

The simplest thermal model is that of a single spherical source with a radius, R, emitting blackbody radiation. The blackbody intensity, I_ν, spectrum is given by the Planck function,

$$I_\nu = \frac{2h\nu^3}{c^2} \frac{1}{e^{h\nu/kT_b} - 1} , \tag{45}$$

where h and k are the Planck and Boltzmann constants, respectively, and c is the velocity of light. (All equations are in CGS units.) The shape of the spectrum from such a source is completely determined by its temperature, T_b, which is related to the frequency, ν_b, at which the intensity has its maximum value. These two variables are related by the Wien displacement law,

$$T_b/\nu_b = 1.70 \times 10^{-11} \ ^\circ K \ Hz^{-1} . \tag{46}$$

The total luminosity, L, is given by the product of the surface area of the blackbody and the total rate of emission of radiation from an element of surface (from the Stefan-Boltzmann law),

$$L = 4\pi R^2 \sigma T_b^4 . \tag{47}$$

The total infrared radiation, L_{IR}, from the nucleus of NGC 1068 (or from Component I, which produces most of the radiation) is about 5×10^{45} erg s^{-1}. This estimate from Low and Aumann (1970) is about one fifth of the earlier estimate by Kleinmann and Low shown in Table 2. The value of L_{IR} from Component II is about 10^{44} erg s^{-1}. The numerical relationships between T_b (or ν_b) and R for these two values of are illustrated in Figure 13. We see that in order to produce the total amount of radiation observed from Component I and to have the maximum in the spectrum occur at 3×10^{12} Hz (T_b = 50 °K), R must be as large as 1.0×10^{21} cm (≃ 0.3 kpc), a size which is not consistent with the upper limits imposed by the possible variability in any region of the spectrum nor with the apparent lack of resolution of the nucleus at 10 μm reported by Neugebauer *et al.* (1971). If we take $\nu_b = 5 \times 10^{12}$ Hz (which is about as high as could be consistent with the 100-μm observation), we find that $R = 3.7 \times 10^{20}$ cm (≃ 0.1 kpc). This size is still not consistent with the upper limits imposed by the possible variability in any region of the spectrum, but does not conflict with the lack of resolution of the nucleus at 10 μm.

We note here that the size of the region producing Component I is not necessarily restricted by the observations of variability, since the presence of Component I is based only on the reported measurements made at 100 μm (where there is no evidence of variability) by Low and Aumann (1970) [see also Low (1970) and Kleinmann and Low (1970)]. The resolution limit of this observation is about 7', or much larger than the entire NGC 1068 galaxy. The presence of 100-μm radiation from the center of our own galaxy has been discovered by Hoffmann and Frederick

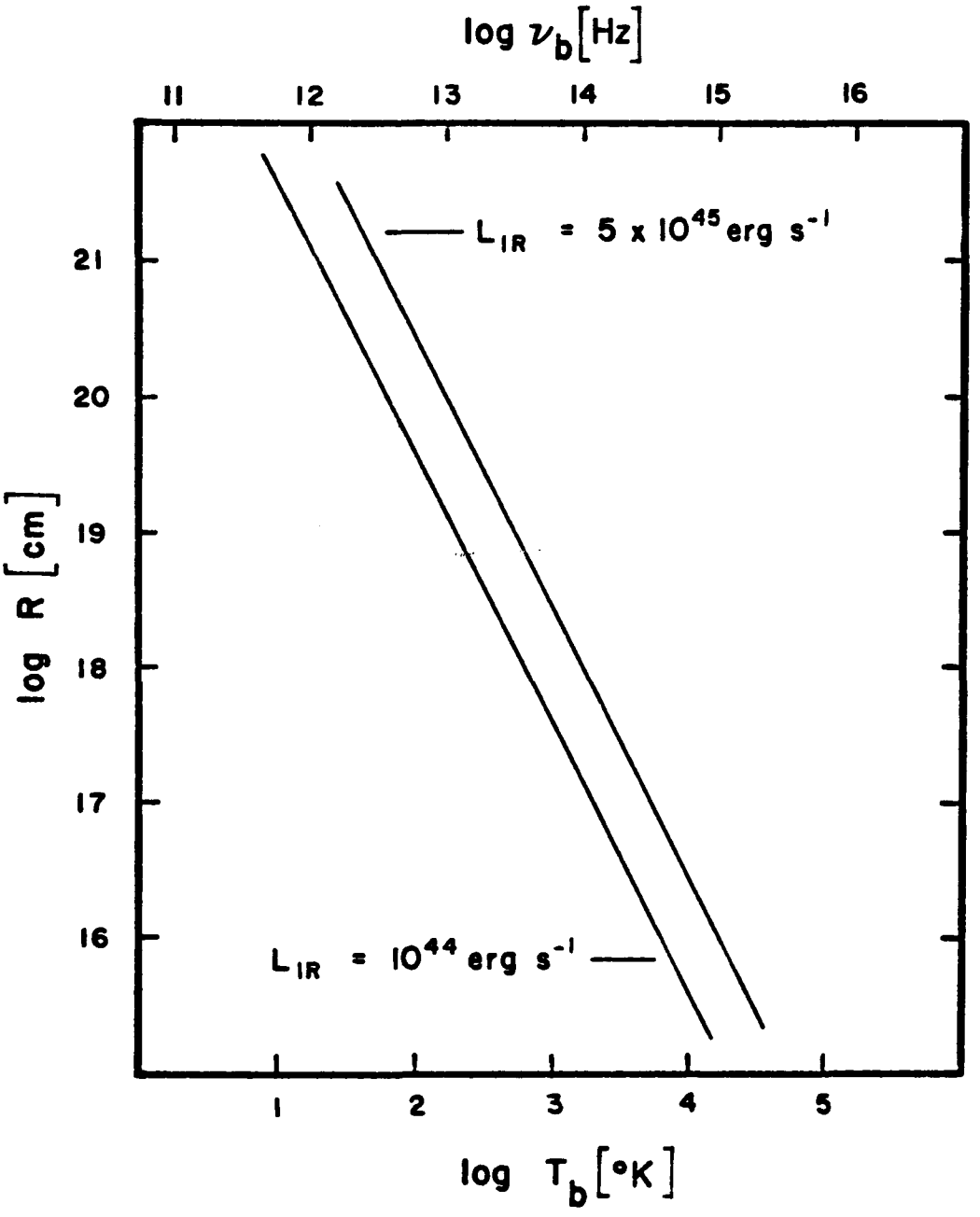

Figure 13. The T_b (or ν_b) vs. R Relationship for Two Values of L_{IR}

(1969). In that case the source of the far infrared radiation is known to be extended with a linear size of about 1 kpc, a size which is comparable to that which would be required by a blackbody emission mechanism for the nucleus of NGC 1068. Nevertheless, we shall continue to restrict the source size of the model for the nucleus of NGC 1068 to much smaller dimensions than 1 kpc to satisfy the most restrictive conditions required by the reported observations of variability.

The size of the region which produces Component II must be 3×10^{18} cm (1 pc) in order to radiate 10^{44} erg s^{-1} with the maximum of the spectrum at 2×10^{13} Hz (T_b = 350 °K). This size is in direct conflict with the observations of possible rapid variability at 2.2 μm, and exceeds by a factor of 10 the upper limit on the size imposed by the variability of the 10-μm flux. In order to produce 10^{44} erg s^{-1} in an emitting region of radius 3×10^{17} cm, it would be necessary to have $\nu_b = 6 \times 10^{13}$ Hz (and T_b = 1100 °K), which is too high (by a factor of 2) to be consistent with the observed spectrum of NGC 1068. For $\nu_b = 3 \times 10^{13}$ Hz, the highest frequency consistent with the spectrum of Component II, $R = 1.3 \times 10^{18}$ cm is required. This value of the radius is still about 3 or 4 times the size limit imposed by the variability of the 10-μm flux.

Whereas it is possible to produce the observed rate of radiation with the maxima in agreement with the observations (if the size restrictions imposed by the variability of the flux are ignored), the spectra of these two blackbodies, shown as the solid curves in Figure 14, are a poor fit to the observed spectrum of NGC 1068. A best visual fit of blackbody spectra, shown as the dashed curves in Figure 14, is an

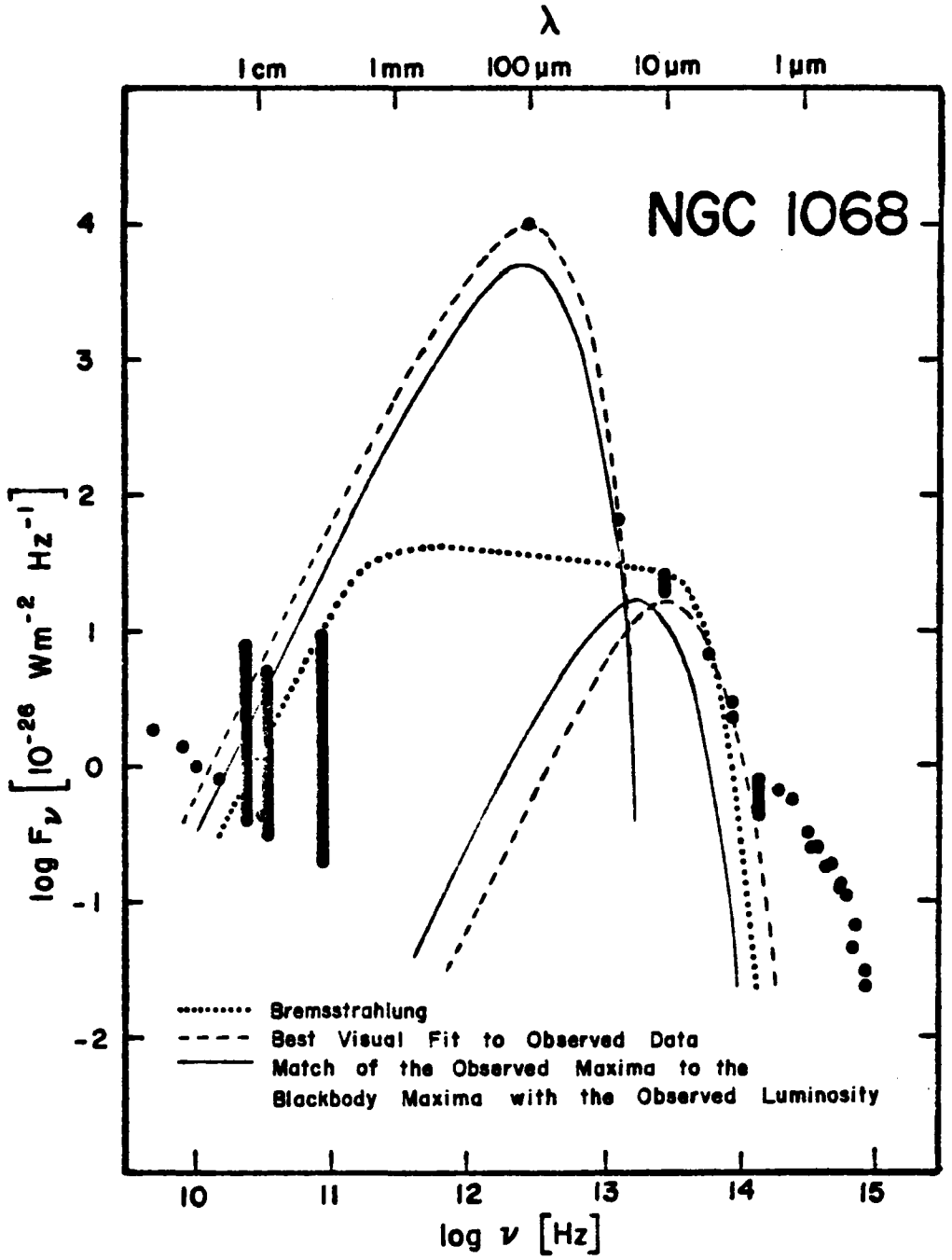

Figure 14. Thermal Models of the Observed Spectrum of NGC 1068

The dots and bars represent the observed flux and the observed variability of the flux, respectively. The data are cited in Figure 11.

improvement over the spectra where only the blackbody maxima must match the observed maxima of the spectrum and the total luminosities must equal the observed luminosities. The parameters of the best visual fit for both Components I and II are given by the following:

	ν_b[Hz]	T_b[°K]	R[cm]
Component I	3.0×10^{12}	50	1.4×10^{21}
Component II	3.4×10^{13}	600	1.4×10^{18} .

Since the maximum amount of thermal radiation from a source of a given size and temperature occurs when the radiation can be characterized by a blackbody, any other mechanisms of thermal radiation will require sizes even larger than those for the blackbodies given above. Thus it is not profitable, unless the restrictions on the sizes are relaxed, to investigate carefully the mechanisms, for example, of free-free radiation by a thermal gas (bremsstrahlung) or of reradiation in the infrared region by a shell of dust grains of radiation originally emitted in the ultraviolet by a central source. In particular, if there is variability of the flux on a time scale of less than one year (and this seems to be the case for NGC 1068), then it does not seem likely that any thermal model can explain the observed radiation. In spite of this condition (or in case improved observations of the variability indicate longer time scales of variability than are now thought to be real), we will comment briefly on these latter two radiation processes.

Bremsstrahlung

The emission of radiation by a gas of electrons and protons with equal number density, N_e, according to the free-free mechanism

(bremsstrahlung) is described by the following equations (for a summary see, for example, Allen 1963) for the volume emission coefficient (per unit solid angle), ε_ν, and absorption coefficient, κ_ν, as functions of frequency:

$$\varepsilon_\nu = 5.443 \times 10^{-39}\ g\ e^{-h\nu/kT_e}\ T_e^{-1/2}\ N_e^2\ , \qquad (48)$$

$$\kappa_\nu = 3.692 \times 10^{8}\ g\ (1 - e^{-h\nu/kT_e})\ T_e^{-1/2}\ \nu^{-3}\ N_e^2\ , \qquad (49)$$

where the Gaunt factor, g, is of the order of unity in the visual and near ultraviolet region; and in the radio region,

$$g = 1.2695\ (2.78 + \log T_e - \tfrac{1}{3} \log N_e)\ . \qquad (50)$$

At sufficiently low frequencies where the optical depth, τ_ν, is greater than 1, the flux has a spectral index = 2.0. In the optically thin region the flux spectrum is almost flat up to the frequency at which $h\nu/kT_e \approx 1$, where the spectrum begins to decrease exponentially. Thus a bremsstrahlung spectrum, which is a thermal spectrum, is very similar to a blackbody spectrum, except that the bremsstrahlung spectrum tends to be much broader. Therefore there is no conceivable way to fit a bremsstrahlung spectrum to the very narrow Component I of the flux spectrum from the nucleus of NGC 1068.

It is possible to make a much better fit, however, to Component II and the millimeter regions of the spectrum. Suppose that we have a homogeneous, spherical (with radius R) distribution of thermal electrons and protons. If we require that the source have an optical depth of unity at a frequency, $\nu_i = 3 \times 10^{11}$ Hz:

$$1 = \tau_\nu = \int_0^S \kappa_\nu\ ds \approx \kappa_\nu\ R, \qquad (51)$$

that the flux in the flat (optically thin) region is about 50 f.u.:

$$50 \times 10^{-23} = F_\nu = \int\int I_\nu \cos\theta \sin\theta \, d\theta \, d\phi \approx \frac{4\pi R^3}{3D^2} \quad , \qquad (52)$$

and if we require that the spectrum begin to decrease exponentially at a frequency, $\nu_e \lesssim 10^{14}$ Hz:

$$1 = \frac{h\nu_e}{kT_e} \, , \qquad (53)$$

then we can solve these three equations for the three unknowns N_e, T_e, and R. In the above equations s is the path length up to the maximum, S, in the line of sight, θ and ϕ are spherical coordinates in the system where the observer is at the origin, and D is the distance from the observer to the source of the radiation and in this case is the distance to NGC 1068, taken to be 13 Mpc. [For a discussion of the parameters of the radiation field see, for example, Appendix I of Pacholczyk (1970a).] The three parameters are required to have the following values in order to fit a bremsstrahlung model to both Component II and the millimeter wavelength regions of the observed spectrum of NGC 1068:

$$T_e = 4000 \ ^\circ K \, ,$$
$$N_e = 7.2 \times 10^5 \ cm^{-3} \, ,$$
$$R = 4.2 \times 10^{19} \ cm.$$

This model is shown as the dotted curve in Figure 14. The fit is not impossibly bad (except perhaps in the confused millimeter wavelength region), but a size of 4.2×10^{19} cm (13 pc) greatly exceeds the maximum sizes indicated by the reported variability of the flux in both the infrared and millimeter regions.

Radiation from Dust

One of the reasons for the suggestion that dust might explain the infrared emission in the nuclei of Seyfert galaxies is the presence of the sharply peaked component of the spectra in so many otherwise diverse objects (Low 1970). There seems to be no *a priori* reason for this striking similarity in these objects; but if the infrared radiation is due to dust, the emission would not occur at higher frequencies than the infrared, because the temperatures required for emission at higher frequencies would be sufficiently high to evaporate any reasonably expected dust grains. Another reason suggestive of the presence of dust is the probable correlation (Wampler 1967) between infrared emission by dust and the observed Balmer decrements, the ratio of the strengths of successive Balmer lines of hydrogen, in Seyfert galaxy nuclei. In several Seyfert galaxies, the Balmer decrements are very large and do not agree with any of the usual theoretical calculations (Osterbrock 1968). However, dust, if present in sufficiently great quantities, may be able to produce the amount of reddening needed in order to explain simultaneously the large observed Balmer decrements and the high infrared flux.

An explanation of the observed infrared radiation from Seyfert galaxies in the wavelength range from 2.2 μm to 22 μm in terms of emission by dust grains has been presented by Rees *et al.* (1969). In their model they have assumed that a spherically symmetric distribution of dust grains absorb radiation in the visual and ultraviolet region of the spectrum from a source at the center of the galaxy. The absorption efficiency of the grains is assumed to be independent of frequency in the frequency region where the absorption occurs (visual and ultraviolet)

and is taken to have a power-law dependence on frequency in the infrared region where the radiation is reemitted. No specific distribution of sizes of grains is assumed, but only an average efficiency for all grain sizes is used. The density of the grains is assumed to have a power-law dependence on distance from the central source. The dependence of the grain temperature on the distance from the center is determined by assuming that the grain temperature is in equilibrium; that is, for each grain the total amount of energy absorbed in the visual and ultraviolet is equal to the total energy radiated in the infrared. Rees *et al.* then fitted this model to the observed spectrum of NGC 1068 in the region designated as Component II in Figure 11 (and throughout this dissertation) in order to determine the temperature dependence on the distance from the central source and the exponents of the power laws for the frequency dependence of the absorption efficiency and radial dependence of the grain density.

It is found that the maximum allowed temperature of 2000 °K (no reasonably expected grains can survive higher temperatures) occurs at a distance of 1 pc, and a temperature of 185 °K (having a maximum emission at a wavelength of 20 μm) occurs at 150 pc. A very slight concentration of the grains toward the center (depending on the ≈ -2/3 power of the distance) is required, and the dependence of the absorption efficiency of the grains on frequency is similar to what would be expected for the anticipated grain sizes and composition. The total mass of the grains, $\lesssim 10^5$ solar masses, is much less than the total amount of mass of the nucleus of NGC 1068 (Burbidge, Burbidge, and Prendergast 1959) as would be required.

As expected, the difficulty with a dust model is the inability to produce enough radiation in a small volume. The dust model suggested by Rees *et al.* cannot have significant variability of the flux on time scales < 0.1 year at 2 μm or < 5 years at 10 μm. Both of these time scales are in strong disagreement with the observations if the shortest reported time scales of variability are assumed. If the reported very rapid variability at 2.2 μm is not real and if the 10-μm flux is produced in Component I, a dust model may adequately explain Component II.

Synchrotron Radiation Mechanisms

The only non-thermal radiation process which will be considered in this dissertation is the synchrotron radiation, or magnetic bremsstrahlung, process by relativistic electrons. Pacholczyk (1970a) has presented a comprehensive discussion of synchrotron radiation processes, and the formalism employed herein will follow his treatment closely.

The Homogeneous Model

The simplest synchrotron radiation model of the source of the infrared radiation from the nucleus of NGC 1068 is that of a spherical, homogeneous distribution of isotropic, relativistic electrons with energy, E, spiraling around magnetic field lines. If we assume that the electrons in the cloud of radius, R, have a number density per unit volume and energy described by a power law,

$$N(E) = N_o E^{-\gamma} , \tag{54}$$

and that the magnetic field strength has a homogeneous value, H, while the direction of the field is sufficiently random (tangled field lines)

so that any small scale anisotropy of the radiation can be ignored, then the volume emission coefficient (per unit solid angle), ε_ν, and absorption coefficient, κ_ν, are given by

$$\varepsilon_\nu = c_5(\gamma)\ N_o\ H^{(\gamma+1)/2} \left(\frac{\nu}{2c_1} \right)^{(1-\gamma)/2} , \tag{55}$$

$$\kappa_\nu = c_6(\gamma)\ N_o\ H^{(\gamma+2)/2} \left(\frac{\nu}{2c_1} \right)^{-(\gamma+4)/2} , \tag{56}$$

where the constants,

$$c_5(\gamma) = \frac{\sqrt{3}}{16\pi} \frac{e^3}{mc^2} \frac{(\gamma+7/3)}{(\gamma+1)} \Gamma\left(\frac{3\gamma-1}{12}\right) \Gamma\left(\frac{3\gamma+7}{12}\right) , \tag{57}$$

$$c_6(\gamma) = \frac{\sqrt{3}\pi}{72} e\ m^5\ c^{10}\ (\gamma+10/3)\ \Gamma\left(\frac{3\gamma+2}{12}\right) \Gamma\left(\frac{3\gamma+10}{12}\right) , \tag{58}$$

are tabulated in Table 11 for various values of γ. Γ is the gamma function [for a discussion of the gamma function see, for example, Whittaker and Watson (1963)], e and m are the electronic charge and mass, respectively, and c is the velocity of light. The magnetic field and the electron energy are related to a frequency called the critical frequency, ν_c, by the relation,

$$\nu_c = c_1\ H\ E^2 , \tag{59}$$

$$c_1 = \frac{3e}{4\pi m^3 c^5} = 6.27 \times 10^{18}.$$

The significance of ν_c is that the maximum synchrotron emission as a function of frequency by a single particle occurs at a frequency = $0.29\ \nu_c$. The total radiated power, p, emitted by a particle, which is the same as the rate of loss of particle energy due to synchrotron radiation, is given by

Table 11. The Constants[a] c_5, c_6, and c_{14} for a Range of Values of γ

γ	c_5	c_6	c_{14}
0.5	2.66 E-22	1.62 E-40	3.38 E 29
1.0	4.88 E-23	1.18 E-40	1.33 E 30
1.5	2.26 E-23	9.69 E-41	2.38 E 30
2.0	1.37 E-23	8.61 E-41	3.48 E 30
2.5	9.68 E-24	8.10 E-41	4.65 E 30
3.0	7.52 E-24	7.97 E-41	5.89 E 30
3.5	6.29 E-24	8.16 E-41	7.22 E 30
4.0	5.56 E-24	8.55 E-41	8.51 E 30
4.5	5.16 E-24	9.24 E-41	9.94 E 30
5.0	4.98 E-24	1.03 E-40	1.14 E 31
5.5	4.97 E-24	1.16 E-40	1.30 E 31
6.0	5.11 E-24	1.34 E-40	1.45 E 31
7.0	5.85 E-24	1.88 E-40	1.78 E 31
8.0	7.31 E-24	2.82 E-40	2.14 E 31
9.0	9.86 E-24	4.47 E-40	2.52 E 31
10.0	1.42 E-23	6.83 E-40	2.68 E 31

[a] The meaning of the notation is indicated by the following example: 2.66 E-22 = 2.66×10^{-22}.

$$p = c_2 H^2 E^2, \tag{60}$$

$$c_2 = \frac{2e^4}{3m^4c^7} = 2.37 \times 10^{-3}.$$

The spectral index, α, in the optically thin (relatively higher frequency) region of synchrotron emission is related to the index in the electron energy spectrum by the relation,

$$\gamma = 1 - 2\alpha. \tag{61}$$

In the optically thick region of the spectrum, $\alpha = 5/2$ and is independent of any of the parameters of the model.

If we now apply the formalism with the assumptions outlined above to a model of the infrared radiation from NGC 1068, we can determine the magnetic field and the particle density if some information obtained from the observed spectrum is supplied. The observed spectral index $\simeq -2.5$ between 100 μm and 2 μm corresponds to $\gamma = 6.0$. If a single source must produce the entire infrared spectrum, the size of the source must be restricted by the shortest observed time scale of variability; and then $R \leq 10^{15}$ cm. If the turnover in the spectrum is due to the source becoming optically thick to its own radiation at frequencies less than 3×10^{12} Hz, we can use equations (51) and (56) to describe this condition:

$$1 = \tau_\nu = \kappa_\nu R. \tag{62}$$

The condition that $F_\nu = 1$ f.u. at a frequency of 10^{14} Hz (in the optically thin region) can be expressed by means of equations (52) and (55):

$$10^{-23} = F_\nu = \frac{4\pi R^3}{3D^2} \varepsilon_\nu, \tag{63}$$

where the distance, D = 13 Mpc = 4×10^{25} cm. We then have two equations in the two unknowns, H and N_o. The solution of equations (62) and (63) for the magnetic field is given by the well-known relation,

$$H = \frac{\nu_1^{\gamma+4}}{[c_{14}(\gamma)]^2} \left(\frac{\Omega}{F_\nu \nu^{-\alpha}}\right)^2 , \tag{64}$$

between the magnetic field and the frequency, ν_1, at which the source becomes optically thick to its own radiation, the solid angular size of the source, $\Omega = \pi R^2/D^2$, and the flux density at some frequency, $\nu > \nu_1$. The constant, $c_{14}(\gamma)$, is listed in Table II for various values of γ.

With all the assumptions and spectral information cited above, we find that the magnetic field $H = 10^{-3}$ gauss; and using this value of the field in either equation (62) or (63), we find that $N_o = 5.8 \times 10^3$. (We have assumed $R = 10^{15}$ cm.) Since an electron radiates most of its energy near the frequency = 0.29 ν_c, we find the lower limit, E_l, and the higher limit, E_h, of the range of energy of the particles from equation (59) and from the low frequency, ν_l, and the high frequency, ν_h, limits of the observed flux spectrum in the optically thin region:

$$E_{l,h} = \left(\frac{\nu_{l,h}}{0.29\ c_1\ H}\right)^{1/2} . \tag{65}$$

The numerical values are $E_l = 2.3 \times 10^{-2}$ erg and $E_h = 2.3 \times 10^{-1}$ erg. The particle energy, Γ, in units of the electron rest mass is

$$\Gamma = \frac{E}{mc^2} . \tag{66}$$

Γ ranges from 3×10^4 to 3×10^5. The lifetime of the electrons, t, before losing half of their energy through synchrotron radiation is found

from equation (60):

$$t = (c_2 H^2 E_1)^{-1}, \tag{67}$$

and is about 1.6×10^{10} sec ($\simeq$ 500 years). According to equation (60), the energy loss rate depends on the square of the energy, so that the higher energy electrons will radiate away a significant portion of their energy and become relatively lower energy electrons before the initially lower energy electrons have lost a significant portion of their energy. Therefore the low energy limit of the electrons is used in equation (67) since these have the longer lifetime. The total density of relativistic electrons, n, is found by equating the total luminosity to the total energy of all the particles divided by the lifetime of an electron:

$$L = \frac{4\pi R^3}{3} n \frac{E_1}{t}. \tag{68}$$

The low energy limit of the electrons is used in equation (68). The energetics of the source are determined by the low energy electrons, because of the much greater density of low energy electrons ($\gamma = 6$). The high energy electrons help determine the shape of the spectrum, but do not add significantly to the total energy. The density of the relativistic electrons found in this manner for $L = 5 \times 10^{45}$ erg s^{-1} is 4.7×10^{11} cm^{-3}, an unusually high value, which represents a total mass in the 10^{15} cm region (if we assume that there is a proton present for each electron) of 3.3×10^{33} grams or $\simeq$ 3 solar masses. This value of the density of the relativistic electrons is a minimum estimate because we have used the energy corresponding to the frequency of the turnover in the spectrum. But this turnover is assumed to be present because

the source is optically thick at lower frequencies. The low energy cut-off in the electron energy spectrum can, of course, occur at any lower value of the energy; and since the density of relativistic electrons increases very fast with decreasing energy, the total density can be much higher than is found from equation (68).

Besides the unlikelihood of this high value of the density, there is another objection concerning the effect of a plasma on the synchrotron radiation. It has been shown [see equation (4.4) of Pacholczyk (1970a)] that one effect of a plasma on the synchrotron emission is to cause a very steep (exponential) cut-off in the spectrum in the frequency range,

$$\nu \lesssim \nu_s = 20 \frac{N_e}{H} , \tag{69}$$

where N_e is the electron density. (The equation is in CGS units.) In the case under discussion, if the synchrotron radiating electrons are considered to be the plasma, then we need to have the equivalent expression for ν_s in the case of a relativistic plasma. This equivalent expression has been given by Sazonov (1970) as

$$\nu_s = 20 \frac{N_e}{H} \frac{2}{3} \frac{\ln \Gamma}{\Gamma} \tag{70}$$

for a monoenergetic distribution of electron energies. Let us now derive ν_s for the case of a power-law distribution of electron energies. The final form of ν_s contains the plasma frequency squared, ν_o^2, so we need only to find the plasma frequency for a relativistic plasma, ν_o^{Γ}. We can begin with equation (4) of Sazonov,

$$\left(\nu_o{}^r\right)^2 = -\frac{e^2\nu}{3k}\int_{E_1}^{E_h} dE\ \frac{\partial}{\partial E}\left[\frac{N(E)}{p^2}\right] v\ p^2\ \ln\left(\frac{2\pi\nu + kv}{2\pi\nu - kv}\right), \qquad (71)$$

where p, v, and E represent the momentum, velocity, and energy, respectively, of an electron, and k is the wave vector. This equation represents the solution of the linearized kinetic equations of an electron plasma without collisions. If the index of refraction differs little from unity, we can take $k = 2\pi\nu/c$; and if the electrons are highly relativistic ($E >> mc^2$), it can be shown that

$$\begin{aligned} E &\simeq pc\ , \\ \beta &= v/c \simeq 1\ , \\ \beta\ \ln\left(\frac{1+\beta}{1-\beta}\right) &\simeq 2\ \ln\Gamma\ , \end{aligned} \qquad (72)$$

from which it follows that

$$\left(\nu_o{}^r\right)^2 = -\frac{e^2c^2}{3\pi}\int_{E_1}^{E_h} dE\ \frac{\partial}{\partial E}\left[\frac{N(E)}{E^2}\right] E^2\ \ln\left(\frac{E}{mc^2}\right). \qquad (73)$$

Now if N(E) is given by equation (54) and if $E_h >> E_1$, it is readily shown that

$$\left(\nu_o{}^r\right)^2 = \frac{e^2}{3\pi m}\,\frac{\gamma+2}{\gamma}\,\frac{\ln\Gamma_1}{\Gamma_1}\,N_o\,E_1{}^{-\gamma+1}\ . \qquad (74)$$

Since the electron density is given by

$$\begin{aligned} N_e &= \int_{E_1}^{E_h} N_o\,E^{-\gamma}\,dE \\ &\simeq N_o\,E_1{}^{-\gamma+1}\,(\gamma-1)^{-1}\ , \end{aligned} \qquad (75)$$

then we find that

$$\left(\nu_o{}^r\right)^2 = \nu_o{}^2 \frac{(\gamma+2)(\gamma-1)}{3\gamma} \frac{\ln \Gamma_1}{\Gamma_1} , \tag{76}$$

where the non-relativistic plasma frequency, ν_o, is given by

$$\nu_o{}^2 = \frac{e^2 N_e}{\pi m} ; \tag{77}$$

and finally it can be shown [in a manner similar to the derivation of equation (69)] that

$$\nu_s = 20 \frac{N_e}{H} \frac{(\gamma+2)(\gamma-1)}{3\gamma} \frac{\ln \Gamma_1}{\Gamma_1} , \tag{78}$$

where Γ_1 is the lower energy limit of the electron distribution. For the case under discussion, $N_e = n = 4.7 \times 10^{11}$ cm^{-3} and $\Gamma_1 = 3 \times 10^4$, and therefore $\nu_s = 6.7 \times 10^{12}$ Hz. Below ν_s the spectrum would have an exponential decrease and the peak at 100 μm could not be present. This is not in good agreement with the observed spectrum of NGC 1068 since the peak frequency is assumed to be 3×10^{12} Hz, or at the highest, 5×10^{12} Hz. This is a low estimate of ν_s since the value for N_e used in equation (78) corresponds to the minimum density of electrons required to produce the observed luminosity. If the low energy cut-off of the electron energy distribution is even slightly less than E_1, the density of electrons is much higher (since $\gamma \approx 6$) and ν_s is correspondingly much higher. For instance, if the electron distribution is cut off at an energy one third of the energy corresponding to the frequency at which the source becomes optically thick, the value of the total density is increased significantly (by a factor of ≈ 7); and in this latter case we would find that $\nu_s = 4.8 \times 10^{13}$ Hz. It seems that it is not

likely that the 100-μm peak in the spectrum could occur with the size $\lesssim 10^{15}$ cm if the magnetic field is determined in the above manner.

There is an even more severe difficulty with the homogeneous model concerned with scattering according to the inverse Compton process of the synchrotron radiation off the relativistic electrons. It can be shown [see equation (5.60) of Pacholczyk (1970a)] that the ratio r of the energy loss rates of an electron, dE/dt, by means of the synchrotron radiation process to the inverse Compton scattering process is just equal to the ratio of the energy densities of the magnetic field, $H^2/8\pi$, to the radiation field, u_{rad}:

$$r = \frac{\frac{H^2}{8\pi}}{u_{rad}} = \frac{\left(\frac{dE}{dt}\right)_{sync}}{\left(\frac{dE}{dt}\right)_{Comp}} \tag{79}$$

If this ratio is << 1, the electron's energy is transferred to the photons produced by the synchrotron process such that the final photon energy is a factor Γ^2 greater than its original energy (Γ is the electron energy in units of mc^2) with the consequences that the electron energy is rapidly depleted and part of the original distribution of photons (the spectrum with peak frequency ν_1) is shifted to a new frequency region with the peak frequency,

$$\nu_{cs} = \Gamma^2 \nu_1 , \tag{80}$$

at the expense of the energy of the electrons. The ratio r is also equal to or greater than (it is greater if there is a second scattering of the spectrum peaked at a frequency ν_{cs} to a higher frequency or if the radiation at ν_{cs} is produced by causes other than the scattering

from the spectrum peaked at ν_1) the ratio of the observed luminosity in the original spectrum with peak frequency ν_1 to the observed luminosity in the shifted spectrum with peak frequency ν_{cs}. The condition that the relative electron energy loss rate be equal to or greater than the relative luminosities in the two regions of the spectrum can be expressed as a condition on the magnetic field:

$$H \geq \left(\frac{32\pi^2 r}{c\, c_{14}}\right)^{2/5} \nu_1^{7/5} , \tag{81}$$

where the radiation density has been calculated under the condition that the source is optically thick to its own radiation at the frequency, ν_1, and that the spectrum is sharply peaked around ν_1. In the model under discussion we have found that $\Gamma = 3 \times 10^4$ and thus the peak frequency of the Compton-scattered spectrum would be about 3×10^{21} Hz (in the γ-ray region with a photon energy of about 12 Mev). At the present time there are no observations of NGC 1068 in this spectral region. Therefore there is no way of giving a precise value to the ratio r. If we arbitrarily assume that the γ-ray luminosity is equal to the infrared luminosity ($r = 1$), we find from equation (81) that the magnetic field must be $\geq$ 65 gauss. If we assume that the γ-ray luminosity is equal to the upper limit of the X-ray luminosity ($\simeq 5 \times 10^{42}$ erg s^{-1}), then $r = 10^3$ and the magnetic field must be $\geq$ 800 gauss. However, the magnetic field for the homogeneous synchrotron radiation model above is much less than either of these lower limits. In fact, a magnetic field value of 10^{-3} gauss would imply that $r = 8 \times 10^{-13}$, and the γ-ray luminosity would be about 10^{58} erg s^{-1}, an entirely unreasonable value.

There are several ways by which we can improve the homogeneous synchrotron radiation model. The key to the improvement lies in noting the very strong dependence of the derived parameters on the observed size of the source (or assumed, if the observations of variability are not sufficiently conclusive) and on the observed (or assumed) frequency of the flux maximum. The dependence of the derived parameters can be shown easily through equations (64) to (68), (78), and (81) and is summarized as follows:

$$
\begin{aligned}
H &\propto R^{4} \; \nu_1^{\gamma+4} \\
E_1 &\propto R^{-2} \; \nu_1^{-(\gamma+4)/2} \\
t &\propto R^{-6} \; \nu_1^{-3(\gamma+4)/2} \\
n &\propto R^{-7} \; \nu_1^{-(\gamma+4)} \\
\nu_s &\propto R^{-9} \; \nu_1^{-3(\gamma+4)/2} \\
r &\propto R^{10} \; \nu_1^{(5\gamma+13)/2} .
\end{aligned}
\tag{82}
$$

We see from the results of equation (82) that we cannot improve the model by assuming the peak frequency is lower than 3×10^{12} Hz, even though the observations would allow it to be as small as 1.5×10^{12} Hz. Lowering the peak frequency would only make ν_s even higher and r still smaller. Clearly by increasing either the assumed size of the source or the peak frequency (or both) we will simultaneously improve the requirements on ν_s and r. Table 12 presents the effect on the derived parameters of varying the assumed parameters. Only two values of the peak frequency, corresponding to the middle and the high frequency end

Table 12. Variation of the Derived Parameters of the Homogeneous Synchrotron Radiation Model

ν_1 [Hz]	3×10^{12}	3×10^{12}	3×10^{12}	5×10^{12}	5×10^{12}	5×10^{12}
R [cm]	10^{15}	10^{16}	3×10^{16}	10^{15}	10^{16}	3×10^{16}
H [gauss]	1.1×10^{-3}	1.1×10^{1}	1.1×10^{3}	1.8×10^{-1}	1.8×10^{3}	1.8×10^{5}
E_1 [erg]	2.3×10^{-2}	2.3×10^{-4}	2.3×10^{-5}	1.8×10^{-3}	1.8×10^{-5}	1.8×10^{-6}
Γ_1	2.8×10^{4}	2.8×10^{2}	2.8×10^{1}	2.1×10^{3}	2.1×10^{1}	2.1
t [s]	1.6×10^{10}	1.6×10^{4}	1.6×10^{1}	7.4×10^{6}	7.4	7.4×10^{-3}
n [cm^{-3}]	4.7×10^{11}	4.7×10^{4}	1.5	2.8×10^{9}	2.8×10^{2}	8.9×10^{-2}
ν_s [Hz]	6.7×10^{12}	6.7×10^{3}	2.1×10^{-1}	3.1×10^{9}	3.1	9.9×10^{-5}
r	7.8×10^{-13}	7.8×10^{-3}	7.8×10^{2}	4.6×10^{-8}	4.6×10^{2}	4.6×10^{7}

of the bandpass of the 100-μm observations, are used. Three values of the assumed radius of the source are used. These correspond to the largest size consistent with every reported possible variability of the flux, and 10 and 30 times the largest size. We can see from Table 12 that, even for the highest peak frequency consistent with the observations, we cannot satisfy the requirement that $r \geq 10^3$ (or 10^2 if the shifted spectrum is in the ultraviolet region of the spectrum) unless the radius of the source is made from 10 to 30 times the largest size consistent with the reported variability of the flux. That is, a size of from 10^{16} cm to 3×10^{16} cm is required in order to satisfy the condition that the losses due to inverse Compton scattering be sufficiently small. However, a size this large is not allowed if the apparent variability of the flux observed at 2.2 μm is real. If the 2.2-μm variability is not real, then a size of 3×10^{16} cm is sufficiently small to satisfy all the other restrictions imposed by variability of the flux.

Even if the difficulties with inverse Compton scattering and the high density of the relativistic electrons are resolved, it is still difficult to match the spectrum of the homogeneous model, shown in Figure 15, to the observed spectrum of NGC 1068. It was pointed out in Chapter 3 (p. 79) that the spectral index between 10^{12} Hz and 3×10^{12} Hz is $\gtrsim 3$, whereas the spectral index for an optically thick, homogeneous source of synchrotron radiation is only 2.5. It would be necessary to invoke some other mechanism to account for the steep cutoff in the frequency range below 3×10^{12} Hz. The flux predicted by the model disagrees strongly with the observed values of the flux in the optically thin region between 50 μm and 10 μm also.

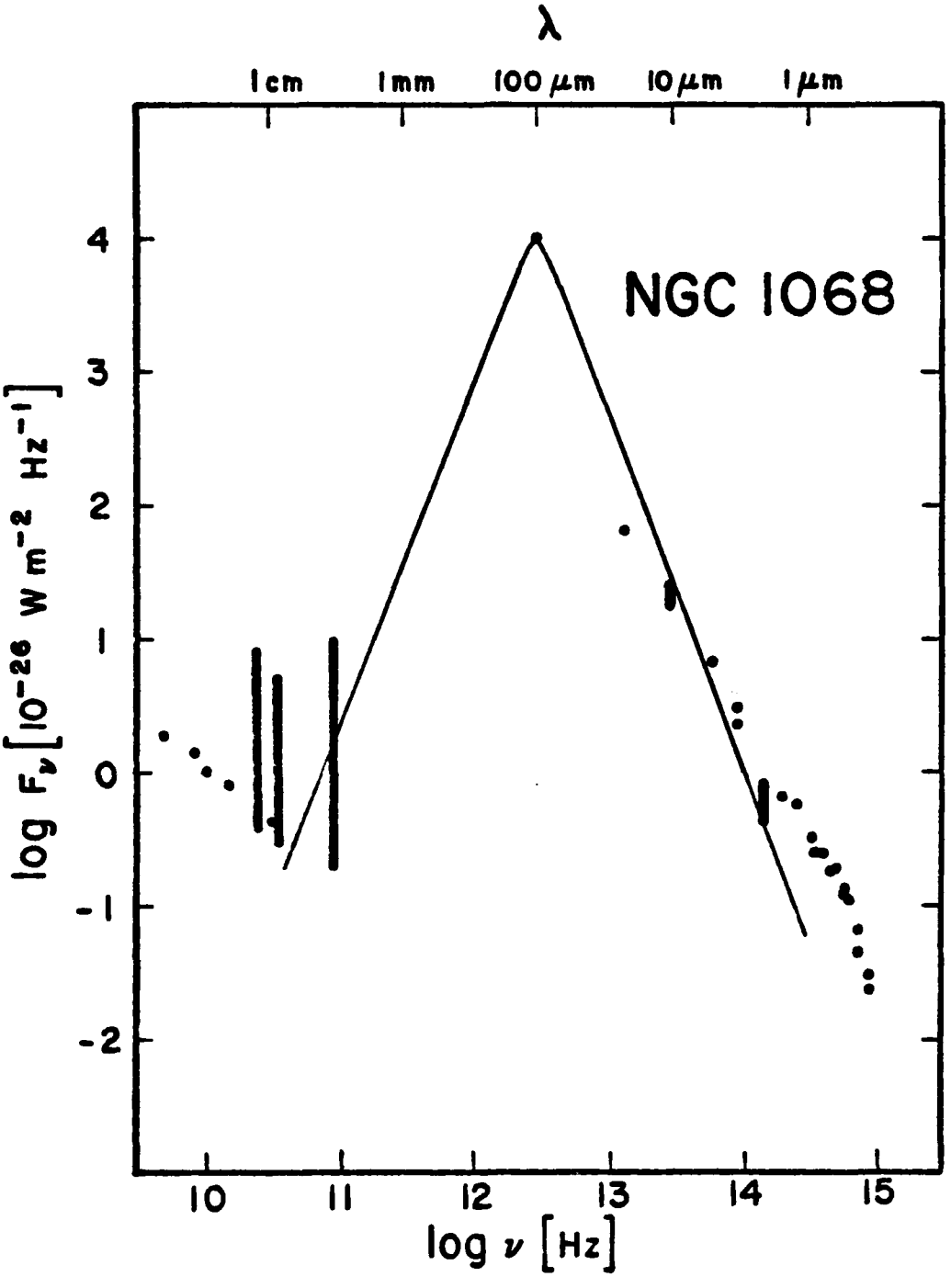

Figure 15. The Homogeneous Synchrotron Radiation Model of the Observed Spectrum of NGC 1068

The data used in this figure are described in the caption to Figure 14.

It follows from the above discussion that it does not seem possible to explain the infrared spectrum from the nucleus of NGC 1068 by means of an optically thick (at 3×10^{12} Hz), homogeneous, spherical source of relativistic electrons radiating by the synchrotron process if the size of the source is restricted by the shortest observed time scale of variability of the flux (suggested, but not shown conclusively, by the 2.2-μm observations) and if we wish to satisfy the condition that the scattering of the photons produced by the synchrotron radiation process off the relativistic electrons by means of the inverse Compton process be sufficiently small to be consistent with the observations of the spectrum of NGC 1068.

A similar model approach to explaining the observed spectrum of NGC 1068 by means of an optically thick, homogeneous, spherical source of synchrotron radiation has been presented by Bergeron and Salpeter (1971). In this model the authors assume (from the observations of NGC 1068) the values of the infrared luminosity ($= 5 \times 10^{44}$ erg s^{-1}, or one tenth the observed value quoted by Low and Aumann), the X-ray luminosity ($= 10^{43}$ erg s^{-1}, or three times the upper limit quoted by Gursky *et al.*), the frequencies ν_1 ($= 6 \times 10^{12}$ Hz, at the extreme edge of the 100-μm bandpass observations) and ν_{cs} ($= 1.1 \times 10^{17}$ Hz), and the index γ ($= 6$). From the two luminosities we determine the value of r ($= 50$). From these assumed parameters they derived the model parameters,

$$H = 300 \text{ gauss},$$

$$R = 2.6 \times 10^{15} \text{ cm},$$

$$\Gamma_1 = 1.2 \times 10^2, \text{ and}$$

$$n = 2.9 \times 10^2 \text{ cm}^{-3}.$$

This model by Bergeron and Salpeter is able to explain the observed flux spectrum of NGC 1068 and allows for variability on a time scale as short as one day. It must be pointed out, however, that the model is successful only with a rather strained interpretation of the observed spectrum. This model also suffers from the drawback of any homogeneous model as indicated above. It does not offer a good fit to the spectrum, but passes through only two points (in a straight line in the log-log plane) of the observed spectrum, the assumed peak and the point at a wavelength of 22 μm. This deficiency of not fitting the spectrum well has been stressed in a subsequent paper (in preparation) by Bergeron and Salpeter (1972), wherein they indicate the need to find a detailed model which attempts to fit all the observed data (as done later in Chapter 5 of this dissertation). It is also pointed out in the subsequent paper that when a more likely value of ν_1 is used, the model is incompatible with the observations, as it gives a too high millimeter flux.

Inhomogeneous Models

The result from the homogeneous synchrotron radiation model that the spectral index in the optically thick region of the spectrum is not large enough to match the observed spectrum in NGC 1068 has been investigated by Ozernoy and Sazonov (1971). They have shown that it is possible to have the spectral index either greater than or less than the normal value of 2.5 in the optically thick region of a source of synchrotron radiation depending on whether the magnetic field increases or decreases, respectively, in going from the center toward the boundary of the source. The assumptions in their model are similar to the

assumptions made in the homogeneous model discussed in the previous section except for the inhomogeneous magnetic field and the fact that their model had plane symmetry rather than spherical symmetry.

The more serious drawback of the homogeneous model is the size restriction inferred from the variability of the flux. Pacholczyk (1970b), in a discussion similar to one presented by Rees and Sciama (1966), has discussed briefly the effect of having an inhomogeneous magnetic field, one decreasing from the center outwards toward the boundary of the source, giving rise to the synchrotron emission. At a given distance from the center, the source would be optically thick to radiation up to a frequency, the value of which would depend upon the specific parameters of the model. At smaller distances (higher magnetic field values) the source would be optically thick up to a higher frequency. Therefore at a given distance the source is optically thin to all radiation transmitted from interior to that distance. Stated differently, we can say that the radiation observed in a given frequency range would arise from a rather narrowly defined range of distance from the center of the source, and radiation of lower frequencies would be emitted primarily at greater distances. It may be possible to satisfy the inverse Compton scattering condition in this way because the magnetic field required to make the source optically thick at a given distance will also be high enough so that the electron energy losses due to inverse Compton scattering are sufficiently less than the synchrotron energy losses.

From equation (64) it can be shown that the following approximate proportionality holds:

$$H \propto \nu_1^{\gamma+4} R^4, \tag{83}$$

where ν_1 is the frequency at which, for a given distance, the source becomes optically thick or the frequency at which most of the radiation is emitted at the given distance. If the time scales of variability of the flux in different regions of the spectrum of NGC 1068 are used to determine the relationship between the distance from the center of the source and the frequency at which radiation is emitted at that distance, then we would expect ν_1 to depend on the -1/2 to -1 power of the distance from the center; and therefore the magnetic field depends on the $-(\gamma - 4)/2$ to $-\gamma$ power. There is a large uncertainty in this exponent, but it does show that the magnetic field must decrease with distance from the center.

According to the results of Ozernoy and Sazonov discussed above, this condition will only make worse the match of the spectrum of the model to the observed spectrum of NGC 1068 in the optically thick range, because an increasing magnetic field from the center of the source is required to achieve the observed more negative value (than -2.5) of the spectral index. Therefore some other mechanism would be required to account for the large spectral index between the millimeter wavelength and the 100-μm regions.

Furthermore, the radiation from a given distance is not emitted at a single frequency, but has a distribution in frequency with a spectral index corresponding to some value of γ. If we sum up the radiation from throughout the source, the resulting spectrum will have a much smaller apparent value of γ because of the smearing out of the frequency

distribution of the radiation. The actual value of γ must be considerably higher than the apparent value. The required values of γ become so high that it is sufficiently accurate to disregard the power-law distribution of electron energies and instead assume that the electrons have a monoenergetic distribution with the value of the energy depending on the distance from the center of the source.

CHAPTER 5

A SYNCHROTRON RADIATION MODEL OF THE NUCLEUS OF NGC 1068

We have shown in the previous chapter that neither blackbody radiation nor thermal bremsstrahlung can explain the infrared spectrum of NGC 1068, and a large dust cloud around a small ultraviolet central source cannot produce the required amount of radiation, if the size of the cloud is restricted by the variability of the 2.2-μm flux (that is, if the light travel time across the cloud is less than the time scale of variability). A model of a homogeneous source of synchrotron radiation, optically thick around a wavelength of 100 μm (a frequency of 3×10^{12} Hz), with the same size restriction requires a magnetic field strength which leads to the condition that the energy losses of the electrons due to inverse Compton scattering are too great compared to the energy loss losses due to synchrotron radiation to be consistent with the observed ratio of the infrared luminosity to the luminosity in any higher frequency region of the spectrum. However, the model of a synchrotron radiation source seems to be improved if we consider a non-homogeneous source, particularly if we assume that the different spectral components are produced in different physical components of the source.

Introductory Remarks

For the inhomogeneous model briefly discussed in the last section of Chapter 4, there is some indication that it may be possible to avoid simultaneously both the inverse Compton scattering problem and the

size restriction by having the size of the radiation region, which emits radiation primarily at a characteristic frequency, restricted by the time scale of variability at this frequency. The disadvantages of this model are that the power-law distribution of electron energy is no longer consistent with the model and that it may be necessary to solve simultaneously the radiation transfer and the electron energy distribution in the energy-coordinate space in more rigorous numerical detail in order to keep the model self-consistent. But it was indicated at the beginning of Chapter 4 that rigorous models are probably not justified by the present accuracy of our knowledge of the infrared spectrum and the variability of the flux from the nucleus of NGC 1068.

The lowest order numerical approximation to the inhomogeneous model (and the simplest improvement over the homogeneous model) is to consider a source with two regions which are themselves homogeneous, but have different physical conditions within. We can satisfy the size restrictions implied by the observed variability of the flux by attributing different parts of the spectrum, which have different time scales of variability, to these physically separate sources of synchrotron radiation.

In the stationary model presented in this chapter, there is a small central source which produces the radiation of Component II of the spectrum and which is restricted in size by the 2.2-μm variability. There is also a source with double (for reasons to be discussed later) structure which is restricted in size by the millimeter variability and which corresponds to Component I of the spectrum. The radiation from both components is produced by electrons radiating according to the

ordinary synchrotron mechanism. It was indicated in Chapters 3 and 4 that the time scales of variability (or even the fact of variability itself) of the flux are not well established. However, the most restrictive conditions on the size, imposed by the shortest reported time scales of variability of the flux of NGC 1068, will be retained in the following model. These restrictions should provide the most difficult case for the model since any model of a larger size should fulfill most of the physical requirements more easily than a smaller model. The model is developed according to the equations presented in Chapter 4 in connection with the homogeneous synchrotron radiation model.

Component I

Let us assume that spectral Component I is produced in two identical homogeneous, spherical sources of electron synchrotron radiation of 3.16×10^{16} cm radius, the restriction from the millimeter variability (the separation between the two components does not necessarily affect the following discussion), and that the density of the relativistic electrons has a power-law distribution in energy given by equation (54). If the turnover in the spectrum at 3.16×10^{12} Hz is caused by the source becoming optically thick on the low frequency side of the 100-μm peak, we can determine the strength of the magnetic field from equation (64), the relation between the field and the frequency at thick the source becomes optically thick, the (solid) angular size of the source, and the flux density at some frequency in the optically thin region. The spectral index, $\alpha = 4$, between the wavelengths of 100 μm and 20 μm leads to a value of $\gamma = 9$ by equation (61). If we take the distance of

NGC 1068 to be 13 Mpc and note that F_ν = 70 f.u. at $\nu = 10^{13}$ Hz for each half of Component I, we find that H = 390 gauss. The magnetic energy density in the source is greater than the radiation energy density by a factor of 130, as shown by equation (81). The low energy limit of the relativistic particles is found from equation (65) to be about 46 times the electron rest mass energy, and therefore we see from equation (80) that the spectrum produced by inverse Compton scattering will peak around 10^{16} Hz. The ratio r (by inspection of the spectrum of NGC 1068 shown in Figure 11) must be $\gtrsim$ 100. The value of 130 seems to just satisfy the inverse Compton scattering condition. The lifetime t of the particles before losing half of their energy through synchrotron losses from equation (67) is 73 sec. Since the lifetime of the source of radiation in NGC 1068 is much greater than this particle lifetime, the particles must be accelerated essentially constantly by some (as yet unspecified) process throughout the 3.16×10^{16} cm region. In order to produce half of the observed luminosity of 5×10^{45} erg s^{-1}, the density n of the relativistic particles from equation (68) must be about 37 cm^{-3} in both parts of Component I. The frequency below which the effect of the relativistic plasma is important [see equation (78)] is sufficiently low so that it satisfies any of the observational conditions.

We can find the effect on the derived parameters of varying the assumed parameters, ν_1 and R, just as for the homogeneous synchrotron radiation model in Chapter 4 (see Table 12). The effects are described by equation (82) and are given in Table 13. Here we have varied the values of ν_1 and R so that r = 300, where ν_1 is allowed to vary as far as the obsevational uncertainties will allow. We see that, if

Table 13. Variation of the Derived Parameters of Component I - Double Structure

ν_1 [Hz]	1.5×10^{12}	3.16×10^{12}	3.16×10^{12}	3.26×10^{12}	5×10^{12}
R [cm]	2.57×10^{17}	3.16×10^{16}	3.44×10^{16}	3.16×10^{16}	7.82×10^{15}
H [gauss]	210	390	550	570	1100
Γ_1	63	46	39	38	27
t [s]	190	73	44	42	15
n [cm^{-3}]	.13	37	21	25	850
ν_s [Hz]	.0025	.51	.24	.29	7.0
r	300	130	300	300	300

$\nu_1 = 1.5 \times 10^{12}$ Hz, a size of 2.6×10^{17} cm, or about three times the assumed size which is consistent with every reported variability of the flux concerned with Component I, is required. However, if $\nu_1 \gtrsim 2.2 \times 10^{12}$ Hz, the size restriction of 3.16×10^{16} cm and the inverse Compton scattering condition can be satisfied simultaneously for any acceptable value of ν_1. For the largest likely value of ν_1 (5×10^{12} Hz), the radius of the source can be as small as 7.8×10^{15} cm, or about one tenth of the upper limit imposed by the variability of the flux.

The spectral index resulting from synchrotron self-absorption in the frequency range below 3×10^{12} Hz is 5/2; but this is not steep enough to be consistent with the quiescent level flux density, 0.2 f.u., at a frequency of 90 GHz. In order to obtain better agreement with the observed overall spectral index in the optically thick region and the observed flux in the short millimeter wavelength range, we propose that the synchrotron radiating double source of Component I is surrounded by an ionized cloud of thermal electrons and protons with electron density, N_e, and temperature, T_e, and a radius, R_t. Suppose the optical depth of the ionized cloud produced by free-free absorption [see equations (49) to (51)] is of the order of unity at a frequency, $\nu_t = 3 \times 10^{11}$ Hz:

$$1 = \tau_\nu{}^t = 1.78 \times 10^{-2} \, g \, \nu_t{}^{-2} \, T_e{}^{-3/2} \, N_e{}^2 \, R_t \, . \qquad (84)$$

This thermal gas is subject to several restrictions. The flux density,

$$F_\nu{}^t = 1.43 \times 10^{-89} \, g \, e^{-h\nu/kT_e} \, T_e{}^{-1/2} \, N_e{}^2 \, R_t{}^3 \, , \qquad (85)$$

of radiation [see equations (48), (50), and (52)] reemitted by the gas

must certainly be less than the observed composite spectrum everywhere and less than the observed upper limits in the ultraviolet, F_{UV}, (Code 1969) and the X-ray, F_X, (Gursky *et al.* 1971) regions. The total luminosity of the thermal gas,

$$L_t = 6.01 \times 10^{-27} \, g \, T_e^{1/2} \, N_e^2 \, R_t^3 \, , \qquad (86)$$

must be no greater than the amount of radiation absorbed, $\simeq 10^{42}$ erg s^{-1}; and if the thermal cloud surrounds the entire source, including Component II (to be discussed in the next section), then the optical depth, τ^T, due to Thomson scattering of the radiation off the electrons must be less than unity:

$$1 > \tau^T = 6.65 \times 10^{-25} \, N_e \, R_t \, , \qquad (87)$$

in order for any of the very short time scale variability of the 2.2-μm flux to be detectable. If the thermal gas surrounds only the two components of Components I, the last restriction can be dropped.

These relationships between N_e and T_e for $R_t = 3 \times 10^{17}$ cm are shown graphically in Figure 16. [The restriction in the ultraviolet is taken more severely than indicated by the observations of Code (1969).] The possible range of the values of N_e and T_e lies on the line representing the solution, $\tau_\nu^t = 1$, and below the lines representing the restrictions described above. A thermal cloud of electrons and protons of radius, $R_t = 3 \times 10^{17}$ cm, with N_e up to 5×10^6 cm^{-3} and T_e up to 6×10^4 °K seems to satisfy all the above conditions. We shall choose the conditions, $T_e = 10^4$ °K and $N_e = 1.6 \times 10^6$ cm^{-3}, for the thermal gas cloud of radius $R_t = 3 \times 10^{17}$ cm which provides the mechanism for

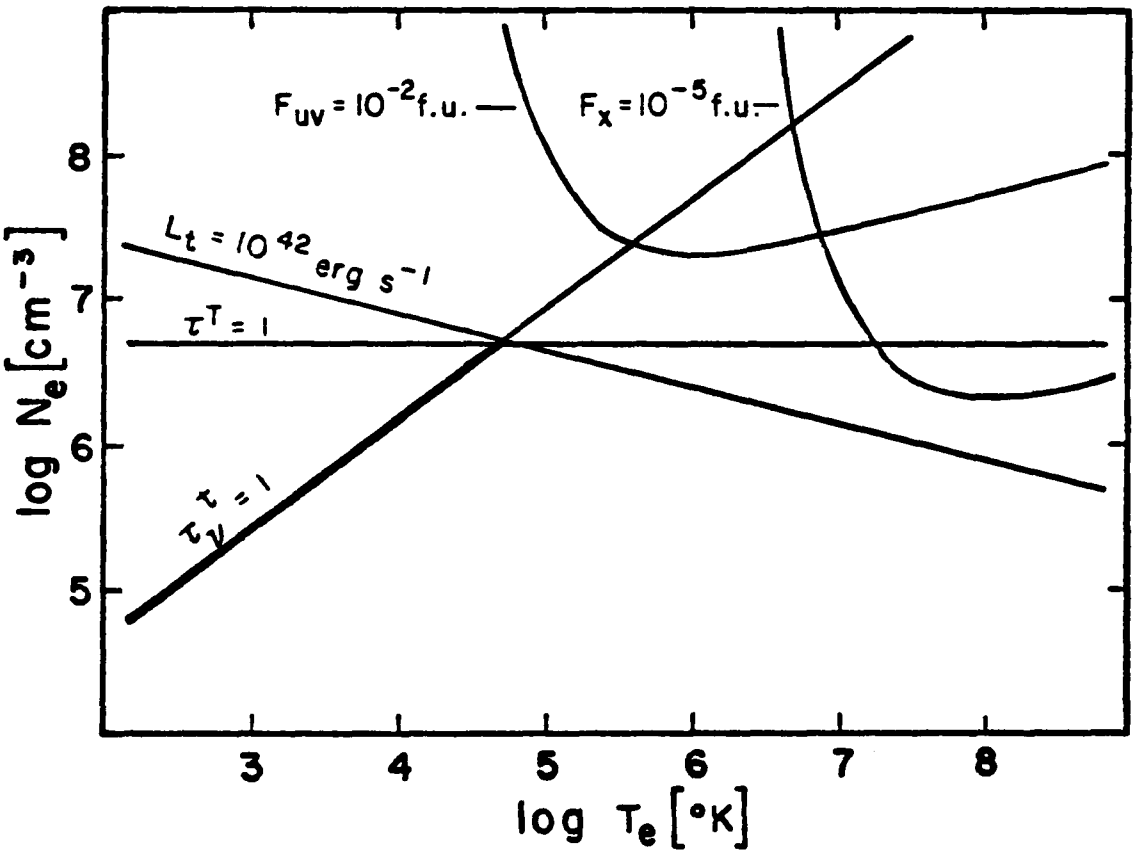

Figure 16. The Possible Values of N_e and T_e of the Thermal Cloud Around Component 1.

The acceptable range of the solution of $\tau_\nu^t = 1$ lies below all the other curves and is indicated by the use of a heavier line.

causing a sharp decrease in radiation in the frequency range below 3×10^{11} Hz.

The spectrum produced by the double source of synchrotron radiation (with $\nu_1 = 3.16 \times 10^{12}$ Hz and $R = 3.16 \times 10^{16}$ cm) surrounded by the thermal cloud described above is shown in Figure 17 as the curve 1, while the flux spectrum from the thermal gas is indicated by F_ν^t.

We can see that the flux of radiation produced by the thermal gas is quite negligible compared to the observed values of the flux in any region of the spectrum, except possibly in the ultraviolet region of the spectrum, where it might be possible to detect such a source if it were present. The Hα luminosity of this gas can be shown [see, for example, Aller (1956), p. 119] to be just slightly less than the observed luminosity of 2.3×10^{41} erg s^{-1} (Pacholczyk and Weymann 1968a). The predicted luminosity in Hα from the thermal gas of this model is of the order of, or slightly less than, 10^{41} erg s^{-1}, and so it might be possible to identify this thermal cloud with the source of, at least, some of the observed hydrogen line emission.

The variation in the flux in the millimeter region could be caused by a variation in the emission in the infrared synchrotron components, which would produce a corresponding change in the millimeter flux, or by a variation in the density of the thermal cloud, which would produce the same relative change in the frequency at which the thermal cloud becomes optically thick. In this latter case the variation in the millimeter flux could be large because of the lateral shifting of an exponentially decreasing curve. Variation of the millimeter flux of any reported amplitude can therefore be ascribed to small changes of the

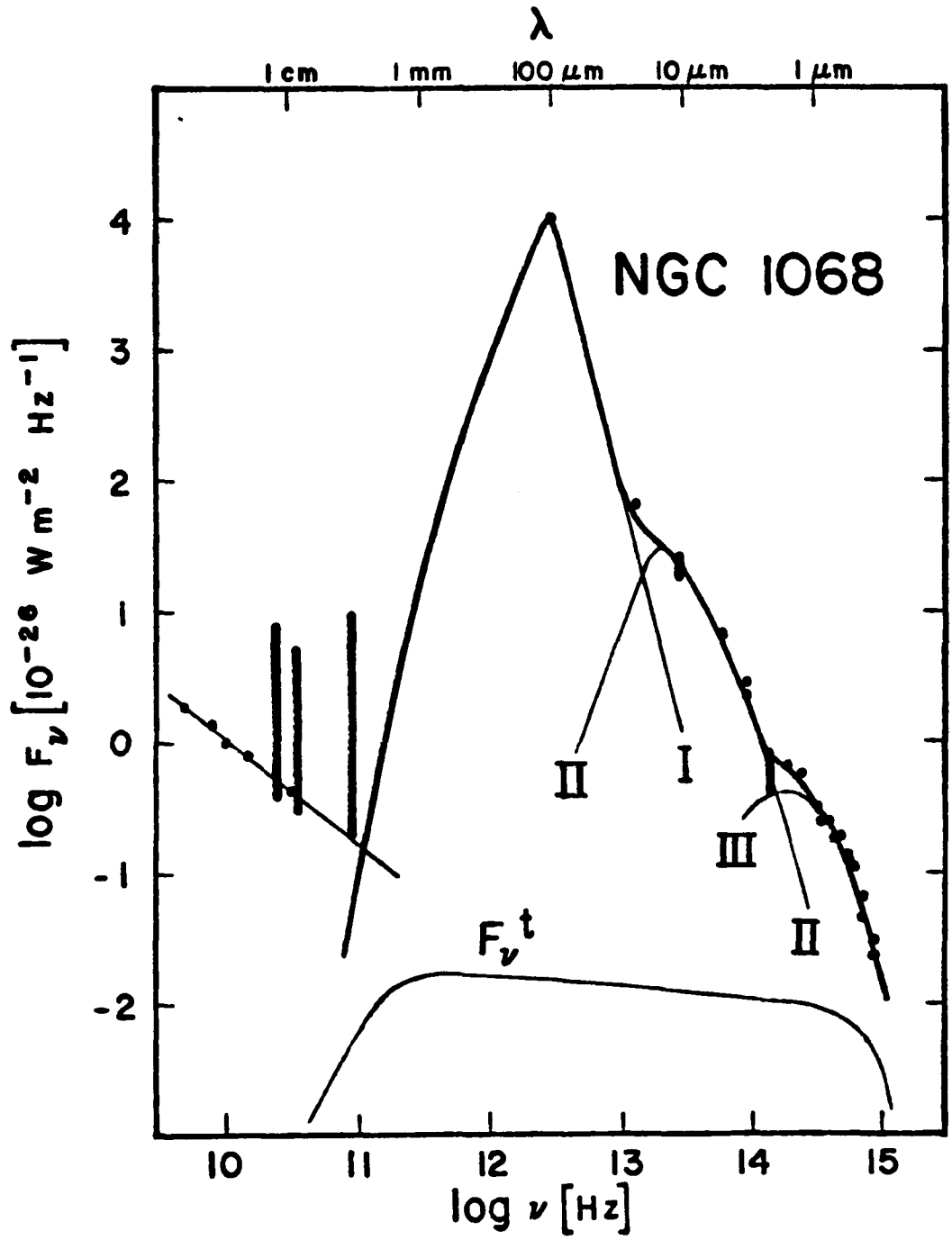

Figure 17. A Synchrotron Radiation Model Spectrum Compared to the Observed Spectrum of NGC 1068

The data used in this figure are described in the caption to Figure 14. The designations I, II, III, and F_ν^t are described in the text.

physical conditions in the radiating regions with an appropriate combination of the above effects. Of course, if the variation were to be caused by changes in the conditions of the thermal gas cloud, this would also produce variation in the hydrogen line emission. We might point out here that Walker (1972) has detected "a quite significant change" in the strength of the Hα line in emission from NGC 1068 between September 1971 and October 1971. Variation of the Hβ line in absorption in another Seyfert galaxy, NGC 4151, has been reported by Cromwell and Weymann (1970).

Component II

If we assume that the radius of the source of the electron synchrotron radiation of Component II is 10^{15} cm (restricted by the reported variability of the 2.2-μm flux), that the source is optically thick to its own radiation at 2×10^{13} Hz, and that $\gamma = 5$ (from $\alpha = 2.0$), then we get a value for the magnetic field from equation (64) of 2.6×10^{5} gauss. This value is easily sufficient to keep the electron energy losses due to inverse Compton scattering much smaller than the energy losses due to synchrotron radiation. The observed spectrum of NGC 1068 would require that $r \gtrsim 100$ to satisfy the inverse Compton scattering condition. We have taken $F_{\nu} = 15$ f.u. at $\nu = 4 \times 10^{13}$ Hz in determining the magnetic field strength. The lower end of the range of the energy of the particles is just moderately relativistic, about 6 times the electron rest mass energy, while the high end is about 40 times the rest mass energy. The lifetime of the particles against synchrotron losses is 1.3×10^{-3} sec, implying that the particles must

be accelerated constantly by some mechanism throughout the source; and the density of the relativistic electrons is 6.9 cm^{-3}. [See equations (65), (67), and (68).]

Let us now look at the effect of varying the assumed parameters as was done for Component I in Table 13. In the case of Component II we will allow ν_1 (within the limits of the observational uncertainties) and R to vary such that we will have r = 100, which is sufficiently large to satisfy the observational restriction imposed by the luminosities in any higher frequency region of the spectrum. The results are given in Table 14. We see that over the entire acceptable range of ν_1 it is possible to choose a size which can simultaneously satisfy the condition, r = 100, and the size restriction, $R \lesssim 10^{15}$ cm, imposed by the shortest reported time scale of variability of the flux (at 2.2 μm). The largest size for any likely value of ν_1 is less that 7×10^{14} cm.

The curvature in the spectrum for frequencies greater than 6×10^{13} Hz can be produced by having a high energy cut-off, or some other divergence from a simple power law [for a discussion, see Section 6.5 of Pacholczyk (1970a)], in the electron energy distribution around an energy of 20 times the electron rest mass energy. The flux spectrum produced by this small source is shown in Figure 17 as the curve II. Component III, described in Chapter 4, is shown as the curve III in Figure 17.

In the discussion of Component II of the spectrum of NGC 1068 in Chapter 4, it was noted that an explanation for the existence of very rapid variability of the flux at 2.2 μm, together with the non-existence of similar variability at 5 μm and 10 μm, would be discussed in this

Table 14. Variation of the Derived Parameters of Component II

ν_1 [Hz]	1.5×10^{13}	2×10^{13}	2×10^{13}	3×10^{13}
R [cm]	6.82×10^{14}	3.95×10^{14}	10^{15}	1.82×10^{14}
H [gauss]	4.3×10^{3}	6.4×10^{3}	2.6×10^{5}	1.1×10^{4}
Γ_1	44	36	5.6	27
t [s]	.64	.34	.0013	.15
n [cm^{-3}]	1.3×10^{3}	4.6×10^{3}	6.9	2.6×10^{4}
ν_s [Hz]	.46	13	3.0×10^{-4}	5.6
r	100	100	1.1×10^{6}	100

section. The explanation of the variability is analogous to the explanation of the millimeter variability suggested at the end of the last section. We have indicated above that a cut-off in the electron energy spectrum would provide the curvature in the spectrum of the model necessary to match the observed spectrum of NGC 1068. We have also seen that the lifetime of the electrons which provide the radiation of Component II is very short. If the mechanism which accelerates the electrons to relativistic velocities is not constant at all times, then the frequency at which the curvature in the intensity spectrum begins, ν_H, would not be fixed. Since the higher energy electrons radiate faster, the higher energy end of the electron energy distribution is depleted first. Therefore if the acceleration mechanism is interrupted, the high energy electrons will be depleted rapidly, and ν_H will decrease correspondingly rapidly. The effect of all this is to decrease the intensity very rapidly at a given frequency; and because the intensity spectrum curves down steeply above ν_H, the variability of the measured flux can occur very rapidly. The amplitude of the variability at a given frequency ν depends very strongly on the closeness of ν to ν_H. Applying all this to the case of NGC 1068, if 6×10^{13} Hz = $\nu_H < 1.4 \times 10^{14}$ Hz (2.2 μm), then the 2.2-μm flux may be able to show rapid variability of a large amplitude, while the variability at 5 μm and 10 μm ($< \nu_H$) might show very rapid variability, but with an amplitude which is not detectable.

Discussion

The homogeneous synchrotron model presented in Chapter 4 was shown to be an inadequate representation of the infrared spectrum of

NGC 1068 primarily as a consequence of the small size implied by the time scale of variability of the flux. The inhomogeneous model in that chapter, while solving some of the problems of the homogeneous model, introduces some drawbacks of its own. The use in this chapter of some features of both models has led to an explanation of the spectrum from the millimeter wavelength region to the visual region which appears to be self-consistent and which provides a satisfactory fit to the observed spectrum of NGC 1068.

It has been noted above that the most restrictive condition on the size of the source in the model, namely that the size assumed in the model corresponds to the shortest reported time scale (at an infrared wavelength of 2.2 μm) of the variability of the continuum flux, may be too strong a constraint if it is shown in the future that the time scale indicated by the observations at 2.2 μm is definitely incorrect. The model presented here should be understood as the most difficult possible case consistent with the observations now available.

In the model presented in this chapter we suggested that there is a very small source of optically thick synchrotron radiation in the center of the nucleus of NGC 1068, giving rise to the higher frequency infrared component (Component II) of the flux spectrum. Separate from this source we suggested the presence of a much larger double source of optically thick synchrotron radiation surrounded by a larger cloud of optically thick electrons and protons absorbing according to the free-free mechanism. The radiation produced by this double source accounts for the lower frequency infrared component (Component I). The physical

conditions derived for these sources in the previous two sections are presented schematically in Figure 18.

There seems to be no reason to require that both spectral Components I and II be produced in the same physical source. On the contrary, the separation into small and large sources appears to be necessary in order to have a self-consistent model of optically thick synchrotron radiation still satisfying the inverse Compton condition. While two concentric sources would not be impossible, it would seem to require a rather unexpected acceleration mechanism in order to produce the different distributions of electrons in the two sources, with the lower energy electrons in the center of the source.

Assuming that the two sources are not concentric, a double structure for the larger source presents a more symmetric model, which might be more likely to be formed. Furthermore, this type of double structure has been detected, or is at least consistent with the observations, in the quasi-stellar objects, 3C 147 (Donaldson and Smith 1971) and 3C 273 and 3C 279 (Knight *et al.* 1971). Another rather weak argument for the proposed type of double structure is the analogy to the large double radio sources of hundred-kiloparsec sizes with relatively lower magnetic fields ($H \approx 10^{-5}$ gauss) and higher particle energies ($\Gamma \approx 10^{3}$ to 10^{5}) and the small variable sources in the centimeter wavelength region of parsec sizes or smaller with relatively higher magnetic fields ($H \approx 10^{-3}$ to 10^{-1} gauss) and lower particle energies ($\Gamma \approx 10^{1}$ to 10^{3}).

In spite of the above arguments for the double-structured source which produces Component I of the spectrum and a separate source which

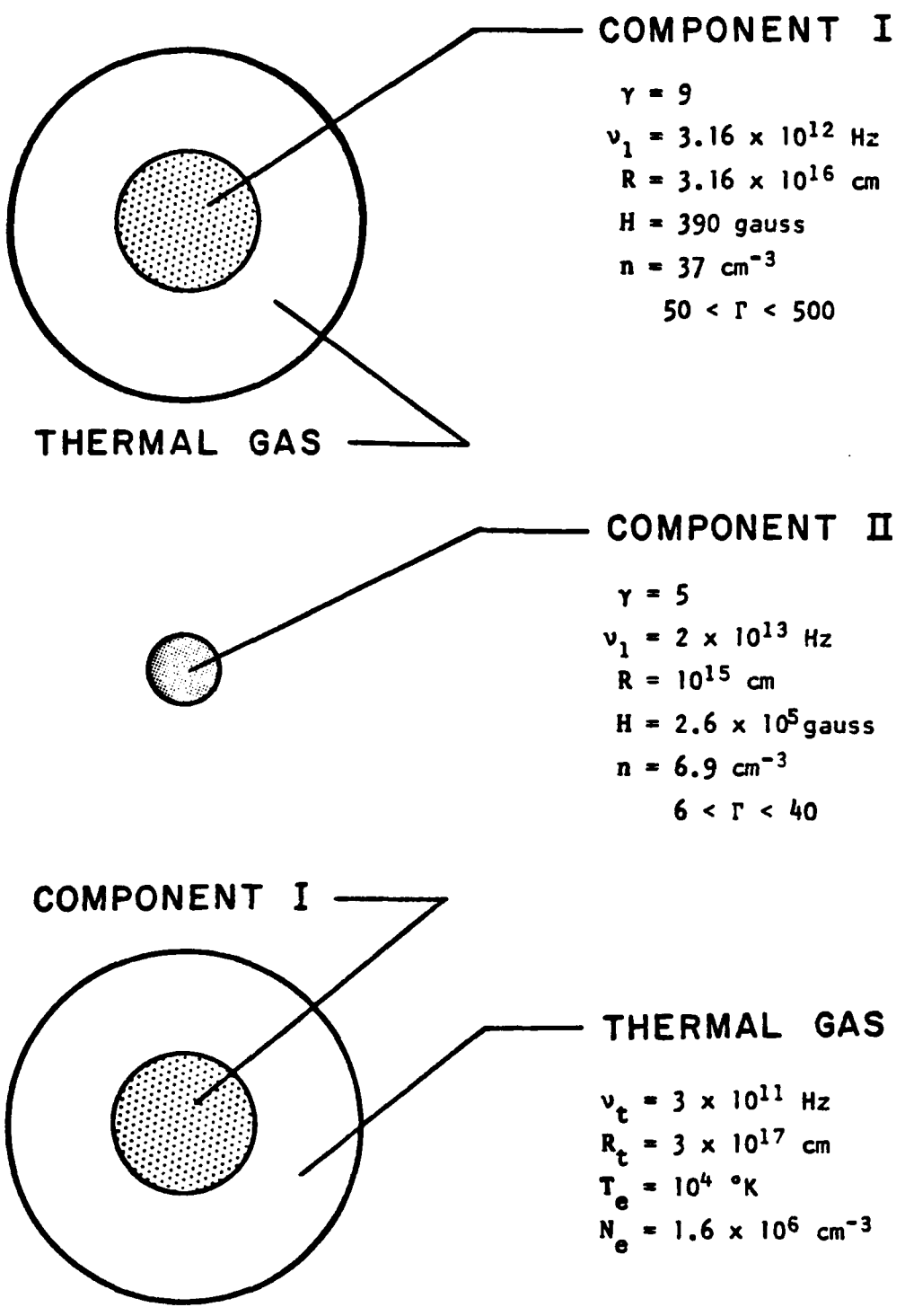

Figure 18. Schematic Presentation of the Infrared Synchrotron Model of the Nucleus of NGC 1068

produces component II, let us look at a source with simpler geometry. Specifically we can look at the case where the double source is replaced by a single source and where Components I and II are concentric and further surrounded by the thermal gas cloud. If we follow the outline of the section Component I in this chapter with the same assumptions and variation of the assumed parameters, the results of the calculations for the variation of the derived parameters of a single source for Component I are given in Table 15. We see that in this case it is slightly more difficult than for the case of the double-structured Component I to satisfy simultaneously the size restriction and the inverse Compton scattering condition, although it is still possible for acceptable values of ν_1 and R. A minimum frequency of $\nu_1 = 2.12 \times 10^{12}$ Hz is required in order to satisfy a size restriction of 10^{17} cm while $\nu_1 = 3.67 \times 10^{12}$ Hz is required in order to satisfy a size restriction of 3.16×10^{16} cm. A choice of parameters, taken from Table 15, for the single structured Component I is shown in the schematic presentation of Figure 19.

Figure 19 shows schematically the simple geometric model where the two synchrotron radiation components and the thermal gas cloud are all concentric. The parameters from Component II and the thermal gas cloud are taken from the previous two sections of this chapter. In this model the radiation produced in the inner sphere is readily transferred through the outer spheres because the frequencies at which the outer sphere will become optically thick to either thermal absorption or synchrotron self-absorption are lower than for the inner sphere. We have also satisfied the condition that the thermal gas cloud is

Table 15. Variation of the Derived Parameters of Component I - Single Source

ν_1 [Hz]	1.5×10^{12}	3.16×10^{12}	3.16×10^{12}	3.67×10^{12}	5×10^{12}
R [cm]	3.63×10^{17}	3.16×10^{16}	4.86×10^{16}	3.16×10^{16}	1.1×10^{16}
H [gauss]	210	98	550	670	1100
Γ_1	63	92	39	35	27
t [s]	190	590	44	32	15
n [cm^{-3}]	.092	300	14	43	600
ν_s [Hz]	.0018	8.2	.17	.45	5.0
r	300	4.0	300	300	300

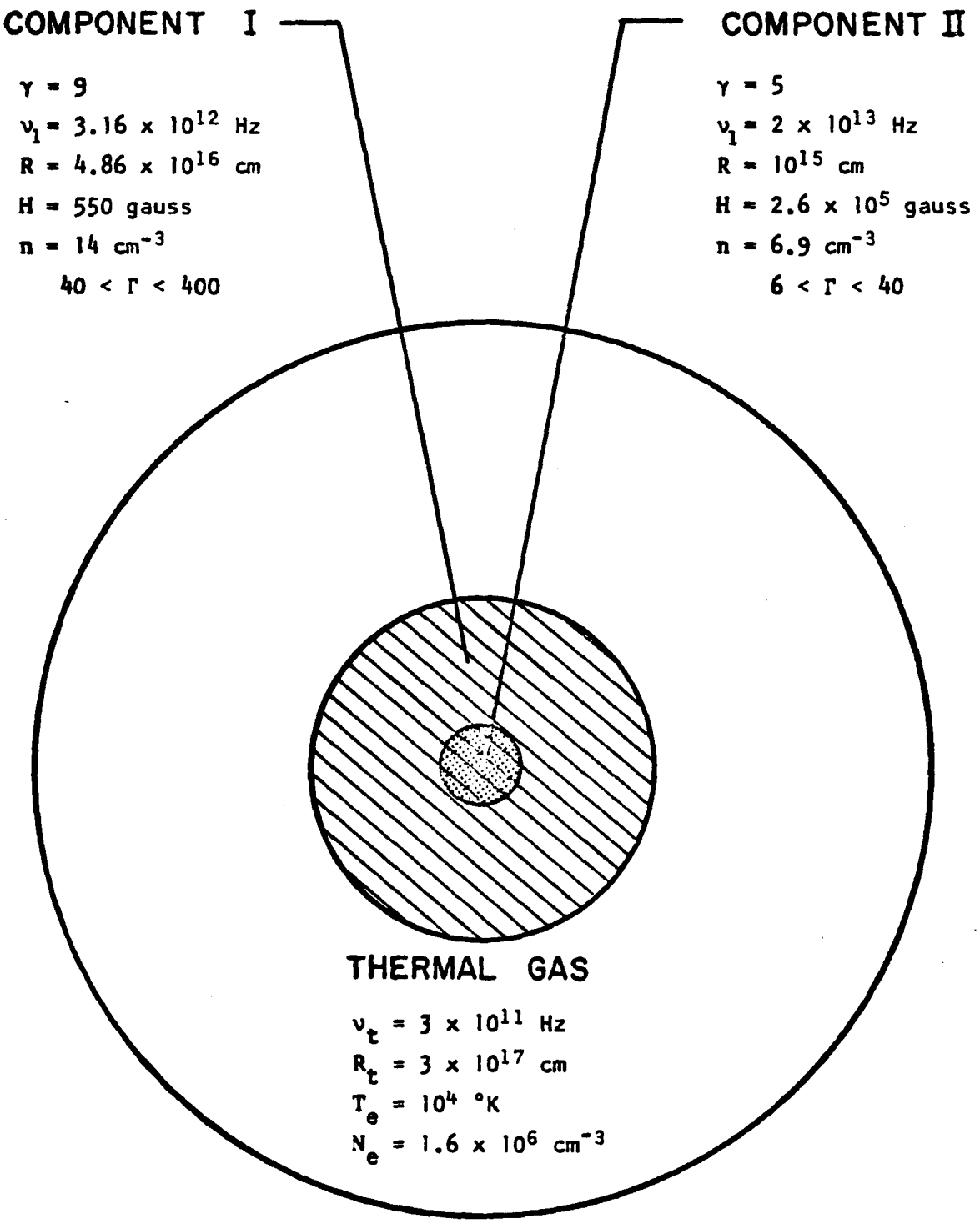

Figure 19. Schematic Presentation of a Concentric Radiation Model of the Nucleus of NGC 1068

optically thin to Thomson scattering, and therefore any variability produced in the inner spheres will not be smeared out in passing through the thermal gas cloud.

CHAPTER 6

PERSPECTIVES

In this last chapter we will summarize the major features of this dissertation and comment briefly on several points which have been accepted with perhaps too little discussion. The overall goals of the research have been the completion of a program of millimeter wavelength observations of Seyfert galaxies and related objects (quasi-stellar objects and N-type galaxies) and the development of a synchrotron radiation model of the infrared spectrum from the nuclei of Seyfert galaxies, in particular of NGC 1068.

Seyfert galaxies have been defined classically as galaxies with very small apparent nuclei, with broad hydrogen Balmer emission lines, and with high excitation conditions in the line-producing region of the nucleus. We have seen that there are several classes of objects which are similar to Seyfert galaxies. These include Zwicky's compact galaxies, N-type galaxies, Markarian objects, and quasi-stellar objects. The classification of Seyfert galaxies is made nearly unambiguous by the simple definition as galaxies whose nuclei show broad emission lines (indicating Doppler line widths $\gtrsim$ 500 km s^{-1}). Seyfert galaxies also tend to have a very high infrared luminosity, and it is not uncommon to have a variable continuum flux density in one or more regions of the flux spectrum.

Summary and Conclusions

The most important information gained from the program of observing a sample of Seyfert galaxies and related objects at a wavelength of 3.3 mm is that the characteristics of the millimeter radiation are related to the longer wavelength radio, rather than to the shorter wavelength infrared, radiation. This seems to be true for both the value of the flux density and the characteristics of the time variability of the flux when the source is clearly variable. The one exception is the case of NGC 1068 where there is some indication that the millimeter flux may be variable, whereas the centimeter flux is quite probably not variable. In general, the millimeter observations indicate that the flux spectra are likely to increase very rapidly with frequency between 10^{11} Hz and a few times 10^{12} Hz. The confidence in the results is demonstrated through a statistical analysis of the characteristics of the overall system errors, an analysis of the results of observing "blank" sky and observations of sources (both strong and weak) whose flux is known to be constant, and by an analysis of variance procedure for seven sources which were observed extensively (monitored for variability).

In discussing the spectrum of NGC 1068, it was indicated that there is considerable controversy concerning the characteristics of the time variability of the continuum flux. The observations of variability in the millimeter region are by no means certain at this time. Continued frequent monitoring of the source is still needed. The shortest time scale of variability, $\lesssim$ 1 day, has been reported for the 2.2-μm flux, but there is some indication that the flux cannot vary by more than a factor of two with this short time scale. The variability of

the 10-μm flux on a time scale of several months, comparable to the time scale of variability of the millimeter flux, appears to be confirmed.

The shortest reported time scales of variability were used to impose restrictions on the sizes of the models of the radiation source from the nucleus of NGC 1068. This was done not to indicate any blind acceptance of the observations, but only to develop a model which might be required to have the small size restrictions if future observations confirm further the presently reported time scales of variability. In addition, determining the size of the source by equating the time scale of variability of the continuum flux to the light-travel time across the source might not be a sufficiently strong constraint on the size if the source does not vary coherently.

Homogeneous models of the source of the infrared radiation from the nucleus of NGC 1068, whether thermal or synchrotron radiation, are not adequate representations of the real source. The thermal models fail because they cannot produce enough radiation in the small volumes, while the synchrotron model requires a magnetic field strength which leads to the condition that electron energy losses are greater for inverse Compton scattering than for synchrotron emission. This condition implies that the luminosity in the Compton-scattered spectrum is greater than in the infrared, contrary to what is observed or presumed for NGC 1068. Synchrotron models with an inhomogeneous magnetic field strength are able to solve some of the problems of the homogeneous model, but they introduce other difficulties involving the energy distribution of the electrons and the spectral index of the resulting spectrum.

The model presented in Chapter 5 is a very simple inhomogeneous model of the infrared radiation from the nucleus of NGC 1068. In that model we have attributed radiation for decreasing frequencies (with increasing observed time scales of variability) to increasing values of the distance from the center of the source and decreasing values of the magnetic field. In the simplest approximation of this inhomogeneous model there are only two numerical values for each of the physical variables: the size of the source, the magnetic field strength, and the density of the relativistic electrons. In this model it is possible to have a magnetic field strength which will cause the observed peak in the spectrum by means of synchrotron self-absorption and which is also consistent with the condition that the energy losses of the electrons via inverse Compton scattering of the synchrotron photons off the relativistic electrons are not significant compared to the energy losses through synchrotron emission of radiation. (See Figure 18 for a schematic summary of the features of the model.) The match of the spectrum of the model to the observed spectrum is quite good; that is, the spectrum of the model falls generally within the errors of observation (see Figure 17). A characteristic feature of the model is that it requires a very narrow range of specification of two observed parameters, the size of the source and the frequency at which the flux density is a maximum. The model does accomodate the presently reported ranges of the values of these two parameters. However, if future observations were to change the assumed parameters, it is quite conceivable that the proposed model would become inapplicable to the case of NGC 1068.

Future Work

The solution of the problem of explaining the source of the infrared radiation from the nucleus of NGC 1068 is achieved here at the expense of not knowing the means for accelerating the electrons to relativistic velocities, the usual area of ignorance in creating synchrotron model of radiation sources. However, in this model the problem is somewhat amplified because of the very short lifetimes of the electrons in the high magnetic fields. The lifetimes are much less than the lifetime of the source of radiation and even much shorter than the observed time scale of variability of the continuum flux. This implies that the particles need to be accelerated essentially constantly throughout the entire source. The problem of the constant replenishment of the energy of the electrons is a major weakness of the proposed model.

There are several areas of the general problem of explaining the source of the infrared radiation from the nuclei of Seyfert galaxies which have not been mentioned in this dissertation. Among the more obvious problems to be investigated in the future (in addition to improving the quality and quantity of the observations of the time variability of the continuum flux) are the feasibility of finding some mechanism to accelerate the electrons to relativistic velocities, the time evolution of the source, and a more careful treatment of the radiation transfer and the diffusion of the relativistic electrons in time and energy. The diffusion of the particles causes the density and the radiation characteristics to differ from the more nearly homogeneous cases, and the boundaries between the different components of the radiation source will become less abrupt. It might prove worthwhile to investigate the effect

of the time evolution of the physical conditions in one source on the physical conditions in the other source and to determine whether the cloud of thermal particles can result from the diffusion and cooling of the relativistic particles. It might also become profitable (with improved observational accuracy) to investigate models having continuously variable magnetic fields and densities of relativistic electrons.

REFERENCES

Abramowitz, M., and Stegun, I. A. 1964, *Handbook of Mathematical Functions*, NBS - AMS 55 (Washington, D. C.: U. S. Government).

Allen, C. W. 1963, *Astrophysical Quantities* (2nd. ed., London: Athlone Press).

Allen, R. J., Barrett, A. H., and Crowther, P. P. 1968, *Ap. J.*, 151, 43.

Aller, L. H. 1956, *Gaseous Nebulae* (New York: Wiley).

Aumann, H. H., and Low, F. J. 1970, *Ap. J.*, 159, L159.

Baars, J. W. M., Mezger, P. G., and Wendker, H. 1965, *Ap. J.*, 142, 122.

Bardin, C., Chopinet, M., and Duflot-Augarde, R. 1967, *Compt. Rend. B*, 265, 1149.

Bennett, A. S. 1962, *Mem. R. A. S.*, 68, 163.

Berge, G. L., and Seielstad, G. A. 1969, *Ap. J.*, 157, 35.

Bergeron, J., and Salpeter, E. E. 1971, *Astrophys. Lett.*, 9, 121.

Bergeron, J., and Salpeter, E. E. 1972, (in preparation).

Bertola, F., D'Odorico, S., Ford, W. K., and Rubin, V. C. 1969, *Ap. J.*, 157, L27.

Blake, G. M., Argue, A. N., and Kenworthy, C. M. 1970, *Astrophys. Lett.*, 6, 167.

Brandie, G. W., and Stull, M. A. 1971, *Nature Phys. Sci.*, 231, 149.

Burbidge, E. M., Burbidge, G. R., and Prendergast, K. H. 1959, *Ap. J.*, 130, 26.

Burbidge, E. M., Burbidge, G. R., and Prendergast, K. H. 1963, *Ap. J.*, 137, 1022.

Burbidge, G. R. 1970, *Ann. Rev. Astron. & Astroph.*, 8, 369.

Burbidge, G., and Burbidge, M. 1967, *Quasi-Stellar Objects* (San Francisco: W. H. Freeman and Company).

Clarke, M. E., Bolton, J. G., and Shimmins, A. J. 1966, *Aust. J. Phys.*, 19, 375.

Code, A. D. 1969, *P. A. S. P.*, 81, 475.

Cogdell, J. R., McCue, J. J., Kalachev, P. D., Salomonovitch, A. E., Moiseev, I. G., Stacey. J. M., Epstein, E. E., Altschuler, E. E., Feix, G., Day, J. W. B., Hvatum, H., Welch, W. J., and Barath, F. T. 1970, *IEEE Trans.*, AP-18, 515.

Cramér, H. 1945, *Mathematical Methods of Statistics* (Princeton: Princeton University Press).

Cromwell, R., and Weymann, R. 1970, *Ap. J.*, 159, L147.

Donaldson, W., and Smith, H. 1971, *M. N. R. A. S.*, 151, 253.

Dupuy, D. Schnitt, J. L., McClure, R., Bergh, S. van den, and Racine, R. 1969, *Ap. J.*, 156, L135.

Dworetsky, M. M., Epstein, E. E., Fogarty, W. G., and Montgomery, J. W. 1969, *Ap. J.*, 158, L183.

Epstein, E. E., Dworetsky, M. M., Montgomery, J. W., Fogarty, W. G., and Schorn, R. A. 1970, *Icarus*, 13, 276.

Epstein, E. E., and Fogarty, W. G. 1968, *A. J.*, 73, 873.

Epstein, E. E., Fogarty, W. G., Hackney, K. R., Hackney, R. L., Leacock, R. J., Pomphrey, R. B., Scott, R. L., Smith, A. G., Hawkins, R. W., Roeder, R. C., Gary, B. L., Penston, M. V., Tritton, K. P., Bertaud, C., Véron, M. P., Wlérick, G., Bernard, A. Bigay, J. H., Merlin, P., Durand, A., Sause, G., Becklin, E. E., Neugebauer, G., and Wynn-Williams, C. G. 1972, (in preparation).

Fairall, A. P. 1971, *M. N. R. A. S.*, 153, 383.

Fitch, W. S., Pacholczyk, A. G., and Weymann, R. J. 1967, *Ap. J.*, 150, L67.

Fogarty, W. G., Epstein, E. E., Montgomery, J. W., and Dworetsky, M. M. 1971, *A. J.*, 76, 537.

Graham, I. 1971, *Nature*, 231, 253.

Guidice, D. A. 1966, *Nature*, 211, 57.

Gursky, H., Kellogg, E. H., Leong, C., Tananbaum, H., and Giacconi, R. 1971, *Ap. J.*, 165, L43.

Hobbs, R. W., Corbett, H. H., and Santini, N. J. 1968, *Ap. J.*, 152, 43.

Hobbs, R. W., Corbett, H. H., and Santini, N. J. 1969, *A. J.*, 74, 824.

Hoel, P. G. 1971, *Introduction to Mathematical Statistics* (4th. ed., New York: Wiley).

Hoffmann, W. F., and Frederick, C. L. 1969, *Ap. J.*, 155, L9.

Johnson, H. L. 1966, *Ap. J.*, 143, 187.

Johnson, N. L., and Leone, F. C. 1964, *Statistics and Experimental Design in Engineering and the Physical Sciences* (Volumes I and II, New York: Wiley).

Kellermann, K. I., and Pauliny-Toth, I. I. K. 1968, *Ann. Rev. Astron. & Astroph.*, 6, 417.

Kellermann, K. I., and Pauliny-Toth, I. I. K. 1971, *Astrophys. Lett.* 8, 153.

Kellermann, K. I., Pauliny-Toth, I. I. K., and Tyler, W. C. 1968, *A. J.*, 73, 298.

Kellermann, K. I., Pauliny-Toth, I. I. K., and Williams, P. J. S. 1969, *Ap. J.*, 157, 1.

Kellogg, E., Murray, S., Tananbaum, H., Gursky, H., Giacconi, R., and Forman, W. 1971, *Bull. A. A. S.*, 3, 477.

Kinman, T. D. 1968, *A. J.*, 73, 885.

Kinman, T. D., and Conklin, E. K. 1971, *Astrophys. Lett.*, 9, 147.

Kleinmann, D. E., and Low, F. J. 1970, *Ap. J.*, 159, L165.

Knight, C. A., Robertson, D. S., Rogers, A. E. A., Shapiro, I. I., Whitney, A. R., Clark, T. A., Goldstein, R. M., Marnadino, G. E., and Vandenberg, N. R. 1971, *Science*, 172, 52.

Kruit, P. C. van der 1971, *Astron. & Astroph.*, 15, 110.

Locke, J. L. 1970, (private communication by letter from J. L. Locke of the Algonquin Radio Observatory, Ottawa).

Low, F. J. 1970, *Ap. J.*, 159, L173.

Low, F. J. 1971, (private communication from F. J. Low of the Lunar and Planetary Laboratory, University of Arizona, Tucson).

Low, F. J., and Aumann, H. H. 1970, *Ap. J.*, 162, L79.

Low, F. J., and Kleinmann, D. E. 1968, *A. J.*, 73, 868.

Low, F. J., and Rieke, G. H. 1971, *Nature*, 233, 256.

Macdonald, G. H., Kenderdine, S., and Neville, A. C. 1968, *M. N. R. A. S.*, 138, 259.

MacLeod, J. M., Andrew, B. H., Medd, W. J., and Olsen, E. T. 1971, *Astrophys. Lett.*, 9, 19.

MacPherson, G. J. 1972, *P. A. S. P.*, 84, 392.

Mayer, C. H., and McCullough, T. P. 1971, *Icarus*, 14, 187.

Medd, W. J., and Ramana, W. V. V. 1967, *Ap. J.*, 142, 383.

Mitton, S., and Ryle, M. 1969, *M. N. R. A. S.*, 146, 221.

Morgan, W. W., and Osterbrock, D. E. 1969, *A. J.*, 74, 515.

Morrison, P., and Sartori, L. 1968, *Ap. J.*, 152, L139.

Neugebauer, G., Garmire, G., Rieke, G. H., and Low, F. J. 1971, *Ap. J.*, 166, L45.

Oke, J. B. 1968, *A. J.*, 73, 849.

Osterbrock, D. E. 1968, *A. J.*, 73, 916.

Ozernoy, L. M., and Sazonov, V. N. 1971, *Astrophys. Lett.*, 8, 231.

Pacholczyk, A. G. 1970a, *Radio Astrophysics: Nonthermal Processes in Galactic and Extragalactic Sources* (San Francisco: W. H. Freeman and Company).

Pacholczyk, A. G. 1970b, *Ap. J.*, 161, L207.

Pacholczyk, A. G. 1971, in *External Galaxies and Quasi-Stellar Objects*, ed. D. S. Evans (Dordrecht: D. Reidel Publishing Company), 165.

Pacholczyk, A. G., and Weymann, R. J. 1968a, *A. J.*, 73, 870.

Pacholczyk, A. G., and Weymann, R. J. 1968b, "Proceedings of the Conference on Seyfert Galaxies and Related Objects," *A. J.*, 73, 836.

Pacholczyk, A. G., and Wisniewski, W. A. 1967, *Ap. J.*, 147, 394.

Pastoriza, M., and Gerola, H. 1970, *Astrophys. Lett.*, 6, 155.

Pauliny-Toth, I. I. K., and Kellermann, K. I. 1966, *Ap. J.*, 146, 634.

Penston, M. V., Penston, M. J., Neugebauer, G., Tritton, K. P., Becklin, E. E., and Visvanathan, N. 1971, *M. N. R. A. S.*, 153, 29.

Rather, J. D. G. 1970, Doctoral Thesis, University of California, Berkeley.

Reber, E. E., 1970, *Icarus*, 12, 348.

Rees, M. J., and Sciama, D. W. 1966, *Nature*, 211, 805.

Rees, M. J., Silk, J. I., Werner, M. W., and Wickramasinghe, N. C. 1969, *Nature*, 223, 788.

Rieke, G. H. 1972, (private communication from G. H. Rieke of the Lunar and Planetary Laboratory, University of Arizona, Tucson).

Ryle, M., Elsmore, B., and Neville, A. C. 1965, *Nature*, 205, 1259.

Sandage, A. 1968, *Ap. J.*, 152, L149.

Sargent, W. L. W. 1970, *Ap. J.*, 160, 405.

Sargent, W. L. W. 1971, Series of lectures at the *Scuola di Fisica Cosmica*, held at Erice, Sicily, Italy from May 21 to June 1.

Sazonov, V. N. 1970, *Soviet Astronomy - AJ*, 13, 797.

Schorn, R. A., Epstein, E. E., Oliver, J. P., Soter, S. L., Wilson, W. J. 1968, *Ap. J.*, 151, L27.

Seyfert, C. K. 1943, *Ap. J.*, 97, 28.

Shimabukuro, F. I. 1966, *IEEE Trans.*, AP-14, 228.

Shimabukuro, F. I., and Epstein, E. E. 1970, *IEEE Trans.*, AP-18, 485.

Shimabukuro, F. I., and Stacey, J. M. 1968, *Ap. J.*, 152, 777.

Solinger, A. B. 1969, *Ap. J.*, 155, 403.

Stacey, J. M. 1970, (private communication from J. M. Stacey of The Aerospace Corporation, Los Angeles).

Ulrich, M. H. 1971, *Ap. J.*, 165, L61.

Vaucouleurs, G. de 1961, *Ap. J. Suppl.*, 5, 233.

Vaucouleurs, G. de, and Vaucouleurs, A. de 1968, *A. J.*, 73, 858.

Wade, C. M. 1968, *A. J.*, 73, 76.

Walker, G. A. 1972, (private communication from G. A. Walker of the University of British Columbia, Vancouver).

Wampler, E. J. 1967, *P. A. S. P.*, 79, 210.

Weedman, D. W. 1970, *Ap. J.*, 161, L113.

Weiler, K. W., and Ekers, R. D. 1972, (private communication from K. W. Weiler and R. D. Ekers of the Radio Observatory Westerbork, Hooghalen, Netherlands).

Whittaker, E. T., and Watson, G. N. 1963, *A Course of Modern Analysis* (Cambridge: Cambridge University Press).

Wilson, W. J. 1970, (private communication from W. J. Wilson of The Aerospace Corporation, Los Angeles).

Wilson, W. J. 1971, *Ap. J.*, 166, L13.

Wisniewski, W. A., and Kleinmann, D. E. 1968, *A. J.*, 73, 866.

Woltjer, L. 1959, *Ap. J.*, 130, 38.

Zwicky, F. 1964, *Ap. J.*, 140, 1467.